Alpha decay and alpha elastic scattering by heavy nuclei

by
Peter Tripe

A thesis submitted to the Faculty of Science
of the University of Cape Town for the
degree of Master of Science in
Physics.

March 1993

Abstract

A simple three parameter cluster model has previously been developed by Buck, Merchant and Perez to successfully describe alpha decay half lives for more than 400 nuclei. An important feature of this model is that it envisages preformed (preformation factor, P=1.0) alpha particles in the parent nuclei to be moving in orbits with a large value of a global quantum number, G. The discontinuity in decay half-lives at the N=126 neutron shell closure is then naturally explained by an increase of G as the alpha particle is forced into a higher orbit by the shell closure. We consider alternative approaches to this model and extend it to consider different values of P, and different changes in G at shell closures. We find the original approach of Buck *et al.*, a radius fit with $\Delta G=2$, is still the most successful, but that a potential fit with $\Delta G=4$ turns out to be competitive, lending support to the suggestion that the proton shell closure is also felt. We have also analysed low energy (24.7MeV) scattering of alpha particles from a number of heavy nuclei in an attempt to find a common set of potential parameters that adequately reproduces both the decay and scattering data. Although not completely successful in this attempt, we find that the potential parameters obtained in the decay calculations provide a good first guess at the scattering potential parameters. The above analysis constrains P to the range $0.01 \leq P \leq 0.1$, with the value of P=1.0 not ruled out.

Acknowledgements

I would like to express my sincere appreciation to the following people for their great help, without which this work would have been impossible.

- My parents; not just for their encouragement and keen interest in this work, but for their unwavering support and love at all times.

- Professor S.M.Perez, my supervisor, for his time and patience, and his willingness to discuss issues at any time. His insight has clarified many a 'muddy' thought and his energy and enthusiasm have been invaluable in getting through some frustrating periods.

- The Foundation for Research Development for their financial support.

CONTENTS

1. INTRODUCTION

> *"The study of* [alpha] *radioactivity itself together with the application of it as a working source of high speed helium nuclei has played a fundamental role in the development of quantum physics. The scattering experiments of Rutherford and his associates gave the picture of the nuclear atom on which all of the success of modern atomic theory depends. Bohr's formulation of quantum postulates to be applied to such a model was a great step in the extension of knowledge of atomic structure and finally culminated in 1925 in the discovery by Heisenberg and by Schrödinger of a reformulation of mechanical laws which has subsequently proved extremely powerful in handling atomic structure problems."*

These words form the opening paragraph of E.U.Condon and R.W.Gurney's paper[1] in The Physical Review of February 1929. Ironically, in lauding the role alpha radiation had already played at the frontier of physics, their analysis of alpha radiation provided yet another fundamental contribution to our understanding of the physics of the nucleus. The understanding of radioactive disintegration as a chance occurrence directly followed the application of the statistical nature of quantum mechanics to a simple model of the nucleus without any further hypothesis. Together with G.Gamow's paper in Zeitschrift fur Physik[2] this paper was arguably the first major application of the 'new' quantum mechanics. Since the days in which alpha decay provided the doorway for great progress in physics, its central role has gradually diminished to the point where its study is relegated to introductory courses in nuclear physics and there is the general feeling that it is a fully understood phenomenon. But contrary to this belief, as the amount of data and the accuracy of the data has grown, so it has become more difficult to overlook the fact that the fundamental model of alpha decay, as set out in the 1930's, is inadequate. With the discovery of exotic decays in 1984[3] there has been a further increase of interest into models of alpha decay - the hope being to extend these models to the emission of particles heavier than alpha particles.

1.1 ALPHA DECAY BEFORE THE APPLICATION OF WAVE MECHANICS

It was less than a hundred years ago that the study of Nuclear Physics began with the discovery of X-rays by Röntgen in 1895. Alpha particles were first identified as the least penetrating of the radiations emitted by naturally occurring radioactive materials[4]. In 1903, Rutherford measured their

charge-to-mass ratio by deflecting α particles from the decay of radium in electric and magnetic fields[5]. Despite the difficulty of these early experiments, Rutherford's result was only about 25% higher than the presently accepted value. In 1908 Rutherford showed that, as suspected, the α particles were in fact helium nuclei[6]; in his experiments the particles entered an evacuated thin-walled chamber by penetrating its walls, and after several days of collecting, atomic spectroscopy revealed the presence of helium gas inside the chamber.

There are 30 α-emitters in the three naturally occurring radioactive chains, known as the uranium, actinium and thorium series. These start at ^{238}U, ^{235}U and ^{232}Th and, after a number of radioactive transformations, finish at ^{206}Pb, ^{207}Pb and ^{208}Pb respectively. One of the most remarkable things about α-radioactivity is the great range of half-lives. There is a range of 30 orders in magnitude between the longest and shortest lived emitters of Table I. Table I also illustrates the extreme sensitivity of the half life to the energy of the decay - a 30 orders of magnitude decrease in $T_{½}$ corresponds to a mere factor of 5 increase in decay energy.

Table I - *A selection of alpha emitters. Note the dependence of the half life ($T_{½}$) on the energy of the decay (Q).*

Parent nucleus	Q (MeV)	$T_{½}$(s)
^{148}Sm	2.007	2.0E+23
^{235}U	4.327	3.9E+17
^{209}Po	5.008	3.3E+09
^{196}Po	6.687	5.5E+00
^{212}Po	8.985	3.0E-07

This relationship between the energy (or range) of the alpha-particle and the half life for emission was noted at an early date by Rutherford[7]. However, it remained for Geiger and Nuttall[8] to examine this relationship systematically and to show that the logarithm of the decay constant changed linearly with the logarithm of the range (the range is related to the energy by log(range)~$1/\sqrt{Q}$). Furthermore, the lines for the three series of natural radioactivities formed a group of nearly parallel lines, see Figure 1.1. This property as used effectively to disentangle certain members of the radioactive series. Today, the original use of the Geiger-Nuttall relation is only of historical interest as it does not actually give any further insight into the alpha decay process. The correlative function it had in disentangling the decay

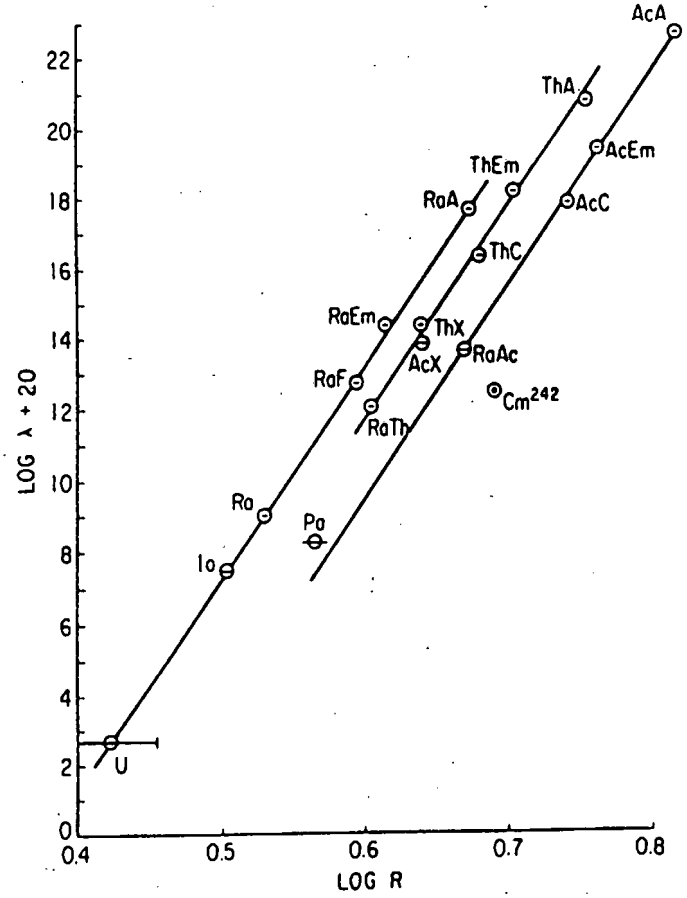

Figure 1.1 - *The Geiger-Nuttall relationship for radioactive series as presented by Rutherford, Chadwick and Ellis,* Radiations from Radioactive Substances *(London and New York: Cambridge University Press, 1930).* λ *is the decay constant (in* sec^{-1}*) and R is range of the emitted alpha particle (in cm of air). The point for* ^{242}Cm *has been inserted to indicate the deficiencies of the Geiger-Nuttall method.*

sequences depends upon the circumstance that among the few alpha energy emitters known at the time, there is an almost monotonic change in alpha energy proceeding down a radioactive decay series. ^{242}Cm, inserted into the plot of Figure 1.1 is but one of many decays later found not to fall on the parallel lines of the radioactive series. Study of these radioactive series in fact obscured for a long time the more fundamental observation that the Geiger-Nuttall relation holds much more closely for a set of nuclei of constant Z, i.e. an isotopic series (see Figure 3.2).

At about the same time, the scattering experiments of Rutherford and his associates gave the picture of the nuclear atom[9]. Bohr's planetary atomic model followed soon in 1913 and was a huge step in the extension of knowledge of atomic structure[10]. There was little progress over the next 15 years towards a satisfactory theory for alpha decay until the development of wave mechanics; although Lindemann[11] was able to obtain an expression which followed the Geiger-Nuttall relation. The hurdle to any understanding of the problem was the statement of classical mechanics that the orbit of a particle is entirely confined to those points in space at which its potential energy is less than its total energy. Classically if a particle is moving in a basin of low potential energy and has not as much total energy as the maximum of potential energy surrounding the basin, it must certainly remain there for all time. This is not true in quantum mechanics. In quantum mechanics most statements of certainty are replaced by statements of probability. And the above statement should be altered to read "...it may remain there for a long time but as time goes on the probability that it has escaped, even without change in its total energy, increases toward unity."

1.2 ONE-BODY MODEL OF ALPHA DECAY

In the Gamow or Condon-Gurney treatment it is assumed that there is a preformed alpha particle moving within a spherical nucleus and confined to the interior by the Coulombic potential barrier. The Schrödinger equation for the motion of the alpha particle in the neighbourhood of the potential is solved with the aid of a number of assumptions which we shall outline briefly. In common with the general applications of wave mechanics to barrier penetration problems it is found that there is a finite probability that the particle can leak through the barrier even though its total energy is less than the potential energy represented by the height of the barrier. Most particles striking the barrier will be reflected but a certain number will 'tunnel' through.

The barrier also operates in reverse, in the case of α-particle scattering by nuclei. Alpha particles incident on the barrier from outside the nucleus usually scatter in the

Coulomb field if the incident energy is well below the barrier height. Tunnelling through the barrier, so that the nuclear force between the particle and target can cause nuclear reactions, is a relatively improbable process at low energy. There is however one exception, and that is if the impinging alpha-particle has an energy very near that corresponding to an energy-level of the compound nucleus, then its chance of penetrating the barrier is greatly enhanced.

The disintegration constant of an α emitter is given in the one-body theory by

$$\lambda_G = fT \qquad (1.1)$$

where f is the frequency with which the α particle presents itself at the barrier and T is the probability of transmission through the barrier. The quantity f is not well defined, but is of the order of v/2R where v is the velocity of the α particle as it moves inside the nucleus and R the radius of the nucleus. The transmission probability, T, must be obtained from a quantum mechanical calculation. To a first approximation, it is sufficient to consider one degree of freedom: we let the coordinate of the particle be r and let the forces be measured by the potential energy function V(r).

The nuclear forces are short range, and outside of the nucleus itself, the only force felt by the α-particle is the Coulomb force with potential energy

$$V(r) = \frac{2Ze^2}{r}. \qquad (1.2)$$

At the edge of the nucleus, assumed to be sharp, the Coulomb potential is replaced by a potential derived from the nuclear forces. This potential is poorly known; an 'average' potential is assumed with constant value throughout the nuclear volume, see Figure 1.2.

For an α-particle of total energy Q, there are three regions of interest. In the region $r<a$ we are inside the nucleus and speak of a potential well of depth $-V_0$, where V_0 is taken as a positive number. Classically, the α particle can move in this region, with a kinetic energy $Q+V_0$, but it cannot escape from it. The annular shell region $a<r<b$ forms a potential barrier because here the potential energy is more than the total available energy Q. The region $r>b$ is a classically permitted region outside the barrier.

From the classical point of view, an α particle in the spherical potential well would sharply reverse its motion every time it tried to pass beyond r=a. Quantum mechanically however, there is a chance of 'leakage', of 'tunnelling' through such a barrier. The complete solution of the wave equation requires a somewhat advanced application of the WKB method. In general the transmission probability, T, or the probability of this 'leaking' occurring with each approach of the

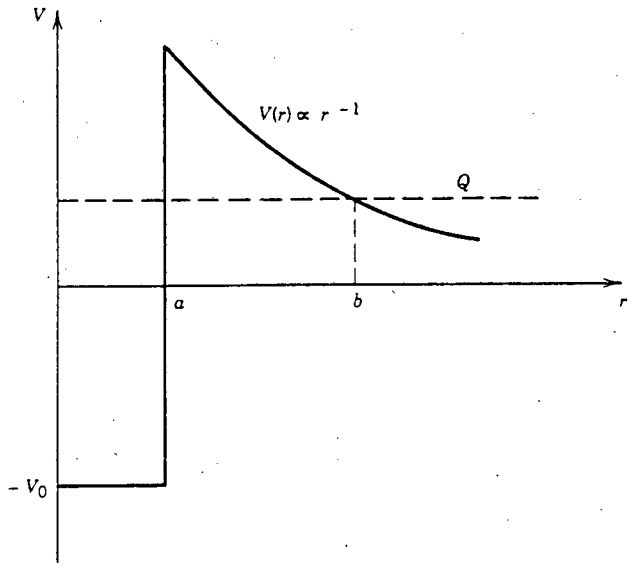

Figure 1.2 - *Potential energy of α-particle, daughter-nucleus system as a function of their separation.*

point r=a is given by:

$$T=e^{-2G} \quad ; \textit{where} \quad G = \sqrt{\frac{2\mu}{\hbar^2}} \int_a^b [V(r)-Q]^{\frac{1}{2}}\, dr \,. \tag{1.3}$$

Due to the simplicity of V(r), G can be evaluated analytically:

$$G = \sqrt{\frac{2\mu}{\hbar^2 Q}}\, 2Ze^2 \left[\arccos\sqrt{x} - \sqrt{x(1-x)}\right] \tag{1.4}$$

where x = a/b. The quantity in brackets is approximately $^{\pi}/_{2}$-$2x^{½}$ when x<<1. Thus the result of the quantum mechanical calculation for the half-life of α decay is

$$T_{\frac{1}{2}} = \frac{\ln 2}{\lambda_G} = \ln 2\, \frac{a}{c} \sqrt{\frac{\mu c^2}{2(V_0+Q)}}\, \exp\left\{2\sqrt{\frac{2\mu c^2}{(\hbar c)^2 Q}}\, 2Ze^2 \left(\frac{\pi}{2} - 2\sqrt{\frac{Qa}{2Ze^2}}\right)\right\} \tag{1.5}$$

which, after grouping of constant terms can be simplified to:

$$\log T_{\frac{1}{2}} = k_1 + \frac{1}{2}\log\left(\frac{\mu}{V_0+Q}\right) + k_2 \frac{Z}{\sqrt{Q}}\left(1 - k_3\sqrt{Q}\right). \tag{1.6}$$

where k_1, k_2 and k_3 are constants. In general $k_3 \ll 1$, and since $\log(\frac{\mu}{V_0+Q})$ varies slowly, we may simplify **(1.6)** to:

$$\log T_{\frac{1}{2}} \approx k_0 + k_2 \frac{Z}{\sqrt{Q}}. \qquad (1.7)$$

From this relationship, the Geiger-Nuttall dependency of $\log(T_{1/2})$ on $1/\sqrt{Q}$ is readily seen. Furthermore, the phenomenon of different isotopic families (each with their particular value of Z) fitting different parallel lines in a Geiger-Nuttall plot is also explained. By substitution one can also see the extreme dependence of the half lives on the decay energy.

1.3 PREFORMATION FACTOR

Alpha decay studies with the one-body model reproduced the general trends of decay constants (over a range of 30 orders of magnitude in $T_{1/2}$), but not the absolute values, even when more realistic potentials than the one above were used. Consequently, an additional term was introduced to **(1.1)** to account for nuclear structure effects.

The preformation factor P (also known as the spectroscopic factor S) is defined as the ratio of the experimental decay constant λ_{exp} over the one-body decay constant λ_G:

$$\lambda_{exp} = P\lambda_G \quad (=PfT) \qquad (1.8)$$

and is interpreted as the probability of nascent α-particle formation. This introduction is not unexpected. We have emphasised that the one-body model requires the existence of *pre-formed* alpha particles within the nucleus. In fact, to explain the existence of the radioactive series, Condon and Gurney proposed the existence of a 'cloud' of such particles orbiting the heavy nucleus, waiting to be successively emitted as the nucleus decays down the series. Such a picture is unlikely; however any given nuclear state will in general contain various configurations, each corresponding to a different mode of motion of the nucleons. In any one nucleus, these configurations will continually be forming and then dissolving to form others. In an assemblage of atoms, there will be, at any time, a certain number of nuclei in each of the configurations, with each configuration having its own probability of occurrence.

Precisely, if Ψ_i is the wave function of configuration *i*, the wave function of the decaying

state is $\Sigma\alpha_i\Psi_i$, and $p_i = |\alpha_i|^2$ is the probability of occurrence of configuration *i*. In some of these configurations, two neutrons and two protons will have come together to form a 'virtual' α-particle. There will then be a certain probability that this cluster will be emitted as an α-particle. If we assume that only one parent configuration is the source of a particular α-decay, we can express the partial decay constant in terms of the probability of that configuration. If Ψ_i is a nuclear configuration that contains an α-particle cluster, and if λ^G_i is the probability that an α-particle of energy Q_i, already formed, will be emitted, we have for the observed decay constant

$$\lambda_i^{exp} = p_i\lambda_i^G = |\alpha_i|^2\lambda_i^G. \qquad \textbf{(1.9)}$$

Thus there are seen to be two aspects of the problem: the determination of p_i, which is a problem of nuclear structure; and the evaluation of λ^G_i, which is what we did in studying the one body model. We refer to p_i as a formation factor and it corresponds directly (assuming that only one parent configuration is the source of the decay) to the preformation factor P that we have introduced.

2. MODERN HISTORY

In this chapter we bring the theory of alpha decay up to date with current understandings in nuclear physics. The approach is much the same as before: the probability of α-formation in a particular state is calculated; the forces this particle feels are represented by an α-nuclear potential; and the rate of decay from a quasi-stationary state of this potential is then determined. The difference lies in a more advanced treatment of each component.

Before developing the alpha-nuclear potential we look at the analogous development of the nucleon-nuclear potential which introduces a number of concepts fundamental to our study of alpha decay.

2.1 NUCLEON-NUCLEAR POTENTIAL

Ultimately we would like to be secure in the knowledge that we could work from first principle knowledge of the nucleon-nucleon interaction (or possibly even quark-quark interactions) to describe the behaviour of any nucleus - its size, 'shape', ground state spin and electromagnetic moments, energy levels and even its behaviour in collisions with other nuclei and the possible reactions it can undergo. Unfortunately there are a number of serious problems with trying to obtain an exact description of the nuclear potential from a microscopic standpoint.

Firstly there is the mathematical difficulty of solving a many-body problem. Even if the interaction potential between individual nucleons were of an exceptionally simple form, the set of coupled equations describing the mutual interactions of A nucleons, where A is greater than 1 or 2, becomes impossible to solve analytically.

Furthermore, these mutual interactions are not of a simple form: to lowest order the interaction between two nucleons consists of an attractive central potential; but there is also a strong exchange dependence; a non-central term, known as the tensor potential; a repulsive term at short distances; and even a dependence on the relative momenta of the nucleons. To obtain an understanding of the nuclear potential from such a microscopic standpoint is currently not feasible, and we resort to a macroscopic 'mean-field' theory.

The basic idea is to think of a 'mean field' felt by a nucleon and not to calculate the effects of the individual interactions directly. The origins of this approach lie in atomic physics with Hartree-Fock self-consistent field methods. We 'freeze' the nucleus so that the interaction of all the other nucleons on a particular 'test' nucleon is given by:

$$V_N(\vec{r}) \approx \sum_{i=1}^{A} v(|\vec{r}-\vec{r}_i|) \tag{2.1}$$

where v is the nucleon-nucleon interaction and the sum runs over all nucleons. Averaging over the positons $\vec{r}_i$ then yields

$$V_N(r) \approx \int \rho(r') v(|\vec{r}-\vec{r}'|) d\vec{r}', \tag{2.2}$$

where ρ(r) is the nuclear density distribution. The nucleon-nucleon interaction is basically attractive and of short range, and may be approximated by a delta function, so that

$$V_N(r) \approx -V_0 \rho(r). \tag{2.3}$$

An analytic form which closely describes the experimental density functions is the Fermi function. The potential then becomes

$$V_N(r) = V_0 f(r) = \frac{-V_0}{1+\exp\left(\frac{r-R}{a}\right)} \tag{2.4}$$

with V_0, R, and *a* the depth, radius and diffuseness of $V_N(r)$ respectively. To construct a nucleus, one puts the nucleons into stationary states of the potential, respecting the Pauli principle. The nucleons then occupy quantum states 1s, 1p, 1d, 2p...etc., of increasing energy.

Figure 2.1 shows measured proton and neutron separation energies, plotted as deviations from the predictions of the semi-empirical mass formula. It is believed that the sharp discontinuities in the separation energy correspond to the filling of major nuclear shells. Figure 2.2 shows additional evidence from a variety of experiments; the sudden and discontinuous behaviour occurs at the same proton or neutron numbers as in the case of the separation energies. These so-called magic numbers (Z or N = 2, 8, 20, 28, 50, 82 and 126) represent the effects of filled major shells, and any successful theory must be able to account for the existence of shell closures at those occupation numbers. The potential in **(2.4)** (with Coulomb potential included) does not result in the correct 'shell structure' for the nucleus and a spin-orbit potential:

$$V_{so}(r) = -\left(\frac{\hbar}{m_\pi c}\right)^2 V_s \frac{1}{r}\frac{df(r)}{dr} \boldsymbol{L}\cdot\boldsymbol{\sigma} \tag{2.5}$$

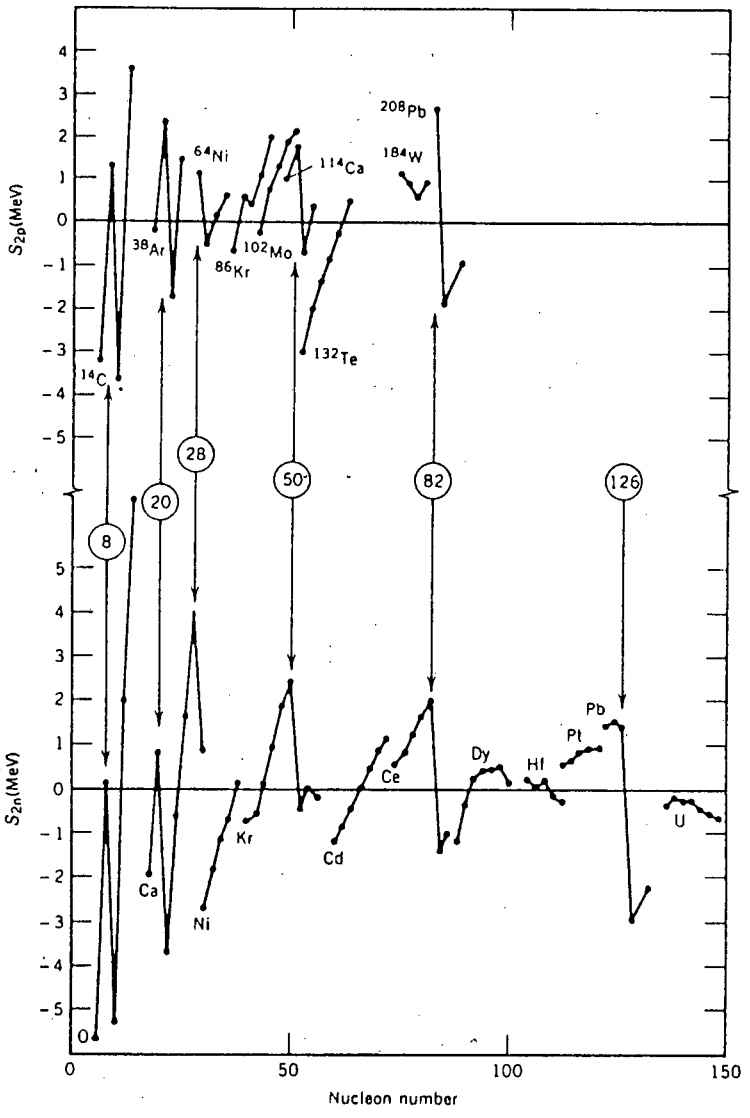

Figure 2.1 - *Two-proton and two-neutron separation energies of sequences of isotones and isotopes respectively. The sudden changes at the indicated 'magic numbers' are apparent.*

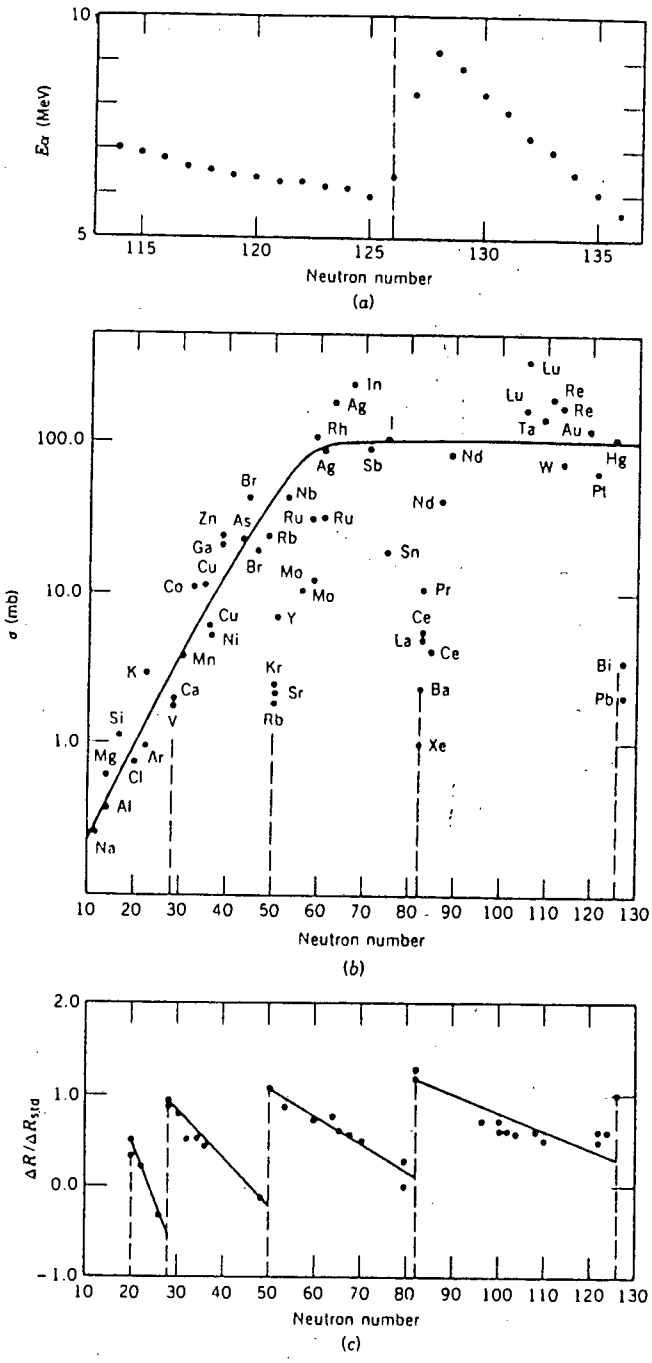

Figure 2.2 - *Additional evidence for nuclear shell structure.*

(a) Energies of α-particles emitted by isotopes of Rn.

(b) Neutron-capture cross-sections of various nuclei.

(c) Change in nuclear charge radius when $\Delta N=2$. (To emphasize shell effects, the radius difference ΔR has been divided by the standard ΔR expected from the $A^{1/3}$ dependence.)

must be added. V_s is the depth of the spin-orbit interaction. This splits the states with orbital angular momentum quantum numbers greater than zero into two components; thus the 1p state splits into the $1p_{3/2}$ and $1p_{1/2}$ states and so on. The energies of the nuclear states may be calculated by solving the Schrödinger equation with the potential,

$$V(r) = V_c(r) + V_N(r) + V_{so}(r), \qquad (2.6)$$

where $V_c(r)$ is the Coulomb electrostatic potential that is present for protons. After adjustment of the parameters the energies and quantum numbers of all the nuclear single-particle states are obtained. The states form bands that automatically give the observed magic numbers corresponding to nuclei of high stability, see Figure 2.3.

This model gives a simple first order account of many properties of the nucleus. However it is an approximation to the potential that a single independent nucleon feels. As pointed out in 1.3, there is the possibility of other quantum states of the nucleus existing in which nucleons have combined to form transient substructures, and among these substructures the alpha-particle is the most likely.

2.2 ALPHA-NUCLEAR POTENTIAL

2.2.1 Motivation

The simplest view of the nuclei of atoms is that they are composed of neutrons and protons. However it is certainly possible for the neutrons and protons to combine together to form transient clusters that survive for a short time before breaking up again into nucleons. Such clustering is expected on energetic grounds[12], especially in the case of alpha-particles with their high binding energies and degree of symmetry. This expectation for α-clustering is supported by several experimental observations:

1. Alpha-decay itself suggests that alpha-particles can be formed in the nuclear surface and can escape by tunnelling through the Coulomb barrier.
2. Alpha-transfer reactions like (d,^{6}Li) and (^{7}Li,t) can be explained by a model which allows alpha-particles to be removed from, or placed into, alpha-particle orbits that are analogous to the nucleon orbits of the nucleon shell model[13,14].
3. Certain rotational bands of light nuclei can be very successfully described as alpha cluster

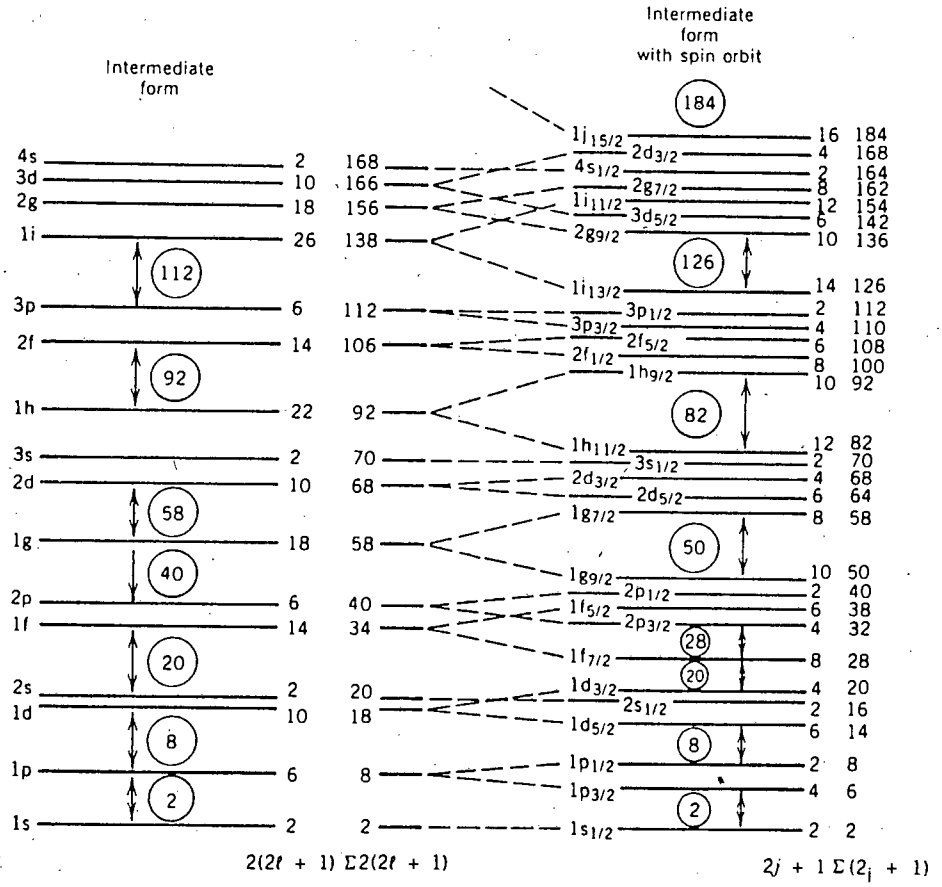

Figure 2.3 - *At left are the energy levels calculated with a Woods-Saxon potential. To the right is shown the capacity and cumulative number of nucleons up to that level. The right side of the figure shows the effect of the spin-orbit interaction, which splits the levels with l>0 into two new levels. The shell effect is quite apparent, and the magic numbers are exactly reproduced.*

states of the nucleus[15,16,17,18].

4. Nuclei formed of an integral number of alpha particles (e.g. ^{12}C and ^{16}O) have particularly stable structures.

Once again, in principle, this behaviour could be described more fundamentally from an individual description of the nucleons, but the mathematical difficulties of doing this are very great. Hence we develop a model that treats the alpha particle as a group or cluster of nucleons in the nucleus as a single entity, rather than as a combination of individual nucleons. In this way, the original many-body problem degenerates once more to a one-body problem similar to the nucleon-nucleus case.

2.2.2 Development

Buck, Dover and Vary[15] presented a simple model for three and four particle cluster states in light nuclei. Studies of alpha-transfer reactions on light nuclei showed that they populate selectively rotational bands of states. The energies and quantum numbers of these states can be calculated as eigenvalues of the alpha potential they propose. The model also gives the widths of the states and electromagnetic transition rates.

As in the development of the nucleon potential, the potential in this model is approximated by a folding potential. Again, using a δ-function form for the nucleon-nucleus interaction, a double folding of the core density $\rho_B(r)$ and the cluster density $\rho_A(r)$ results, due to the composite nature of the α-particle:

$$V_N(r) = -\frac{2\pi\hbar^2}{M}\bar{f}\int\rho_A(r-r')\rho_B(r')d^3r' \quad . \tag{2.7}$$

M, is the nucleon mass and $\bar{f}$, a depth parameter. The densities $\rho_A(r)$ and $\rho_B(r)$ are deduced from electron scattering analyses.

This gives rise to a single particle potential of the form

$$V(r) = V_N(r) + V_{coul}(r) \ , \tag{2.8}$$

which includes a Coulomb potential assumed to arise from a uniform spherical charge distribution. Pauli effects are incorporated by requiring that the nascent α particle be composed of nucleons filling shell-model orbitals above the closed core. This extreme form of the cluster model imposes

restrictions on the possible values of the numbers of nodes n and orbital quantum number L of the alpha particle wave function. The values of n and L are related to the n_i and l_i of the nucleons which make up the cluster by the Wildermuth condition[19]:

$$G = 2n+L = \sum_{i=1}^{n_c} g_i = \sum_{i=1}^{n_c} (2n_i+l_i), \tag{2.9}$$

where n_c is the number of nucleons in the cluster. For ^{20}Ne considered as ^{16}O+α, for example, the lowest-lying states correspond to dropping the four particles into the 2s-1d shell ($2n_i+l_i=2$) rather than the 1s or 1p shell. This procedure is exact in the case of two nuclei whose constituent nucleons are described by single harmonic oscillator wavefunctions sharing a common length parameter. This is not the case here, and so it provides only an approximate treatment. However results for heavy nuclei will be shown not to be very sensitive to the precise value of G employed, and the remaining effects may be absorbed into the effective potential.

There are two factors which set this very successful model aside from other less successful ones. Firstly the folded potential is considerably different to previous Woods-Saxon potentials used (Figure 2.4) - a Woods-Saxon potential with roughly the same geometry gives essentially a degenerate or inverted energy level spectrum. Secondly, the Wildermuth condition ensures that the requirements of the Pauli principle are essentially met.

Figure 2.4 - *Single particle potentials[15] appropriate to the ground state of ^{20}Ne, viewed as α+^{16}O. The solid curves are Woods-Saxon potentials whose depth V_0 was adjusted separately for each state to fit the experimental binding energy. The dashed curve represents the folded potential which succesfully reproduces the spectrum.*

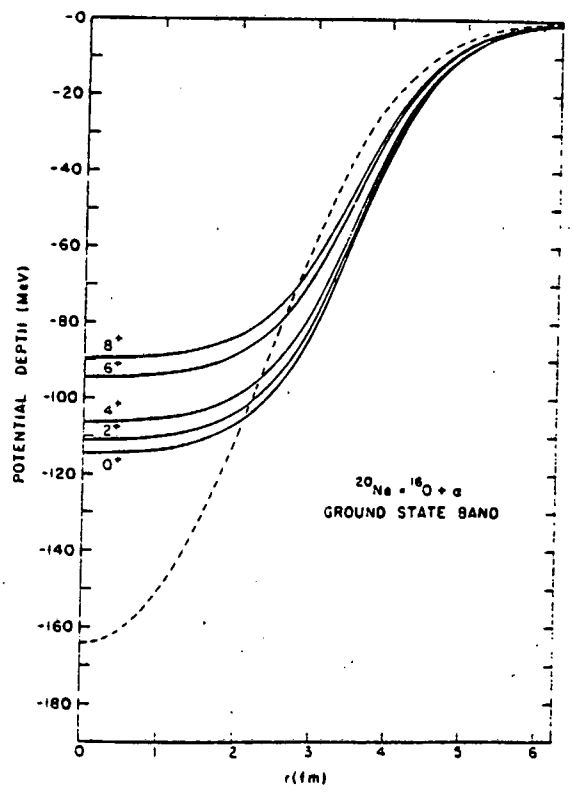

2.3 DECAY WIDTH OF A QUASI-STATIONARY STATE

In the development of the one-body theory of alpha decay, the half-life was seen to have two components

$$T_{\frac{1}{2}} = \frac{ln2}{\lambda_G} = \frac{ln2}{fT} \tag{2.10}$$

where T, the transmission probability, was well determined through quantum mechanical calculations. The quantity f was less strictly dealt with, being roughly of the order of v/2R where v is the velocity of the α particle as it moves inside the nucleus and R the radius of the nucleus.

In applications of the Buck-Dover-Vary model, the single-particle Schrödinger equation is solved with the potential and bound and resonant state solutions identified with states of relative motion of the cluster about the core. The widths of these states are determined by performing cluster-core scattering calculations in which the behaviour of the phase shifts was observed to rise through $\pi/2$ as the energy of the incident particle is increased through the region of resonance. A similar approach to alpha decay is impossible. There one is trying to obtain extremely small widths of $\sim 10^{-26}$eV or less for a state whose energy is around 5 MeV. An alternative approach is to make use of the semiclassical limit of the two potential approach to the decay of a quasi-stationary state developed by Gurvitz and Kalbermann[20]. The quasi-classical limit of the width found in this approach leads to the Gamow formula, but with a well defined pre-exponential factor. Thus

$$\Gamma = PF\frac{\hbar^2}{4\mu}\exp\left(-2\int_{r_2}^{r_3}k(r)dr\right). \tag{2.11}$$

The normalization factor F is given by

$$F\int_{r_1}^{r_2}\frac{1}{k(r)}\cos^2\left[\int_{r_1}^{r}k(r')dr' - \frac{\pi}{4}\right]dr = 1 \tag{2.12}$$

where r_1 and r_2 are the two inner turning points of the total cluster-core potential (which contains nuclear, Coulomb and centrifugal terms) and r_3 the outer turning point. The squared cosine term may be replaced by its average value of ½ without significant loss of accuracy, so that

$$F\int_{r_1}^{r_2}\frac{dr}{2k(r)} = 1 \tag{2.13}$$

with the wave number k(r) given by

$$k(r) = \sqrt{\frac{2\mu}{\hbar^2}|Q-V(r)|} \quad . \qquad (2.14)$$

The α-decay half-life is then related to the width by

$$T_{\frac{1}{2}} = \frac{\hbar\, ln2}{\Gamma} \quad . \qquad (2.15)$$

Thus all the essential ingredients in a one-body theory of α-decay are in place. It remains to determine the preformation probability P, and the parameters: depth, radius and diffuseness of the one-body potential.

3. THE BUCK-MERCHANT-PEREZ MODEL OF ALPHA DECAY

In this section we recount the development of a particularly successful macroscopic model of alpha decay. Through a thorough analysis of this model and its development we give direction to the later work of this thesis in which we explore aspects and implications of the model not previously examined. The development of this model spans a series of nine papers over a period of three years. For convenience we list them in chronological order in Table II, together with the abbreviations by which they will be referred to in this and later sections.

These papers do not deal solely with the alpha decay of heavy nuclei. In fact the original goal was not so much to deal with alpha decays as to provide a model of 'exotic' decays. As it so happens, the model provides a consistent treatment of both exotic decays and alpha decays from heavy nuclei.

Table II - *Publications in the development of the Buck-Merchant-Perez model of alpha decay.*

BM1	B.Buck and A.C.Merchant, *J.Phys. G: Nucl. Part. Phys.* **15**, 615 (1989).
BM2	A.C.Merchant and B.Buck, *Europhys. Lett.* **8**, 409 (1989).
BM3	B.Buck and A.C.Merchant, *Phys. Rev. C* **39**, 2097 (1989).
BMP4	B.Buck, A.C.Merchant and S.M.Perez, *Phys. Rev. Lett.* **65**, 2975 (1990).
BMP5	B.Buck, A.C.Merchant and S.M.Perez, *J. Phys. G: Nucl. Part. Phys.* **17**, 1223 (1991).
BMP6	B.Buck, A.C.Merchant and S.M.Perez, *Mod. Phys. Letters A*, Vol. 6, No. **27** 2453 (1991).
BMP7	B.Buck, A.C.Merchant and S.M.Perez, *J.Phys. G: Nucl. Part. Phys.* **17**, L91 (1991).
BMP8	B.Buck, A.C.Merchant and S.M.Perez, *Phys. Rev. C* **45**, 2247 (1992).
BMPT9	B.Buck, A.C.Merchant, S.M.Perez and P.Tripe, *Phys. Rev. C* **47**, 1307 (1993).

3.1 EXOTIC DECAYS

All nuclei with Z>40 are metastable with respect to radioactive decay into two nuclear fragments with masses M_1 and M_2 for which $Q = [M(A,Z)-M_1(A_1,Z_1)-M_2(A_2,Z_2)]c^2 > 0$. The case $A_2=4$ corresponds to alpha decay; cases in which $A_1 \approx A_2$ correspond to spontaneous fission; and the intermediate cases are the so called exotic decays first observed by Rose and Jones[3]. They may also be referred to as 'heavy-particle radioactivities'[21], or 'cluster decays'[22]. Among the heavy nuclei there are numerous possible two-body decays with positive Q. For most, the decay rates are undetectably low, but for certain combinations corresponding to fragments with nearly closed shells,

Table III - *The experimentally measured cluster decay half-lives. (as of May 1992)*

Parent		Emitted		Experiment
Z	A	Z_e	A_e	$\log T_{1/2}(s)$
88	222	6	14	11.02 ± 0.06
88	223	6	14	15.20 ± 0.05
88	224	6	14	15.90 ± 0.12
88	226	6	14	21.33 ± 0.20
89	225	6	14	17.34 ± 0.30
90	228	8	20	20.86 ± 0.30
90	230	10	24	24.64 ± 0.07
91	231	10	24	23.38 ± 0.08
92	232	10	24	21.06 ± 0.10
92	233	10	24	24.82 ± 0.15
92	233	10	25	
92	234	10	24	25.25 ± 0.05
92	234	12	28	25.75 ± 0.06
94	236	12	28	21.68 ± 0.15
94	238	12	28	25.70 ± 0.25
94	238	12	30	
94	238	14	32	25.30 ± 0.16
96	242	14	34	23.24

the high Coulomb barrier is partly compensated for by a high Q, and the decay may be detectable.

In order to choose favourable cases for experimental study, one needs a quantitative model for decay rates. The models fall into two distinct classes: unified models and cluster models. The unified models, seek to treat alpha and exotic decay along with spontaneous fission as equivalent processes, differing only in the degree of mass asymmetry exhibited. Cluster models assume that a cluster of nucleons forms within the parent nucleus with some probability and that the decay proceeds by barrier penetration along the lines of alpha decay. In BM1, Buck and Merchant propose a cluster model of exotic and alpha decays.

3.2 INITIAL DEVELOPMENT (BM1-3)

Although Gamow[2] and Condon and Gurney[1] immediately succeeded in obtaining qualitative explanation in terms of barrier penetration, the quest for quantitative predictions of the absolute values of alpha decay rates has not met with much more success[23,24]. The traditional approach through R-matrix theory is extremely sensitive to the choice of an arbitrary channel radius[25]. Shell model estimates of preformation factors have generally been restricted to quite severely truncated model spaces for computational reasons, and the subsequent calculation of decay half-lives is then also very sensitive to the largely arbitrary choice of the alpha-core nuclear potential.

In BM1, Buck and Merchant find that a straightforward application of the Buck-Dover-Vary cluster model[15] coupled to the Bohr-Sommerfeld quantization condition, is able to give a consistent and intuitively clear description of all of the then available lifetime measurements of exotic decays from heavy nuclei. They go on to demonstrate that it is also able to reproduce the absolute values of the alpha decay widths of the vast majority (in excess of 80% of more than 400 cases studied across the entire periodic table) of ground state to ground state transitions to within a factor of 10 or better. Furthermore odd-even and odd-odd nuclei are successfully treated on an equal footing to even-even nuclei in contrast to many other theories which can only treat even-even nuclei with any degree of confidence[26]. This success comes without any strong dependence on arbitrary factors and proves to be fairly independent of what nuclear potential is used.

3.2.1 Proposed Model

The determination of the decay width is by the method of Gurvitz and Kalbermann[20]

$$\Gamma = \frac{F\hbar^2}{4\mu} \exp\left(-2\int_{r_2}^{r_3} k(r)dr\right) \tag{3.1}$$

where F and k(r) are as defined in **(2.12)**, **(2.13)** and **(2.14)**. A preformation factor P=1 is assumed.

The double-folding integral of **(2.7)** is used to determine the approximate form of the local central potential $V_N(r)$ which describes the interaction between cluster and core. Buck and Merchant find that this potential may itself be closely approximated by a simple three-parameter cosh form

$$V_N(r) = \frac{-V_0[1+\cosh(R/a)]}{\cosh(r/a)+\cosh(R/a)} \tag{3.2}$$

where V_0 is the depth of the potential and R and a are related to its radius and diffuseness.

Ideally all of these parameters should be determined by some independent means. A series of unique optical potentials derived from alpha-nucleus scattering experiments would be best. However, no such optical potentials are presently available. Indeed, alpha-nucleus scattering experiments are essentially impossible for many of the nuclei of interest because of the short lifetimes and/or extremely low isotopic abundances of the proposed targets.

Values of R and a are assigned by considering ^{212}Po as a ^{208}Pb+α system. Charge densities for ^{208}Pb and ^{4}He are available from electron scattering experiments[27,28]. These were converted to matter densities as suggested by Cook[29] and substituted into **(2.7)**. The shape of the resulting folded potential could be almost perfectly reproduced by assigning the values R=6.3fm and a=0.75fm in **(3.2)**. Buck and Merchant then maintain the diffuseness at a=0.75fm and scale the radii in proportion to $A^{1/6}$ for all the nuclei considered.

The potential depth V_0 is determined for each nucleus, using an adaptation of the WKB method for finding stationary states. The WKB method is normally used to find the energies of stationary states of a potential with known shape and depth. The task here is essentially the inverse of this. In the framework of the cluster model[15], the alpha particle to be emitted fills a state of the alpha-nucleus cluster potential. The energy of this 'state' is well determined by the Q value of the decay. It is the *depth* of the potential that must now be found by application of the WKB method. This is done by applying the Bohr-Sommerfeld quantization condition to place the quasi-bound state of relative motion with n nodes at the energy Q. Hence,

$$\int_{r_1}^{r_2} dr \left[\frac{2\mu}{\hbar^2}[Q - V_N(r) - V_C(r)] - \frac{(L+\frac{1}{2})^2}{r^2} \right]^{\frac{1}{2}} = (2n+1)\frac{\pi}{2} \qquad (3.3)$$

where r_1 and r_2 are the two inner turning points of the total cluster-core potential V(r) (which contains nuclear, Coulomb and centrifugal terms) and n is the number of nodes in the alpha particle's wave function. Note that Buck and Merchant use the Langer modified centrifugal term (in which L(L+1) is replaced by $(L+\frac{1}{2})^2$) to ensure all their integrals are well defined (even for L=0).

The choice of n is obviously critical in determining V_0. The α-particle wave function is one of many solutions (with different nodes n) to the Schrödinger equation involving the cluster-core potential that is being developed. To determine which of these solutions (and hence how many nodes) is relevant, BM1 appeals to the Pauli Exclusion Principle and the extreme form of the cluster model, which assumes the alpha cluster is composed of the most energetic nucleons. As discussed in 2.2.2, this places a lower bound on the possible values of n according to the Wildermuth condition. The main requirements of the Pauli exclusion principle are satisfied by working with those states with quantum numbers n and L (the orbital angular momentum) which obey the Wildermuth condition $2n+L \geq G$, where G is a constant integer chosen large enough to correspond to the microscopic situation in which the cluster nucleons all occupy orbitals above those already occupied by the core nucleons. G, we recall from 2.2.2, is only 'well defined' for harmonic oscillator wave functions but although the values of the calculated potential depths V_0 is sensitive to G, the quality of fit is not. A value of G=22 (n=11 for L=0) is chosen for all nuclei in BM1.

The method of Buck and Merchant has now been defined. They propose a 'cosh' alpha-nucleus potential with free parameters V_0, R and a. R and a are determined for the ^{212}Po ($=^{208}$Pb+α) system. R is scaled according to an $A^{\frac{1}{3}}$ dependence for other nuclei and a is kept constant, a=0.75fm. V_0 is determined by the Bohr-Sommerfeld condition with G=22 (n=11 for L=0). The alpha decay widths are then calculated, following the method of Gurvitz and Kalbermann.

3.2.2 Results

As one might expect, the results are particularly successful for elements with cores around Pb (Po, At, Rn, Fr, Ra, Ac, Th, Pa). Of 169 isotopes having 84 or more protons in the region of the N=126 neutron shell closure, only seven of these decays are not reproduced to within a factor of 10 or better. Decays of elements with lighter cores (Os, Ir, Pt, Au, Hg, Pb, Bi) fare slightly less well, whilst for those with heavier cores (U, Pu, Cm, Bk, Cf, Es and Md) only 50% of the predicted

widths are within a factor of 10 of the data points. Possible sources of error include deformations of some of the heavy nuclei; poorly known spin states; and large uncertainties in certain experimental half lives. In all, the level of success is good: 221 of the 261 widths involving known spins are predicted to within a factor of 10 and a further 36 to within a factor of between 10 and 100.

In Figure 3.1 we reproduce the results of BM1 for the partial alpha decay half-lives of the Pt, Po, and Th isotopes. These elements have cores lighter than Pb, equal to Pb and heavier than Pb respectively. This we do, not merely to illustrate the general level of agreement of the model but in fact to highlight a *weakness* of the model. In the conclusion of BM1, Buck and Merchant comment that it would be interesting to study more closely the (generally small) discrepancies between their predictions and the data with the hope of obtaining some additional nuclear structure information. We choose to do this by plotting $\log(T_{1/2}^{cal}/T_{1/2}^{exp})$ for these same isotopes, in Figure 3.1.

Although the model has roughly reproduced the jump in partial half-lives with the shell closure at N=126 closer examination shows a general tendency to under-estimate the $T_{½}$ for the nuclei with N<126 and over-estimate those with N>126. Before nuclear structure information can be extracted as Buck and Merchant had hoped, an explanation for this global failure of the model is needed.

BM2 and BM3, two later publications, are less comprehensive descriptions of this work which deal with the alpha and exotic decay separately.

3.3 A BETTER DESCRIPTION OF BEHAVIOUR AT N=126 (BMP4-BMP7)

From the perspective of the BM1 model, the α particle to be emitted occupies a particular orbit about the core with a specific global quantum number $G=2n+L$. In BM1-3 it was assumed that G was the same for the entire range of nuclei considered. On reflection there is little justification for this, since the nucleons composing the nascent alpha particles come from different major shells as one increases A through the shell closure at N=126. Buck, Merchant and Perez interpret the discontinuous change in alpha decay widths at N=126, as evidence for distinct orbits with differing G. They propose that G remains constant while a major neutron shell of the daughter nucleus is being filled (i.e. N=52-82, 84-126, 128-164 in the parent nuclei) but is forced to increase abruptly as the shell closure is crossed. In practice this means we use one value of G in the Bohr-Sommerfeld condition of **(3.3)** for parent nuclei with N≤126 and an increased value for those with N>126. All other calculations can be left unchanged.

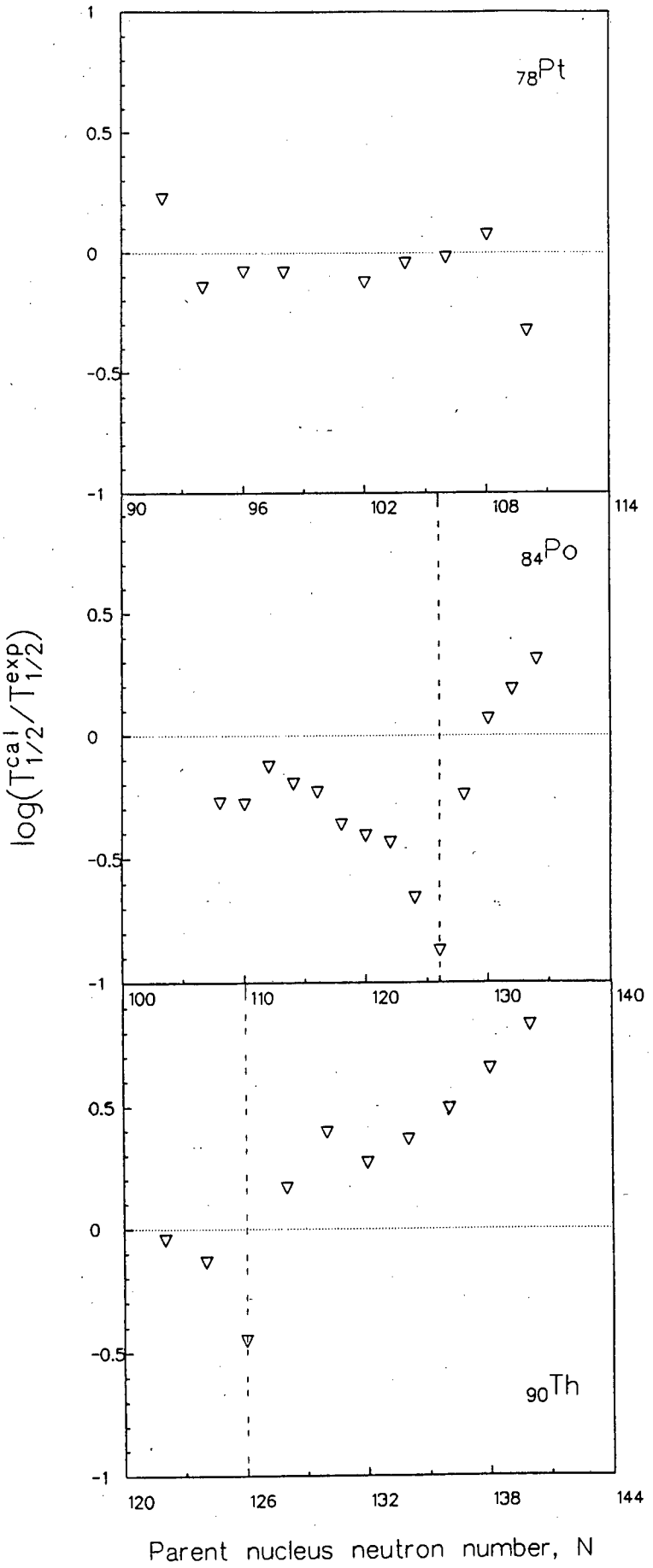

Figure 3.1 - *A comparison of calculated ($T^{cal}_{1/2}$) and experimental ($T^{exp}_{1/2}$) alpha-decay half lives for Pt, Po and Th isotopes using the results of BMP1. $log(T^{cal}_{1/2}/T^{exp}_{1/2})$ is plotted to emphasise the quality of fit.*

The authors choose to change their approach slightly:

1. They restrict the data set to even-even nuclei only. This removes any uncertainties regarding spin assignments as all even-even nuclei have 0^+ ground states.

2. They use a much simpler square well + (surface charge) Coulomb potential, to further reduce the number of variables (no diffuseness term).

$$V = -V_N + \frac{2(Z-2)e^2}{R} \quad (r<R); \quad V = \frac{2(Z-2)e^2}{r} \quad (r>R) \qquad \textbf{(3.4)}$$

3. The decay width **(3.1)** is simplified since by **(2.13)** F=2K/R, with K the constant wave number for r<R. The preformation factor P, is explicitly included, but set to P=1 in the analysis.

$$\Gamma = \frac{P\hbar^2 K}{2\mu R} \exp\left(-2\int_R^{\frac{2(Z-2)e^2}{Q}} k(r)dr\right) \qquad \textbf{(3.5)}$$

4. Instead of scaling R with an $A^{1/3}$ dependence and determining V_N, they set V_N to be the same for all nuclei and calculate R from the Bohr-Sommerfeld condition instead. V_N is varied to obtain the best overall fit to the data.

5. The smallest possible change of G at the closure, $\Delta G=2$, is chosen. They introduce the terms $G_<$= "the value of G for nuclei with N≤126"; and $G_>$= "the value of G for nuclei with N>126". They try a variety of values for $G_>$, and find that values in the range 18-24 give fits which are significantly better than those using higher or lower values of $G_>$.

Following this work, using the best-fit parameter values of

$$P = 1 \qquad V_N = 134\text{MeV} \qquad G_< = 22 \qquad G_> = 24\ ,$$

the partial half-lives for the ground state to ground state α decays of even-even nuclei with 76≤Z≤100 were all calculated to within a factor of ~2. Figure 3.2 shows model fits for the $_{78}$Pt, $_{84}$Po and $_{90}$Th isotopes. The change in behaviour at N=126 is beautifully borne out. On a more precise

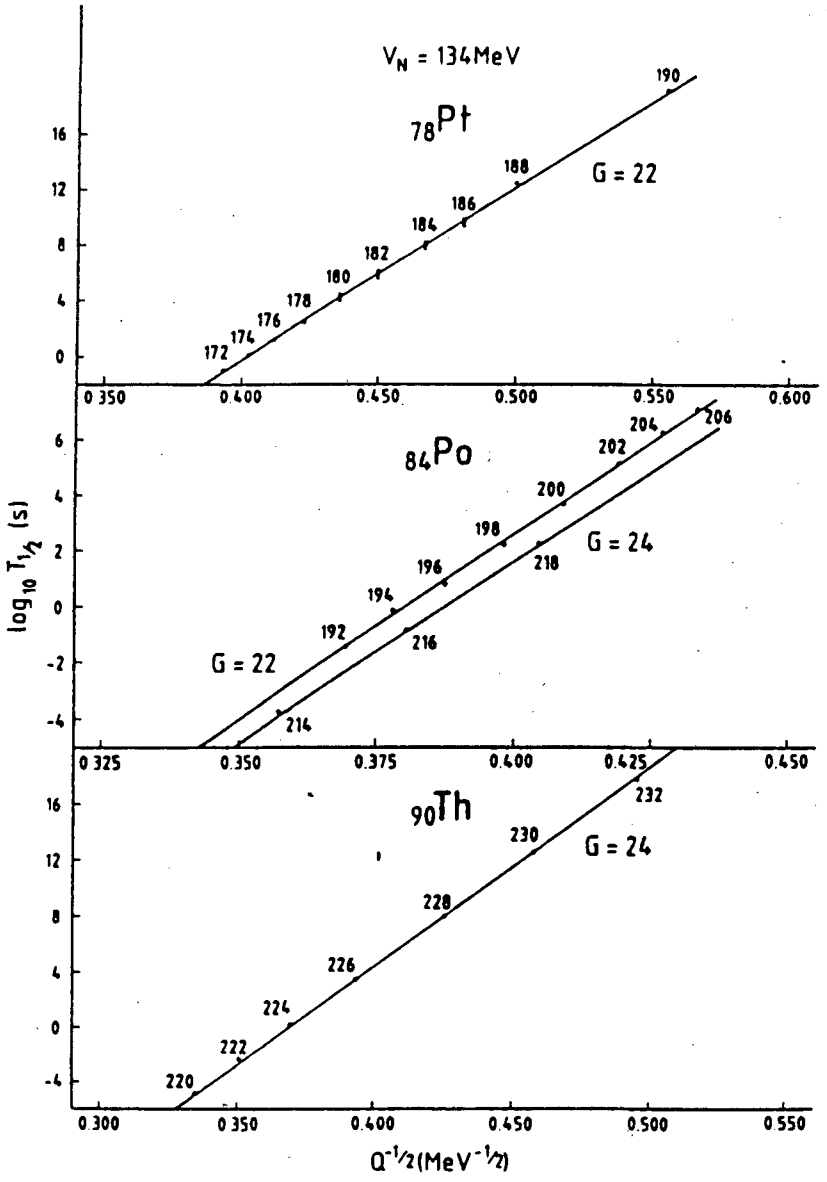

Figure 3.2 - *Geiger-Nuttall plots of experimental (points) and calculated (solid lines) α-decay half lives for Pt, Po and Th parent isotopes. The calculated half-lives are from BMP4, using their best-fit set of parameters: P=1; V_N=134MeV; $G_<$=22; $G_>$=24. Note the success in using an increased global quantum number, G, at the neutron shell closure.*

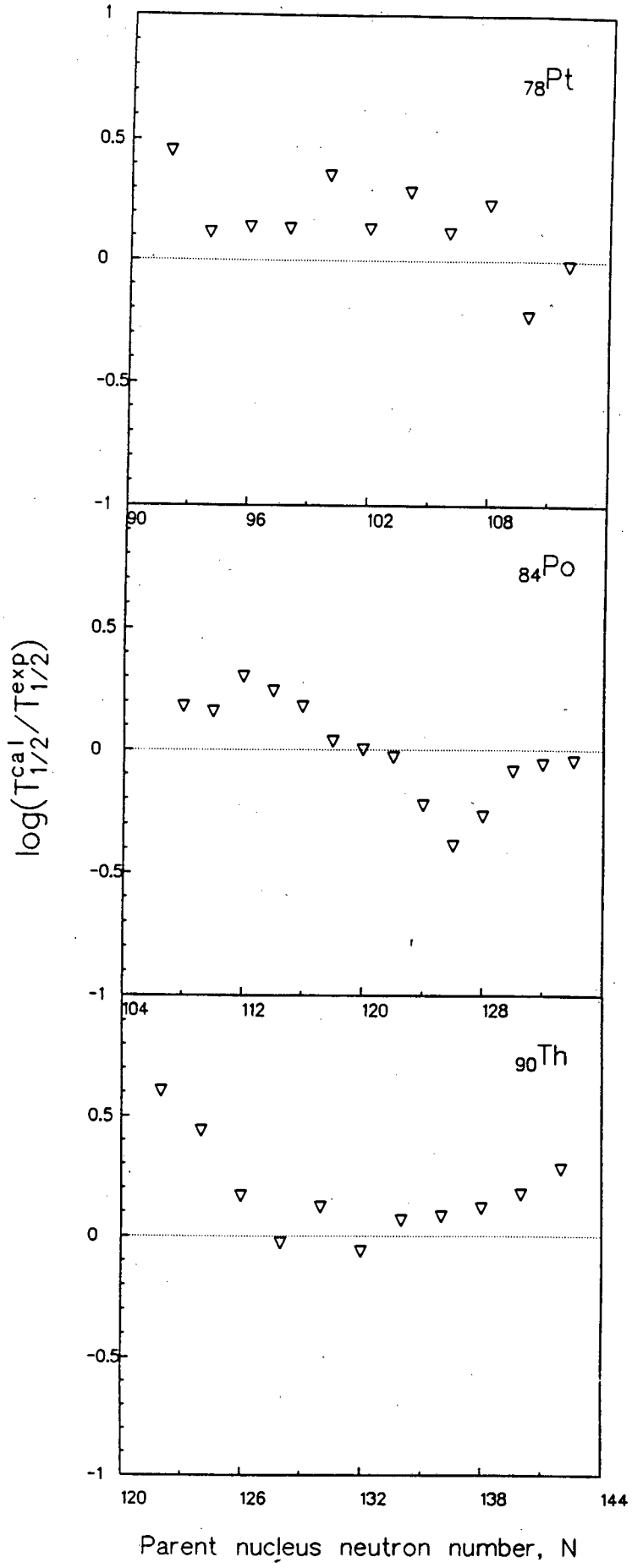

Figure 3.3 - *A comparison of calculated ($T_{1/2}^{cal}$) and experimental ($T_{1/2}^{exp}$) alpha-decay half lives for Pt, Po and Th isotopes using the results of BMP4. $log(T_{1/2}^{cal}/T_{1/2}^{exp})$ is plotted to emphasise the quality of fit.*

level, Figure 3.3 of $\log(T_{1/2}^{cal}/T_{1/2}^{exp})$ for Pt, Po and Th show definite improvement over Figure 3.1.

One issue that has been avoided is that we have until now mentioned only the neutron shell closure at N=126 and not the proton shell closure at Z=82. These closures occur at almost the same point (hence the existence of the 'doubly magic' ^{208}Pb); thus most of the decay data fall into two groups with either N≤126 and Z≤82 (both proton and neutron shells open), or with N>126 and Z>82 (both shells closed). The model fits use $G_<$=22 for the former case, and $G_>$=24 for the latter. This does not determine whether the discontinuity in G is a consequence of the neutron shell closure at N=126, or of the proton shell closure at Z=82, or of a combination of these. The remaining data, involving the transitional nuclei with Z>82 and N≤126, provide some evidence that the proton shell

Table IV - *Deviations between the calculated and experimental half-lives for α decay of $_{86}$Rn and $_{88}$Ra isotopes with N<126.*

Nucleus	N	$\Delta(\log T_{1/2})$
$_{86}$Rn	114	0.39 ± 0.01
$_{86}$Rn	116	0.34 ± 0.03
$_{86}$Rn	118	0.25 ± 0.03
$_{86}$Rn	120	0.25 ± 0.02
$_{86}$Rn	122	0.09 ± 0.05
$_{88}$Ra	118	0.39 ± 0.22
$_{88}$Ra	120	0.28 ± 0.12
$_{88}$Ra	122	0.26 ± 0.02

closure by itself is relatively unimportant. A small effect of this closure could, however, explain the BMP4 results of Table IV for the isotopes of $_{86}$Rn and $_{88}$Ra with N≤126. For these cases, the model with $G_<$=22 consistently overestimates the experimental values of $\log T_{1/2}$ by $\Delta(\log T_{1/2})$~0.3. From a total of 89 decays considered in the analysis of BMP4, only 10 have $|\Delta(\log T_{1/2})| \geq 0.25$, and 7 of these are to be found in Table IV.

BMP5 and BMP6 provide a more extensive description of the work than is afforded in BMP4 but do not introduce any new physics. BMP7 is an extension of this model which successfully describes exotic decays of heavy nuclei.

In conclusion, BMP4 shows that an α-particle-core potential of square-well form, with fixed

depth, and radius given by the Bohr-Sommerfeld condition, reproduces all the α-decay half-lives for heavy even-even nuclei to within a factor of ~2 provided that the α-particle occupies orbits with different global quantum numbers for N≤126 and N>126.

3.4 A REALISTIC POTENTIAL THAT ALSO GIVES A BETTER DESCRIPTION OF BEHAVIOUR AT N=126 (BMP8-9)

Despite the successes of the square well version of the cluster model treatment of α decay, it is open to criticism that the potential is unrealistic and that the half lives deduced from it may somehow be an artifact of the simplified geometry employed. To counter this criticism, BMP8 returns to the cosh potential geometry of **(3.2)**, with a finite diffuseness, and replace the surface Coulomb potential of BMP4 by one appropriate to a point charge α particle interacting with a uniformly charged spherical core:

$$V_C(r) = \begin{cases} \dfrac{Z_1 Z_2 e^2}{r} & for\ r \geq R\ , \\ \dfrac{Z_1 Z_2 e^2}{2R}\left[3 - \left[\dfrac{r}{R}\right]^2\right] & for\ r \leq R\ . \end{cases} \qquad (3.6)$$

The Coulomb and nuclear radii are assumed to be the same. The Langer modified centrifugal potential is again used, so that the cluster-core potential V(r) is

$$V(r) = \frac{-V_0[1+\cosh(R/a)]}{\cosh(r/a)+\cosh(R/a)} + V_C(r) + \frac{\hbar^2}{2\mu r^2}(L+½)^2. \qquad (3.7)$$

Q, the energy appropriate to the decay, is deduced from the measured α particle energy E_α by applying a standard recoil correction, as well as an electron shielding correction in the systematic manner suggested by Perlmann and Rasmussen[30]

$$Q = \frac{A_p}{A_p - 4} E_\alpha + (65.3 Z_p^{7/5} - 80.0 Z_p^{2/5})\ 10^{-6} MeV, \qquad (3.8)$$

where Z_p and A_p are the charge and mass numbers, respectively, of the parent nucleus.

As in BMP4 onwards, the radius parameter R is evaluated separately for each decay by applying the Bohr-Sommerfeld quantization condition. This leaves the free parameters: P

(preformation probability), V_0 and a (potential depth and diffuseness respectively), $G_<$ (G for N≤126), and $G_>$ (G for N>126).

For simplicity, a value of P=1.0 and $\Delta G=G_>-G_<=2$ is again chosen. The search strategy has been to select a value for $G_>$ (G for N>126) and a small starting value for the diffuseness a, and then to search for a value of V_0 to optimise the fit to experiment. Keeping $G_>$ fixed, they increase a by 0.05fm and optimize V_0 again. The incremental increases in a and optimization of V_0 were continued and the least of these minima, and corresponding values of a and V_0, determined. Once these had been established, $G_>$ was changed, and the sequence of stepping through a and optimizing V_0 repeated.

The fitting criterion used to determine the goodness of fit is non-standard. The usual procedure is to minimize some function

$$S_E = \sum \left[\frac{\log_{10} T_{½}^{exp} - \log_{10} T_{½}^{cal}}{\Delta(\log_{10} T_{½}^{exp})} \right]^2 , \qquad (3.9)$$

thus weighting the sum of the squared deviations of the logarithms of the calculated and measured half lives by the experimental errors in the logarithm of the half lives. This is inappropriate for two reasons. Firstly, a handful of nuclei especially amenable to precise measurement (e.g. ^{210}Po and ^{214}Po) have extremely small experimental errors $\Delta(\log T_{1/2}^{exp})\sim 0.00001$ as opposed to the majority of nuclei for which $\Delta(\log T_{1/2}^{exp})\sim 0.1$. These few nuclei so overwhelm S_E that the fitting exercise largely ignores the other nuclei. The weighting of points according to accuracy of experimental values is in general legitimate, but inappropriate in this case for the second reason: there are considerable errors in the determination of $T_{1/2}^{cal}$. The parameter P for example, is set constant for all nuclei. BMP8 estimate a local scatter in P, from nucleus to nucleus, at the level of a factor of about 1.5 to 2. It is therefore unreasonable to weight the deviations with $\Delta(\log T_{1/2}^{exp})$ when $\Delta(\log T_{1/2}^{cal})\sim 0.2$, is typically much larger. They thus replace S_E by

$$S_C = \sum \left[\frac{\log_{10} T_{½}^{exp} - \log_{10} T_{½}^{cal}}{\Delta(\log_{10} T_{½}^{cal})} \right]^2 , \qquad (3.10)$$

where they take $\Delta(\log T_{1/2}^{cal})$ to be equal for all nuclei. Its precise value is arbitrary, and given that it is equal in all cases, may simply be factored out of S_c. They thus minimise the quantity S given by

$$S = \sum (\log_{10} T_{½}^{exp} - \log_{10} T_{½}^{cal})^2 \ . \qquad (3.11)$$

Table V gives the results of fits to values of $G_>$ in the range 18-24. Reducing $G_>$ below 18 or increasing it above 24 leads to worse fits. Of the possible potentials, Buck *et al.* choose that with $G_>$=22. (A straightforward application of the Wildermuth condition to the valence protons and neutrons outside a ^{208}Pb core yields $G_>$=22.)

Using the best-fit parameters for this choice of G values -

V_0 = 162.3MeV a=0.40fm ; [$G_<$=20 $G_>$=22 P=1.0] ,

they calculate the half lives of all the 154 ground state to ground state decays of even-even nuclei listed in Tables 1-5 of BM1. Figure 3.4 shows $\log(T_{1/2}^{exp}/T_{1/2}^{cal})$ as a function of parent nucleus neutron number for 147 even-even nuclei. Broken lines indicate that the deviation between experimental and calculated half lives is within a factor of 2. The degree of agreement is remarkable. Figure 3.4 can also be used to search for systematic trends in the deviations of the two quantities. To highlight any possible effects of the Z=82 proton shell closure, the parent nuclei having Z>82 and N≤126 are plotted by open circles and the remainder by crosses. There may be a weak effect seen in the number of circles below the $\log(T_{1/2}^{cal}/T_{1/2}^{exp})$=0 line. This was noted in BMP4 by the tendency for the calculated half-lives to be larger than the measured values for $^{200}_{86}$Rn....$^{208}_{86}$Rn and $^{206}_{88}$Ra.....$^{210}_{88}$Ra.

In conclusion, the more realistic 'cosh' α-particle-core potential with fixed depth; radius given by the Bohr-Sommerfeld condition; diffuseness and global quantum number determined by a best-fit procedure, continues to reproduce almost all the α-decay half-lives for heavy even-even

Table V - *Values of V_o, a, and $G_>$ which yield good fits to α-decay data. In all cases, P=1 and $\Delta G = G_> - G_< = 2$.*

V_0 (MeV)	a (fm)	$G_>$ (for N>126)	S [see eq.(3.11)]
141.9	0.70	18	1.11
152.5	0.55	20	1.07
162.3	0.40	22	1.11
172.0	0.25	24	1.21

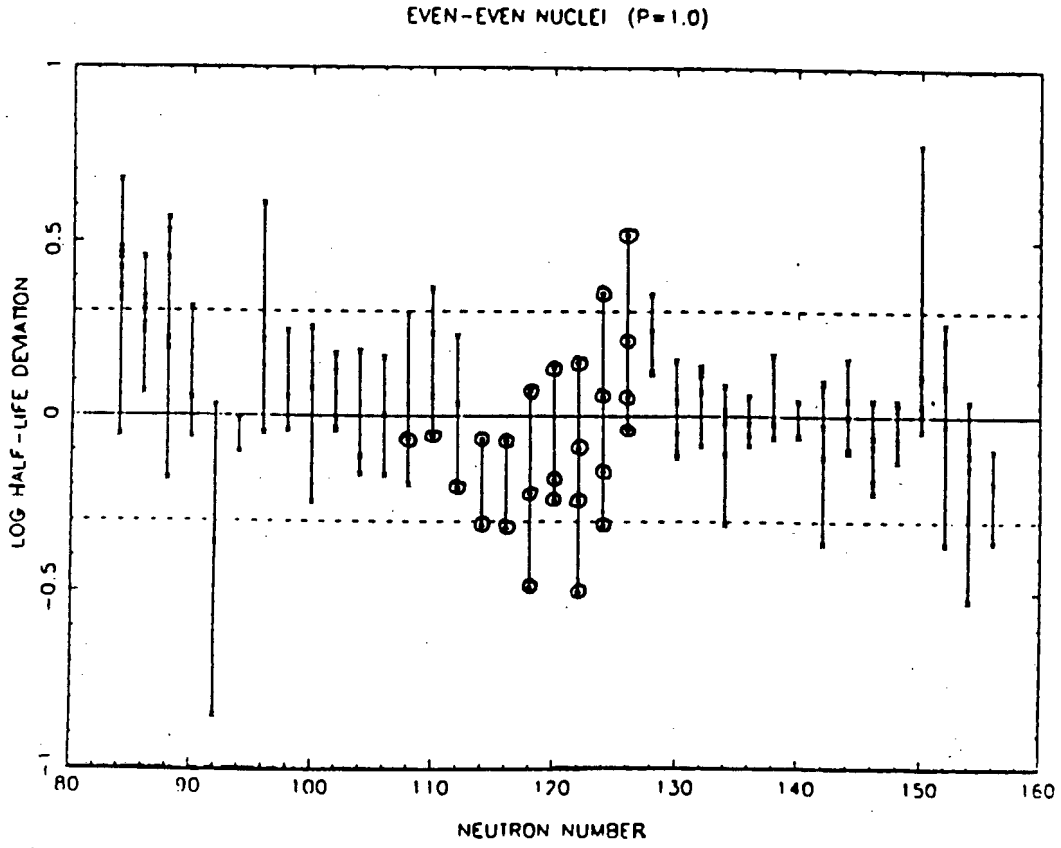

Figure 3.4 - *Plots of* $\log(T^{exp}_{1/2}/T^{cal}_{1/2})$ *as a function of parent neutron number N for even-even nuclei. Results for individual parent nuclei with* $Z>82$ *and* $N\leq 126$ *are labeled by open circles, and the remainder by crosses. Lines are drawn connecting each set of isotones. Factor of 2 deviations between theory and experiment are indicated by broken lines. The model parameters are* $V_N=162.3$ *MeV,* $G_>=22$ *(for* $N>126$*),* $G_<=20$ *(for* $N\leq 126$*),* $a=0.40$*fm, and* $P=1$.

nuclei to within a factor of ~2. Once again, orbits with different global quantum numbers for $N \leq 126$ and $N > 126$ are required. BMPT9 applies the realistic potential to exotic decays, reproducing their half lives to within a factor of 2.

3.5 FORMATION FACTORS

In 1.3, the preformation factor P, or spectroscopic factor S, was introduced to describe the preformation probability due to nuclear structure effects. Through BM1 to BMPT9, Buck *et al.* have maintained a constant preformation factor of P=1, seemingly without detriment to their results. This is not to suggest that they claim P=1. Instead, as mentioned in BMP8, they find little dependence of the goodness of fit on P provided $P \geq 10^{-4}$.

Although the BMP results do not shed any light on the precise value of P, they are interesting in suggesting the fluctuation in the value of P from nucleus to nucleus is small. P enters into the calculation of decay half lives after all the other parameters have been determined, when it appears in the formula for the decay width **(3.5)**. Thus, even if we had all the other parameters 'spot on' and the calculations 100% correct, a fluctuation in P of an order of magnitude would see data points much more widely scattered in a graph of $\log(T_{1/2}^{cal}/T_{1/2}^{exp})$ than seen in Figure 3.4. At most there seems to be a fluctuation up to a factor of 2 from nucleus to nucleus. This result is surprising as it suggests P is fairly insensitive to the structure of the nucleus. We turn now to look at the theoretical and experimental determination of P.

To obtain a measure for a particular type of clustering, one has to define a pure two-cluster state or a subspace of such states. Then one characterizes the cluster content of any other state, by projecting it onto this subspace. Traditionally, the spectroscopic factor, defined as the integral of the modulus square of such projections, is used to quantify the clustering properties of states. The spectroscopic factor is identified with the probability of clustering, and the related amplitude function with the probability amplitude of finding two clusters at a given distance.

It was a frustrating fact for theorists that calculated and measured spectroscopic factors, using this interpretation, differed by several orders of magnitude for several decades. The first attempt to treat alpha decay as a many-body problem was made by Thomas[31] in 1954, but the most significant early work was in the application of the nuclear shell model to alpha decay by Mang[23]. The most striking feature of the experimental data is the sharp drop by a factor of about five in the reduced width of α-emitters with 126 or fewer neutrons. Mang was able to explain this phenomenon in terms of a shell-model. In Figure 3.5 one can see that the model provides very

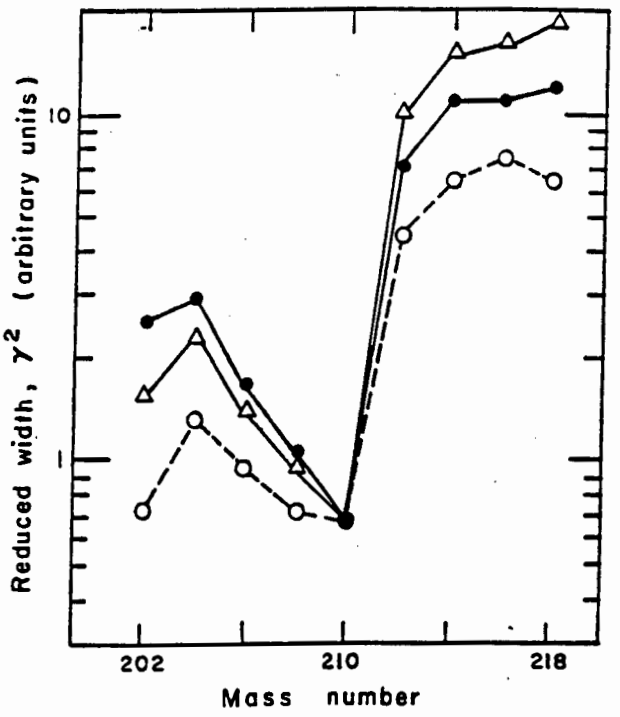

Figure 3.5 - *Reduced widths of even-even polonium isotopes (in arbitrary units) given as a function of mass number. -•-, computed from measured decay constants with the help of Igo's optical-model potential; -Δ-, also computed from measured decay constants, but a pure Coulomb potential has been used with a cutoff at 9.3fm; —○— ,calculated from the shell model.*

satisfactory agreement with the observed trend. The calculated data have been normalized by fitting the value for ^{210}Po to experiment and hide the fact that although the trend was reproduced, the absolute values of the decay constants are still smaller by a factor between 10 and 1000 depending on the parameters used and what alpha-nucleus potential is used. It was believed that if account of some clustering in the diffuse nuclear boundary were taken by some additional shell model configuration mixing, one would increase all the values without essentially altering their ratios.

Fliessbach[32] however, claimed that the problem lay in the interpretation of the role of the spectroscopic factor and introduced a renormalized amplitude to carry the proper probability meaning. It has since been shown by Beck *et al.*[33] that neither interpretation is entirely well-defined. They show however, that it is still possible to quantify the amount of clustering by defining a 'weight' of a cluster-model component in a wave function. This 'weight' they show to be equal to the norm square of Fliessbach's renormalized amplitude. Hence the measured spectroscopic factors (and our preformation factor P) should rather be compared with Fliessbach's "new spectroscopic factor", than the traditional spectroscopic factor. This replacement, typically increases the calculated preformation factors by a factor of 300 or 400, bringing the results more in line with experimental spectroscopic factors[34,35].

Despite this success, there is still little certainty in the absolute probability of alpha formation. One possible reason for this has been given by Fliessbach and Okabe[36]. They

Table VI - *Values of spectroscopic factor calculated according to Fliessbach's renormalization and some experimental values.*

Parent nucleus	Preformation factor	Comment	Source
^{212}Po	3×10^{-3}	pure configuration	Fliessbach and Okabe[36]
	3×10^{-2}	configuration mixing	
^{212}Po	0.302	parameter free microscopic description	Varga *et al.*[37]
^{222}Ra	5.9×10^{-2}	Following method of Fliessbach	Blendowske *et al.*[35]
^{223}Ra	5.4×10^{-2}		
^{224}Ra	6.7×10^{-2}		
^{222}Ra	1.5×10^{-2}	Experimental determination	
^{223}Ra	6.9×10^{-4}		
^{224}Ra	1.8×10^{-2}		
even (Z)	6.3×10^{-3}	Experimental determination	Blendowske and Wallis-er[62]
odd (Z)	3.2×10^{-3}		

investigated the effect of shell model configuration mixing in heavy nuclei and showed that the degree of clustering can be arbitrarily increased by successively more extensive mixing. Table VI compares recent values of S calculated according to the definition of Fliessbach's with 'experimental' measurements.

The 'experimental' spectroscopic factor S_{exp}, is given by

$$S_{exp} = \frac{\lambda_{exp}}{\lambda_G} . \qquad \textbf{(3.12)}$$

λ_{exp} is of course the measured decay constant and is well defined. But λ_G involves the Gamow factor **(1.3)** and can be evaluated accurately only if one has a very good idea of the nuclear potential $V_N(r)$. Thus the 'experimental' spectroscopic factor is not strictly experimental. Reproduction of 'experimental' spectroscopic factors by microscopic calculation is only meaningful if there is certainty that a realistic potential has been used in the calculation of λ_G. To illustrate what care must be taken, it must be considered that typically, a change of 10% in the radius of the nuclear potential results in a factor of 10 difference in λ_G (and hence S_{exp}). Fliessbach and Okabe[36] estimate that uncertainty in this potential introduces about a factor 2 to 3 up or down in the experimental spectroscopic factor. In chapter 5 we shall show that this estimate of the uncertainty is somewhat optimistic.

To conclude this study of the preformation factor - very little can be said with certainty. Although the extremely small spectroscopic factors of the early work by Mang and others have been ruled out, there is little agreement beyond limiting the values to $P \geq 10^{-3}$. The more recent work of Varga *et al.*[37] however, suggests a value of P=0.3. This is much larger than any previously calculated values, and if correct, justifies the assumption of a high degree of preformation in BM1-BMPT9. It remains to be seen whether we can obtain any constraint on P ourselves, either from a more detailed study of the decay data or through some alternative means. A determination of P within a consistent potential model which reproduces both the alpha decay and alpha scattering data would be especially valuable.

4. NEW DEVELOPMENTS WITH THE BMP MODEL

4.1 SUMMARY OF THE BMP WORK AND QUESTIONS IT POSES

Using the cluster model of Buck, Dover and Vary, Buck and Merchant apply a cluster-core folding potential, alternatively represented by a three parameter cosh potential, to the decay of heavy nuclei by alpha or exotic emission. This potential has 3 parameters: V_0, R and a. R and a are fitted to ^{208}Pb; for other nuclei R is scaled by $A^{1/3}$ and a is kept constant. Individual V_0's are determined by applying the Bohr-Sommerfeld condition to each decay in turn. Into the B-S equation goes a constant global quantum number G determined by the Wildermuth condition for the heavy region of the periodic table.

In later work it is realised that a change $\Delta G=2$ in G at the neutron shell closure reproduces better the discrete jump in alpha decay half lives at N=126. The potential is simplified to a square well and hence the parameter a disappears; V_N is held constant throughout whilst individual R's are determined by the B-S condition for each decay.

The third round brings us back to the more realistic cosh potential but with a change $\Delta G=2$ in G at the neutron shell closure. V_0 and a are held constant throughout and, as for the square well model, individual R's are determined by the B-S condition for each decay.

The following questions may be asked.

1. Why a jump of $\Delta G=2$, what about $\Delta G=4$? In the extreme cluster model (alpha particle composed solely of nucleons above the core) with pure harmonic oscillator orbitals we expect to see a change in G both at a proton closure and at a neutron closure. After they have both closed, the change in G should be $\Delta G=4$.
2. Which of the following variants is best ?
   a) Fix r_0 (and thus $R=r_0A^{1/3}$) and a throughout, and determine individual V_0's by applying the B-S condition to each decay in turn. (Referred to as 'potential fits' from here on.)
   b) Fix V_0 and a throughout, and determine individual R's by applying the B-S condition to each decay in turn. (Referred to as 'radius fits' from here on.)
   c) Fix r_0 (and thus $R=r_0A^{1/3}$) and V_0 throughout, and determine individual a's by

applying the B-S condition to each decay in turn. (Referred to as 'diffuseness fits' from here on.)

3. Can any further information about P be extracted?

4.2 PREPARATIONS

We next describe our attempts at answering the above questions. In this section, we first define what model we use and what calculations are to be performed. Next we define what range of parameters are allowed and what data set is to be used. In Section 4.3 we perform a simple sensitivity analysis in which we immediately show that fixing individual diffusenesses by the B-S condition is not feasible. In section 4.4 we in turn examine fixing individual V_0's or individual R's by the B-S condition, using first a value of ΔG=2 and ΔG=4. Section 4.5 repeats the work of 4.4 but includes transitional nuclei before coming to a conclusion about which is the better approach to fitting the data and what value of ΔG must be used. Section 4.6 concludes with a look at different values of preformation factor P.

4.2.1 Relevant equations of models used

The equations used in this chapter and the calculations made have all been extensively discussed in Chapter 3. Nevertheless, for clarity and convenience we repeat the relevant equations we will be using in this section with a brief explanation of the approach used.

We use a cosh nuclear potential, with a uniform charge density Coulomb potential (with same radius as the cosh potential), and a Langer modified centrifugal barrier.

$$V(r) = V_N(r) + V_C(r) + \frac{\hbar^2}{2\mu r^2}(L+\tfrac{1}{2})^2 , \qquad (4.1)$$

where μ is the reduced mass of the cluster-core system. $V_N(r)$ is the nuclear potential

$$V_N(r) = \frac{-V_0[1+\cosh(R/a)]}{\cosh(r/a)+\cosh(R/a)} \qquad (4.2)$$

V_0 is the depth; a is the diffuseness and R the radius. $V_C(r)$ is the Coulomb potential

$$V_C(r) = \begin{cases} \dfrac{Z_1 Z_2 e^2}{r} & \text{for } r \geq R\,, \\ \dfrac{Z_1 Z_2 e^2}{2R}\left[3 - \left[\dfrac{r}{R}\right]^2\right] & \text{for } r \leq R\,. \end{cases} \tag{4.3}$$

The classical turning points of the potential (r_1, r_2 and r_3 in order of increasing distance from the origin) are found by solution of the equation V(r)=Q, where Q is the energy appropriate to the decay under consideration. We next choose a value for the global quantum number G=2*n*+L (*n* being the number of nodes in the radial wave function, and L the corresponding orbital angular momentum). We now have three free parameters: V_0, r_0 (or equivalently $R=r_0A^{1/3}$) and *a*; and one further piece of information, the Bohr-Sommerfeld (B-S) condition. We keep two parameters fixed for all nuclei and calculate the third one from the B-S condition. The first two parameters are varied to determine the best overall fit to the alpha decay half lives. If the potential depth V_0 say, is the quantity determined by the B-S condition, we say that we are "fitting the V's". Similarly if r_0 or *a* is the dependent variable.

The B-S condition is:

$$\int_{r_1}^{r_2} dr \left[\frac{2\mu}{\hbar^2}[Q - V_N(r) - V_C(r)] - \frac{(L+\frac{1}{2})^2}{r^2}\right]^{1/2} = (2n+1)\frac{\pi}{2}\,. \tag{4.4}$$

The decay width is given by

$$\Gamma = \frac{PF\hbar^2}{4\mu} \exp\left(-2\int_{r_2}^{r_3} k(r)dr\right), \tag{4.5}$$

where P is the alpha-particle preformation probability and the normalization factor F is given by

$$F\int_{r_1}^{r_2} \frac{dr}{2k(r)} = 1\,, \tag{4.6}$$

with the wave number k(r) given by

$$k(r) = \sqrt{\frac{2\mu}{\hbar^2}|Q - V(r)|}\,. \tag{4.7}$$

The alpha-decay half-life is then related to the width by

$$T_{\frac{1}{2}} = \frac{\hbar \ln 2}{\Gamma} \quad . \tag{4.8}$$

The strategy for determining the best-fit is to search for values of the independent variables that minimize the quantity S given by

$$S = \sum (\log_{10} T_{½}^{exp} - \log_{10} T_{½}^{cal})^2 \quad . \tag{4.9}$$

For the purposes of these calculations we have developed our own computer codes which have been checked by repeating the calculations of BMP8.

4.2.2 Parameter space investigated

On the one hand we would like to explore the parameter space of the cosh model as extensively as possible. On the other hand, we obviously have to place some restriction on the size of the parameter space. This is not merely to save time and effort, but if the model requires that the diffuseness say, of ^{208}Pb, is 2fm, we should start looking elsewhere for something more realistic. To make the search as extensive as possible within physical restrictions we choose the following (fairly generous) 'window' of parameter space in which to search:

$G_<$	~	20 ± 6	
V_0	~	150 ± 80 MeV	
r_0	~	1.25 ± 0.30 fm	($R=r_0A^{⅓}$)
a	~	0.60 ± 0.40 fm	

The one parameter not specified here is P. It was mentioned earlier in 3.4 and 3.5, that the decay calculations give almost no indication of what the preformation factor is. Changing P from 1.0 to 0.1 was found not to change the quality of the fit, but deepens the potential at which this best fit occurs by ~20MeV[40]. In accord with earlier calculations we keep P=1.0 during these initial surveys. In the concluding section of this chapter we consider a range of P values. These results serve two roles: they exhibit the dependence of the qualities of fit on P; and are used in chapter 5, where we wed decay and scattering calculations.

4.2.3 Data set used

We obviously want to have the largest data set possible, but there are two major considerations which limit our selection.

Firstly, we don't want to be misled by very poor data. Fitting procedures usually guard against this by weighting data points according to their experimental uncertainty. With good reason, we have forsaken this protection as described in section 3.4. We thus manually exclude from the data set, any nuclei for which the α-decay half life is poorly known.

The second consideration is to determine whether the change in half lives is due to the neutron shell closure, the proton shell closure, or both. The clearest way to test whether one or two shell closures is felt, is to look at the case where both shells are definitely open, then look at those where both shells are definitely closed and see whether a jump of $\Delta G=2$ or $\Delta G=4$ between the two regions, gives the better fit. For this reason, we exclude at first nuclei which fall in between these two groups. Nor do we want extremely light or extremely heavy nuclei which may fall into another major shell. The following restrictions were thus placed on our choice of nuclei, where N (Z) refers to the neutron (proton) number of the parent:

1. Even-even ground state to ground state decays. For these $0^+ \rightarrow 0^+$ transitions, the α- particle is necessarily emitted with L=0. For odd mass nuclei a value of L cannot be assigned uniquely, even when the parent and daughter spins are known.

2. A>144. We do not want to consider complications such as another change in G from the N=82 closure. The decays of the very light nuclei are also at the limit of measuring techniques and subject to considerable error.

3. N≤152. A possible shell closure for neutrons in 'deformed' nuclei occurs at N=152. The nucleon potential discussed in 2.1 predicts the next shell closure after 126 is at 164. A nucleus with this many neutrons falls into the range of very heavy nuclei, for which deformation of the nucleus is expected. When this effect is included, there is a shifting of energy levels such that this shell closure moves to N=152 (Figure 4.1). This 'deformed' shell closure' has been detected by a change in the alpha decay data similar to that at N=126, but not as strong (Figure 4.2).

4. No nuclei with: Z≥84, N≤126 - closure of Z shell but not of N shell. To test whether $\Delta G=2$

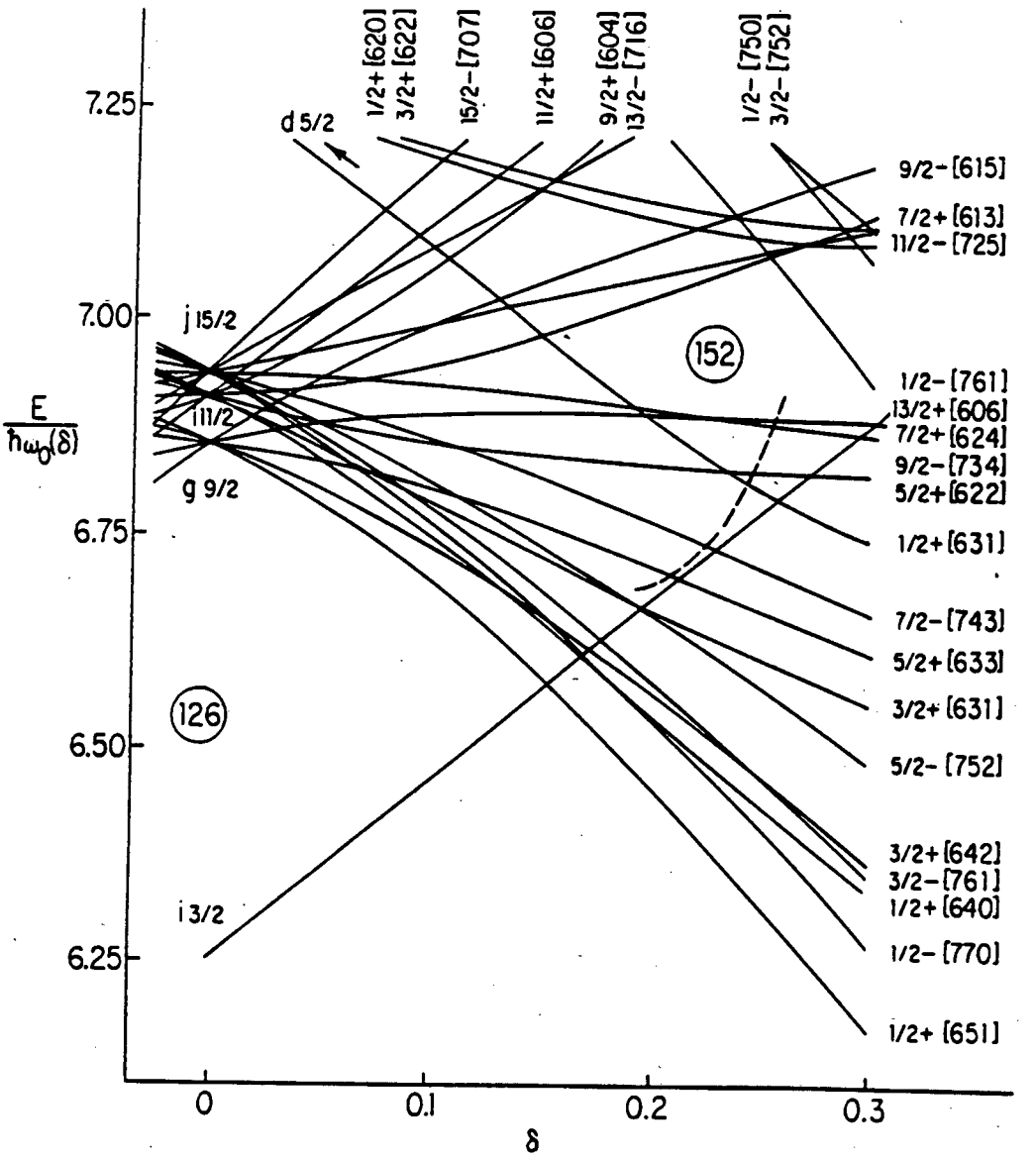

Figure 4.1 - *Energy level diagram for neutrons in the region $126 \leq N \leq 160$ as a function of prolate nuclear deformation. The ordinate indicates the energy of the various levels.*

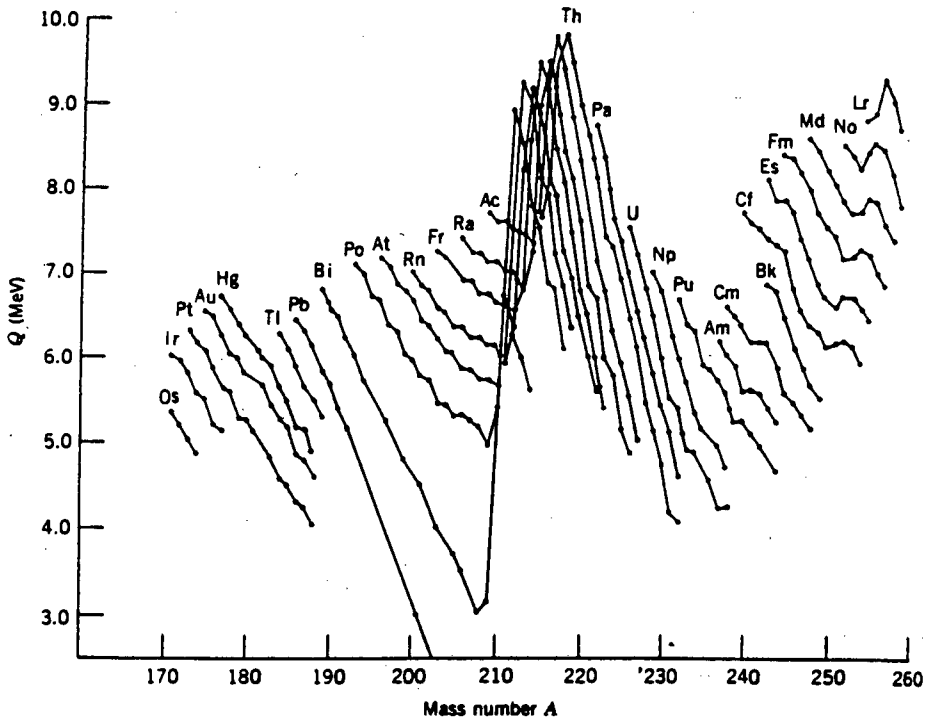

Figure 4.2 - *Energy released in α decay for various isotopic sequences of heavy nuclei. The effects of the shell closures at N=126 (large dip in data) and N=152 (small dip near A=255) can be seen.*

or $\Delta G=4$, we restrict the set to nuclei where both shells are closed or both open. We shall include these 'transitional' nuclei in a later discussion.

5. As for 4 above, we exclude the alternative case where $N \geq 128$ and $Z \leq 82$.

6. No uncertainties in experimental $T_{½}$ greater than 100%.

Using these conditions we found a sample of 110 nuclei (see Appendix A). An interesting point is the fact that the half-lives of nuclei with N<126 are in general much more poorly known than those with N>126. Examination of Appendix A will show that of the 56 nuclei in our sample, with N<126, only 8 have half lives known to 3 significant figures or more. Of the 54 nuclei with N>126, 31 are known to 3 significant figures or better.

In section 4.5 the transitional nuclei are incorporated into the data set we have just established. A further 26 nuclei which satisfy the other conditions listed above are thus included into the data set (see Appendix B).

4.3 SENSITIVITY ANALYSIS

4.3.1 Sensitivity to search approach

With respect to question 2 of section 4.1, as to which parameters are best kept constant and which should be fitted by the Bohr-Sommerfeld condition we first undertake an examination of the sensitivity of the model to changes in its parameters. The need for this becomes clear when considering the possibility of fixing V_0 and r_0 and determining the diffuseness from the B-S condition.

Our calculation always has two parts to it: two parameters (the independent variables) are held constant whilst the third (the dependent variable) is determined for each nucleus by the B-S condition; the half life is then calculated with these parameters and a measure of the fit is determined. (The first two parameters are then incremented, the procedure repeated and a best fit is eventually found once the parameter space has been exhausted.) This introduces the possibility of the B-S integral being sensitive to the values of the independent variables and relatively insensitive to the dependent variable. If this happens, and unless the independent variables are set 'spot on' to their correct values, an unphysically large or small value for the dependent variable may be needed to satisfy the B-S condition. We test for this by performing the following calculations:

1. Set two of the parameters according to the best-fit values of previous BMP work e.g. for ^{230}U we use: $G_>$=24, V=162.3MeV, R=7.602fm, a=0.40fm.
2. Vary the third parameter through a range near its best-fit value.
3. Calculate and plot the deviations of the B-S integral and $T_{½}$ relative to their best-fit values.

The Pt, Po and U isotopic families were all used to get a wide range of nuclei above, below and crossing the N=126 closure and ensure we were not just seeing 'local' behaviour in the calculations. The behaviour was very similar for all nuclei considered. Figure 4.3 of the respective tests on ^{230}U is typical. Table VII shows the approximate change in the B-S integral and the value of $\log(T_{1/2}^{cal})$ when a change of 5% is made in one parameter.

From Table VII, the B-S integral is very sensitive to R and V_0 but not to the diffuseness *a*. Thus if *a* is the dependent variable and either R or V_0 is perturbed slightly, the diffuseness has to be changed by such a degree to ensure the Bohr-Sommerfeld condition is still met, that it takes on physically unreasonable values. Unless the values of V_0 and R are spot on for every nucleus in the sample, the insensitivity of the B-S integral to the diffuseness requires unrealistic values of *a*. Using

(a)

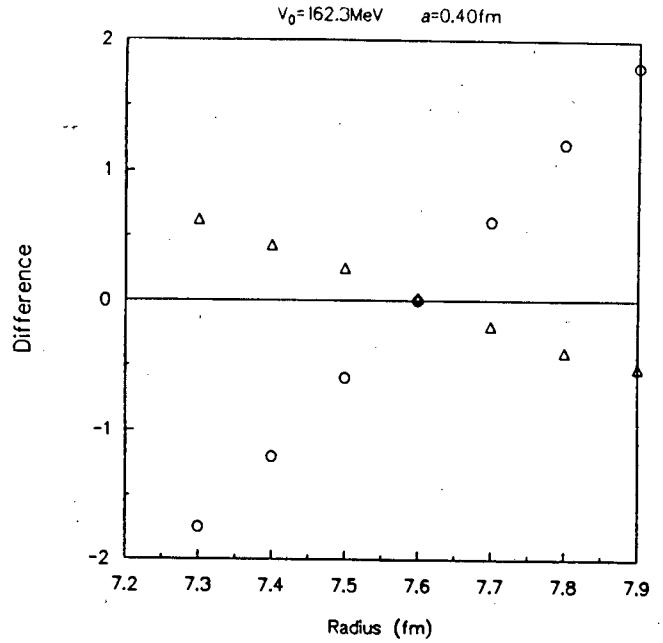

(b)

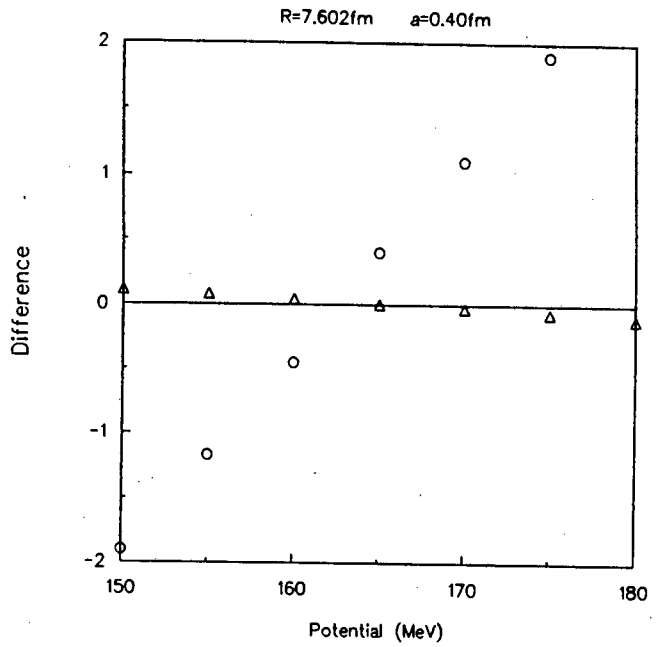

Key: △ - $log(T_{1/2}^{cal})$
○ - *B-S integral*

(c)

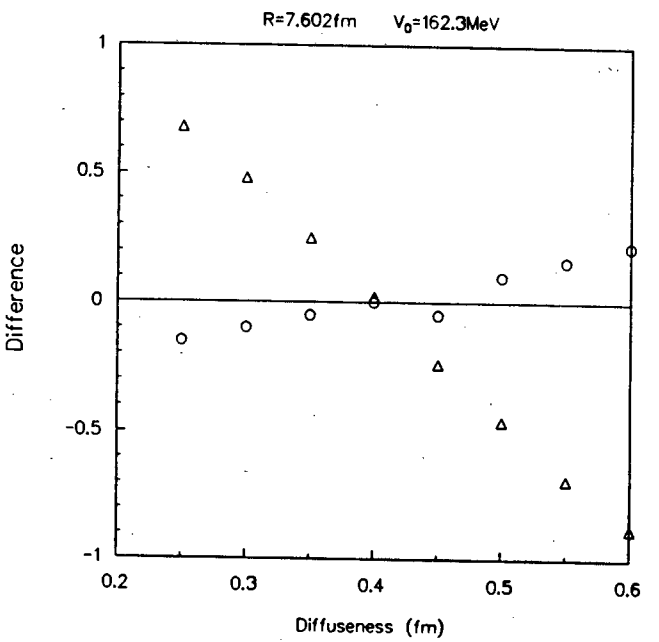

Figure 4.3 - *The effect of perturbing one parameter on the Bohr-Sommerfeld integral and the* $log(T_{1/2}^{cal})$ *of* ^{230}U. *(Parameters used, are best fit parameters of BMP8:* $G_{>}=24$; $V_0=162.3MeV$; $R=7.602fm$; $a=0.40fm$) *(a) Perturbing radius.*
(b) Perturbing potential depth.
(c) Perturbing diffuseness.

Table VII - *The effect of making a 5% perturbation in one parameter on the Bohr-Sommerfeld integral and the log($T^{cal}_{1/2}$) of ^{230}U. (Best fit parameters used, are those of BMP8: G>=24; V_0=162.3MeV; R=7.602fm; a=0.40fm)*

Parameter perturbed		Change in B-S integral	Change in log($T_{½}$)
Radius	(R)	2.20	0.80
Potential	(V_0)	1.40	0.08
Diffuseness	(a)	0.10	0.08

our sample set of nuclei it was impossible to find a set of V_0 and R parameters that ensured all the diffusenesses fell into our physical window of 0.20-1.0fm. Searching on diffuseness is thus unstable and is no longer pursued.

4.3.2 Sensitivity to data set

In the course of analysis, we have plotted graphs of the form "log($T^{cal}_{1/2}/T^{exp}_{1/2}$) vs N" to see the goodness of fit for individual nuclei. Even using best-fit parameters, these plots invariably show ^{166}W to be very poorly predicted (see Figure 4.4). In fact it typically contributes 20% of the value of S (when S~5.0). To see the effect of excluding this point, we reran several fits without it. Although the values of S were all significantly reduced, the position of the minima was unchanged. With this indication that the whole procedure is fairly stable to small changes in input nuclei, we retain ^{166}W for future calculations.

An even more vigorous test of the sensitivity to the data set has been made in which the data set was reduced by almost a third using the data set of Buck *et al.* in BMP8 and repeating the radius fits of Buck *et al.* The values of S obtained with the reduced data set are significantly lower than those obtained with our data set (~1.0 as opposed to ~5.0). This is due largely to the poorer (but still very good) fits obtained for the lighter nuclei (BMP8 includes no nuclei with Z<76, whilst we have 25 such nuclei). Nevertheless the best-fit parameters hardly altered: the potential depths differ by <5MeV, and the value of $G_>$ required for an optimal fit is decreased by 2 using our data set.

It is interesting at this point to consider the contribution to S that the scatter in P values is expected to make. In BMP8 it was shown that the variation in P from nucleus to nucleus is surprisingly small. They estimated the scatter in P from the scatter of individual points about

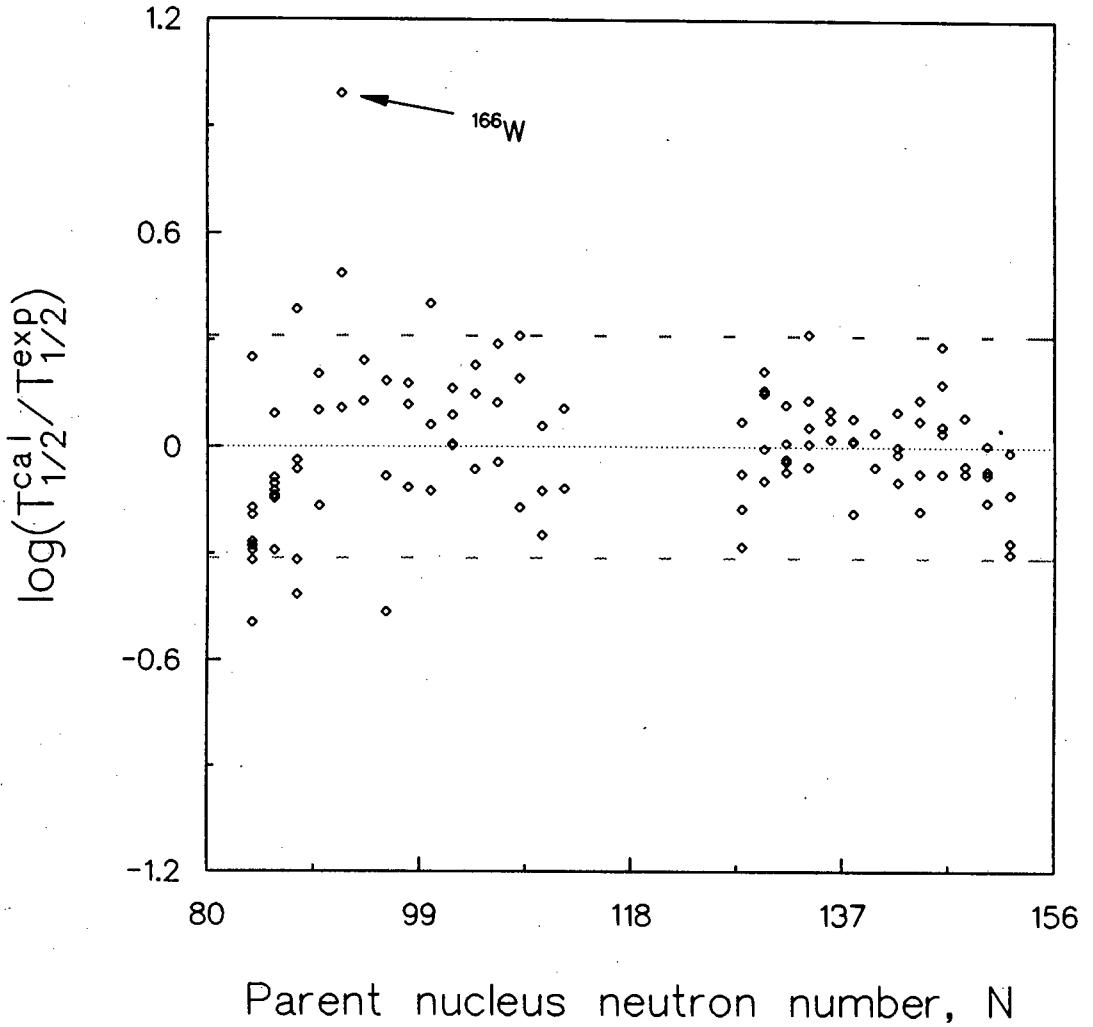

Figure 4.4 - *Plot of* $\log(T^{cal}_{1/2}/T^{exp}_{1/2})$ *using the parameters:* $P=1.0$; $V_0=137MeV$; $a=0.35fm$; $G_<=18$; $G_>=20$. *Factor of two deviations between theory and experiment are indicated by broken lines. The large error in* ^{166}W *in general makes the largest contribution to S.*

Geiger-Nuttall lines statistically fitted to the decay data for each series of isotopes. This resulted in an average scatter of $|\Delta(\log T_{1/2})| \sim 0.2$, and hence to their estimate of a scatter in P of about 50%. Clearly, even if experimental half lives and all other aspects of the theory were exact, S would still have a non-zero value due to a variation in P. In this case, where the contributions to S are purely from a scatter in P, S reduces to

$$S = \sum_i \left[\log(P_i) - \log(\bar{P})\right]^2 = \sum_i \left[\log\left(\frac{P_i}{\bar{P}}\right)\right]^2 \qquad (4.10)$$

where $\bar{P}$ is the constant value of P assumed for all nuclei, and P_i is the preformation factor for the i'th nucleus. In 4.4 it will be seen that S~4.6 for the optimized fits for the 110 nuclei included in our study. This leads to an average scatter

$$\left|\log\left(\frac{P_i}{\bar{P}}\right)\right|_{av} = \sqrt{\frac{4.6}{110}} \sim 0.2 \qquad (4.11)$$

This corroborates well with the findings of Buck *et al.* in BMP8. Further, though not noted in BMP8, the fits themselves can be used to give an absolute upper limit to the scatter in P for the nuclei included in the fit. For our fits a scatter of ~50% is found, emphasising the remarkable consistency of P from nucleus to nucleus.

4.4 BEST FITTING APPROACH (EXCLUDING TRANSITIONAL NUCLEI)

Having shown that both radius and potential fits to the B-S condition are feasible we explore parameter space and answer some of the other questions/objections to earlier choices of G and fitting method. Both the radius and potential fitting methods will be used to examine a variety of G values and different values of ΔG at shell closure; the data set is the one described in 4.2.3. The value of $G_<$ ranges from 14 to 24 and ΔG is either 2 or 4.

The results of both radius and potential fits, with $\Delta G=2$ and $\Delta G=4$ are presented in Table VIII-Table XI. So as not to lose our perspective through a detailed analysis of the exact behaviour of the fits and values of the various parameters in the different tables we briefly summarise the results. In all cases our conclusions are based on fits obtained with parameters in the physical window described in 4.2.2. At times better fits may be obtained with parameter sets outside of our

Table VIII - *Radius fits with $\Delta G=2$ (transitional nuclei excluded). The tabulated quantities are the optimum values of S (quality of fit) as a function of the diffuseness and the global quantum number, G. The subscripted quantity is the potential depth (in MeV) at which the best fit occurs. The shaded regions mark absolute best fits within a family of G values and the dotted line demarcates those values of G and a which require potential depths, V_0, outside the parameter range we consider physically acceptable.*

Diffuseness (fm)	Values of $G_<$ and $G_>$					
	14-16	**16-18**	**18-20**	**20-22**	**22-24**	**24-26**
0.20	9.94_{93}	6.19_{109}	4.71_{127}	4.71_{147}	5.63_{169}	7.13_{193}
0.25	9.25_{95}	5.89_{111}	4.61_{130}	4.84_{151}	5.95_{174}	7.57_{199}
0.30	8.59_{97}	5.51_{114}	4.62_{133}	5.00_{155}	6.29_{179}	8.06_{205}
0.35	8.03_{99}	5.24_{117}	4.57_{137}	5.24_{159}	6.67_{184}	8.60_{211}
0.40	7.47_{102}	5.01_{120}	4.63_{141}	5.49_{164}	7.12_{190}	9.20_{218}
0.45	6.92_{104}	4.86_{123}	4.73_{145}	5.82_{169}	7.63_{196}	9.88_{226}
0.50	6.41_{107}	4.72_{127}	4.89_{149}	6.24_{174}	8.23_{203}	10.6_{234}
0.55	5.99_{110}	4.70_{131}	5.11_{154}	6.68_{180}	8.87_{210}	11.4_{227}
0.60	5.61_{113}	4.68_{134}	5.39_{159}	7.21_{187}	9.62_{218}	12.3_{252}
0.65	5.32_{116}	4.72_{139}	5.77_{164}	7.81_{193}	10.4_{0226}	13.3_{262}
0.70	5.07_{120}	4.84_{143}	6.19_{170}	8.49_{201}	11.3_{235}	14.3_{274}
0.75	4.94_{124}	5.04_{148}	6.73_{176}	9.26_{209}	12.3_{245}	15.5_{286}
0.80	4.82_{128}	5.36_{154}	7.31_{182}	10.1_{217}	13.3_{256}	16.7_{300}
0.85	4.78_{132}	5.70_{159}	7.97_{191}	11.5_{224}	14.4_{268}	18.3_{311}
0.90	4.87_{137}	6.16_{166}	8.71_{199}	12.0_{237}	15.6_{281}	19.33_{331}
0.95	5.01_{142}	6.66_{172}	9.53_{208}	13.1_{248}	16.8_{296}	20.8_{350}
1.00	5.27_{147}	7.26_{180}	10.7_{216}	14.1_{261}	18.2_{312}	22.2_{370}

Table IX - *Radius fits with $\Delta G=4$ (transitional nuclei excluded). The tabulated quantities are the optimum values of S (quality of fit) as a function of the diffuseness and the global quantum number, G. The subscripted quantity is the potential depth (in MeV) at which the best fit occurs. The shaded regions mark absolute best fits within a family of G values and the dotted line demarcates those values of G and a which require potential depths, V_0, outside the parameter range we consider physically acceptable.*

Diffuseness (fm)	Values of $G_<$ and $G_>$					
	14-18	**16-20**	**18-22**	**20-24**	**22-26**	**24-28**
0.20	70.3_{101}	50.6_{118}	36.3_{137}	26.1_{158}	18.7_{182}	13.6_{207}
0.25	67.6_{103}	48.3_{121}	34.4_{141}	24.6_{163}	17.6_{187}	12.8_{213}
0.30	64.6_{106}	46.0_{124}	32.6_{145}	23.2_{167}	16.5_{193}	12.0_{220}
0.35	61.9_{109}	43.8_{127}	30.8_{149}	21.7_{172}	15.5_{198}	11.3_{227}
0.40	59.0_{111}	41.4_{131}	29.0_{153}	20.3_{178}	14.4_{205}	10.6_{235}
0.45	56.1_{114}	39.1_{135}	27.2_{158}	19.0_{183}	13.5_{217}	9.93_{243}
0.50	53.3_{117}	36.9_{139}	25.4_{163}	17.7_{189}	12.5_{219}	9.33_{252}
0.55	50.4_{121}	34.6_{143}	23.7_{168}	16.4_{196}	11.7_{227}	8.81_{262}
0.60	47.5_{124}	32.4_{147}	22.0_{174}	15.2_{203}	10.9_{236}	8.35_{271}
0.65	44.7_{128}	30.2_{152}	20.4_{180}	14.0_{211}	10.1_{245}	7.99_{284}
0.70	41.0_{132}	28.1_{158}	18.9_{186}	13.0_{219}	9.51_{256}	7.72_{296}
0.75	39.2_{137}	26.0_{163}	17.4_{194}	12.0_{228}	8.97_{267}	7.57_{310}
0.80	36.6_{141}	24.1_{169}	16.1_{202}	11.2_{238}	8.57_{279}	7.52_{326}
0.85	34.1_{147}	22.3_{176}	14.8_{210}	10.5_{249}	8.26_{293}	7.60_{342}
0.90	31.7_{152}	20.6_{183}	13.7_{219}	9.86_{261}	8.10_{308}	7.79_{361}
0.95	29.4_{158}	19.0_{191}	12.8_{230}	9.40_{274}	8.06_{325}	8.10_{382}
1.00	27.4_{164}	17.6_{200}	11.0_{241}	9.07_{288}	8.13_{343}	8.52_{405}

Table X - *Potential fits with $\Delta G=2$ (transitional nuclei excluded). The tabulated quantities are the optimum values of S (quality of fit) as a function of the radius and the global quantum number, G (the radius of each nucleus is given by $R=r_0A^{1/3}$). The subscripted quantity is the diffuseness at which the best fit occurs. The shaded regions mark absolute best fits within a family of G values.*

Radius (r_0) (fm)	Values of $G_<$ and $G_>$					
	14-16	**16-18**	**18-20**	**20-22**	**22-24**	**24-26**
1.15	$6.02_{0.71}$	$6.28_{0.65}$	$6.50_{0.60}$	$6.68_{0.56}$	$6.87_{0.52}$	$6.99_{0.49}$
1.16	$5.90_{0.69}$	$6.15_{0.63}$	$6.35_{0.58}$	$6.53_{0.54}$	$6.72_{0.50}$	$6.85_{0.48}$
1.17	$5.84_{0.67}$	$6.05_{0.61}$	$6.23_{0.56}$	$6.39_{0.52}$	$6.58_{0.48}$	$6.67_{0.46}$
1.18	$5.72_{0.64}$	$5.96_{0.58}$	$6.13_{0.54}$	$6.28_{0.50}$	$6.45_{0.47}$	$6.52_{0.44}$
1.19	$5.66_{0.62}$	$5.85_{0.56}$	$6.06_{0.52}$	$6.18_{0.48}$	$6.34_{0.45}$	$6.39_{0.42}$
1.20	$5.62_{0.59}$	$5.79_{0.54}$	$5.96_{0.49}$	$6.11_{0.46}$	$6.25_{0.43}$	$6.29_{0.40}$
1.21	$5.57_{0.57}$	$5.78_{0.51}$	$5.89_{0.47}$	$6.06_{0.43}$	$6.17_{0.40}$	$6.21_{0.38}$
1.22	$5.58_{0.54}$	$5.71_{0.49}$	$5.85_{0.45}$	$5.99_{0.41}$	$6.10_{0.38}$	$6.15_{0.36}$
1.23	$5.56_{0.52}$	$5.71_{0.47}$	$5.86_{0.43}$	$5.94_{0.39}$	$6.05_{0.36}$	$6.10_{0.34}$
1.24	$5.59_{0.49}$	$5.72_{0.44}$	$5.83_{0.40}$	$5.92_{0.37}$	$6.01_{0.34}$	$6.08_{0.32}$
1.25	$5.63_{0.47}$	$5.73_{0.42}$	$5.83_{0.39}$	$5.94_{0.35}$	$6.00_{0.32}$	$6.08_{0.32}$
1.26	$5.67_{0.44}$	$5.78_{0.39}$	$5.89_{0.36}$	$5.99_{0.32}$	$6.02_{0.30}$	$6.09_{0.28}$
1.27	$5.75_{0.41}$	$5.83_{0.37}$	$5.91_{0.33}$	$5.99_{0.30}$	$6.07_{0.28}$	$6.13_{0.26}$
1.28	$5.85_{0.39}$	$5.91_{0.34}$	$5.99_{0.31}$	$6.05_{0.28}$	$6.15_{0.26}$	$6.20_{0.24}$
1.29	$5.93_{0.36}$	$6.02_{0.32}$	$6.07_{0.28}$	$6.15_{0.26}$	$6.20_{0.23}$	$6.27_{0.21}$
1.30	$6.05_{0.33}$	$6.10_{0.29}$	$6.17_{0.26}$	$6.22_{0.23}$	$6.26_{0.21}$	$6.32_{0.19}$

Table XI - *Potential fits with $\Delta G=4$ (transitional nuclei excluded). The tabulated quantities are the optimum values of S (quality of fit) as a function of the radius and the global quantum number, G.(the radius of each nucleus is given by $R=r_0A^{1/3}$). The subscripted quantity is the diffuseness at which the best fit occurs. The shaded regions mark absolute best fits within a family of G values.*

Radius (r_0) (fm)	Values of $G_<$ and $G_>$					
	14-18	**16-20**	**18-22**	**20-24**	**22-26**	**24-28**
1.08	$5.07_{0.83}$	$5.14_{0.77}$	$5.36_{0.72}$	$5.62_{0.67}$	$5.91_{0.64}$	$6.20_{0.60}$
1.09	$5.04_{0.81}$	$5.09_{0.75}$	$5.28_{0.70}$	$5.57_{0.66}$	$5.76_{0.62}$	$6.03_{0.59}$
1.10	$5.03_{0.79}$	$5.05_{0.73}$	$5.21_{0.68}$	$5.45_{0.64}$	$5.67_{0.60}$	$5.90_{0.57}$
1.11	$5.03_{0.77}$	$5.02_{0.71}$	$5.16_{0.66}$	$5.36_{0.62}$	$5.61_{0.58}$	$5.82_{0.55}$
1.12	$5.05_{0.75}$	$5.00_{0.69}$	$5.12_{0.64}$	$5.31_{0.60}$	$5.57_{0.56}$	$5.79_{0.54}$
1.13	$5.06_{0.72}$	$5.00_{0.67}$	$5.10_{0.62}$	$5.26_{0.58}$	$5.48_{0.55}$	$5.66_{0.52}$
1.14	$5.06_{0.70}$	$5.02_{0.65}$	$5.08_{0.60}$	$5.23_{0.56}$	$5.41_{0.53}$	$5.58_{0.50}$
1.15	$5.07_{0.68}$	$5.05_{0.63}$	$5.08_{0.58}$	$5.22_{0.54}$	$5.37_{0.51}$	$5.53_{0.48}$
1.16	$5.11_{0.66}$	$5.07_{0.60}$	$5.09_{0.56}$	$5.21_{0.52}$	$5.35_{0.49}$	$5.52_{0.46}$
1.17	$5.19_{0.62}$	$5.08_{0.58}$	$5.11_{0.54}$	$5.21_{0.50}$	$5.34_{0.47}$	$5.52_{0.44}$
1.18	$5.23_{0.61}$	$5.11_{0.56}$	$5.14_{0.52}$	$5.23_{0.48}$	$5.34_{0.45}$	$5.51_{0.43}$
1.19	$5.28_{0.59}$	$5.16_{0.54}$	$5.20_{0.50}$	$5.25_{0.46}$	$5.36_{0.43}$	$5.49_{0.41}$
1.20	$5.38_{0.57}$	$5.25_{0.52}$	$5.27_{0.47}$	$5.28_{0.44}$	$5.38_{0.41}$	$5.49_{0.39}$
1.21	$5.44_{0.54}$	$5.31_{0.49}$	$5.30_{0.45}$	$5.33_{0.42}$	$5.42_{0.39}$	$5.51_{0.37}$
1.22	$5.53_{0.52}$	$5.38_{0.47}$	$5.36_{0.43}$	$5.39_{0.40}$	$5.47_{0.37}$	$5.54_{0.36}$
1.23	$5.63_{0.49}$	$5.49_{0.45}$	$5.44_{0.41}$	$5.48_{0.38}$	$5.52_{0.35}$	$5.59_{0.33}$

Table XII - *Minimum value of S obtained from each fit*

Fitting method	ΔG=2	ΔG=4
Potential fit	5.6	5.0
Radius fit	4.6	≥10

window, but this is of no use to our study. If anything, such results indicate that the approach used is unsuitable.

The results of Table VIII seem to suggest a lower value of G than that of BMP8 ($G_<\sim 18$ as opposed to $G_<\sim 22$). We checked the accuracy of our calculations by repeating the calculations of BMP8 with their data set. Their results were reproduced exactly, thus the difference in the results must be due to the altered data set.

In Table XII we summarise the results of Table VIII-Table XI by listing the minimum value of S obtained for each fitting method. The most striking feature is the very poor fit obtained when fitting the radii with ΔG=4. This approach is definitely ruled out.

The potential fit with ΔG=2 is also not very attractive. If we recall that ^{166}W contributes about 20% of the value of S, to exclude it would lower all the values of S in Table XII by about 1.0. In that case, a potential fit with ΔG=2 has an S of 4.6 as opposed to 3.6 for a radius fit with ΔG=2. Furthermore, we can expect some contribution from the scatter in P. Though difficult to quantify, a contribution of ~4 is to be expected from the estimates of Buck *et al.* (see 4.3.2). If we take this into account, the difference in the two values of S becomes much more significant and points definitely towards a radius fit with ΔG=2 rather than the potential fit with ΔG=2. This conclusion will be reinforced when we include the 'transitional' nuclei.

The potential fit with ΔG=4 cannot immediately be so discarded. Firstly, the value of S (=5.0) is not considerably greater than the 4.6 of the radius fitting approach even after taking into account the effect of ^{166}W and the scatter in P. Secondly, it has the attractive feature of being the only approach which has a definite absolute minimum in S which occurs within the physical window.

In conclusion we are faced with two alternatives: the radius fitting approach with ΔG=2; or the potential fitting approach with ΔG=4. The former has the advantage of providing the best fit of all, but the disadvantage that a value of ΔG=4 is preferable in the framework of the model used. The potential fitting approach does suggest ΔG=4 but does not give quite as good fits. To

discriminate further between the two approaches we have next investigate which one describes the 'transitional' nuclei better.

4.5 BEST FITTING APPROACH (INCLUDING TRANSITIONAL NUCLEI)

By excluding the transitional nuclei we have considered only those nuclei for which the neutron and proton shells are either both closed, or both open. The analysis as to whether there should be a change in ΔG of 2 or 4 between these two groups, has been inconclusive. We hope to resolve the difficulty here by including the transitional nuclei. The transitional nuclei are nuclei for which just one shell, the proton shell (Z=82), has closed. If the picture that says $\Delta G=4$ between the 'both shells open' and 'both shells closed' groups is correct, there should be a change of $\Delta G=2$ in going from the 'both shells open' group to the 'one shell open, one shell closed' group (unless the proton closure is weak until it occurs in conjunction with the neutron closure). In this section we repeat the potential and radius fits of 4.4, but with a new data set which includes the transitional nuclei. There are three possible assignments of global quantum number that we consider:

	Both open	Transi-tional	Both closed	Comment
1	$G_<$	$G_<$	$G_<+2$	We assume the proton closure is not felt and that $\Delta G=2$.
2	$G_<$	$G_<+2$	$G_<+4$	Both proton and neutron closures are felt independently.
3	$G_<$	$G_<$	$G_<+4$	The proton closure is very weak or absent until it occurs in conjunction with the neutron closure, when $\Delta G=4$.

The first and the last options are essentially a repeat of 4.4 but with the transitional nuclei incorporated into the group of nuclei with both shells open. As such, they provide a standard against which to test the hypothesis that both shell closures are felt independently.

The potential fitting and radius fitting results are tabled in Appendix C. Table XIII summarises these tables by listing the minimum values of S obtained by each approach. Again, a

Table XIII - Minimum value of S obtained from each fit (including transitional elements).

Fitting method	ΔG=2 (1)	ΔG=2/4 (2)	ΔG=4 (3)
Potential fit	9.6	10.4	7.0
Radius fit	6.8	≥15	≥20

radius fit with any assignment of G other than ΔG=2 is unacceptable.

The potential fits show a clear preference for ΔG=4 to ΔG=2 but when we assign a transitional G to the transitional nuclei, the fits are severely worsened. A possibility is that the value of the preformation factor varies markedly in the transitional region and, in particular, that a decrease of P in this region then masks an increase in G. Such an effect has already been tentatively proposed by Buck *et al.* in BMP8 to explain the number of transitional nuclei for which calculated half-lives are overestimates (see Figure 3.4). Such a structure effect is, however, beyond the scope of our potential model.

Within the model, we are forced to accept that the effects of the proton closure appear secondary to those of the neutron closure. Either they are largely absent (as in the ΔG=2 radius fits) or their effects are only felt in conjunction with the neutron shell closure (as in the ΔG=4 potential fits). We are therefore left with no strong preference for either type of fit. Because of the greater proven range of validity of the radius fits (in particular in the vicinity of the N=82 shell closure[38]) we concentrate on the radius fits in the following sections. However, it should be stressed that there are some positive aspects associated with our new potential fits with ΔG=4:

1. Both the radius fits of BMP8 and the present potential fits result in an absolute minimum at $G_{>}$~20. This value of $G_{>}$ is consistent with an equal role of neutron and proton shell closures, and ΔG=4 is indicated.

2. As noted in BMP4-6, the radius fits require a discontinuous jump in the radius of about 0.4fm at the neutron shell closure. The density overlap technique for determining the alpha-core potential (see 2.2.2) would then require a corresponding discontinuous jump in the nuclear density distribution of the core. The analogous discontinuity in the potential depth

required by the potential fits would be less controversially catered for by a corresponding change in the strength of the effective interaction.

It is thus interesting to see that our study shows an equally good fit using the $\Delta G=4$ potential fit and the $\Delta G=2$ radius fit.

4.6 CHANGING THE PREFORMATION FACTOR P

In BMP8 it was claimed that the results were independent of the value of P assumed, provided that it was greater than about 10^{-4}. To test this claim we have repeated the radius fitting calculations (with $\Delta G = 2$) for values of P ranging from 10^{-1} to 10^{-4}. The results are tabled in Appendix D.

We did repeat these calculations using potential fits ($\Delta G=4$) for a few different values of P but found their behaviour relative to the radius fits was identical to that already discussed in 4.4 and 4.5. In other words, there was not a point at which the potential fits became superior to the radius fits and our conclusions from 4.4 and 4.5 (that a radius fit with $\Delta G=2$ is the best approach) still hold. We thus include only the results of our study with radius fits.

A number of observations can be made on study of the tables in Appendix D:

1. The potential depth at which the minima in S occur changes from ~140 MeV when P=1.0 to ~200 MeV when $P=10^{-4}$.

2. The global quantum number at which the minima in S occur, increases rapidly from G~18 for P=1 to G~30 for $P=10^{-4}$. Such large values for G are not acceptable and P must thus definitely be greater than 10^{-4}; 10^{-3} seems to be the lower limit. Values of P between 0.1 and 0.01 suggest G~22, the value predicted by the extreme cluster model with harmonic oscillator orbitals. This may be weak evidence for P falling in this range.

3. In Table XIV we list the lowest values of S for each different value of P. Once more these results indicate a value of P in the range 0.1 to 0.01, with values as high as P=1 or as low as $P=10^{-3}$ not ruled out.

From these observations we see that although the dependence on the value of P used is weak, there

Table XIV - *Minimum value of S obtained with different values of P (by radius fits with ΔG=2).*

Preformation factor used	Minimum value of S
1.0	4.57
0.1	4.46
0.01	4.39
0.001	4.54
0.0001	5.00

is a slight change in the quality of the fit suggesting P lies in the range 0.001 to 1.0.

4.7 CONCLUSION

By including the transitional nuclei we have tested the hypothesis that two shell closures are felt (and hence ΔG=2/4). The results showed that unless we want to complicate matters by introducing some kind of behaviour where the proton closure is only felt in conjunction with the neutron closure or the preformation factor is significantly reduced for the transitional nuclei, we have to assume that the proton closure is not felt. This requires ΔG=2; and hence that fitting the radii according to the B-S condition would appear to be the more appropriate technique particularly given its proven reliability in the vicinity of the N=82 shell closure[38]. We thus accept that radius fits with ΔG=2 are required and all further work is based on this conclusion. This notwithstanding, we note that the ΔG=4 potential fits remained competitive on the inclusion of the transitional nuclei, and that the complications alluded to above will need to be addressed.

Until now all studies of the BMP model have minimised the number of free variables by fixing P=1.0 for all nuclei. The degree of success obtained has vindicated this rather extreme assumption and furthermore provided evidence that the variation in P from nucleus to nucleus is surprisingly small. It also suggests that the real value of P may not be significantly smaller. This cannot be concluded however without examining the dependence of the fits and the fitted parameters to varying values of P.

We have performed such a study by repeating the radius fits (ΔG=2) with values of P=0.1,

0.01, 0.001 and 0.0001. A weak relationship between the quality of the fit and the value of P was found and values of P in the range 0.001 to 1.0 give the best fits for the parameter space investigated. These results are important in lending experimental support to the theoretical results of Table VI which suggests preformation factors of this order.

We stress again that 'experimental' spectroscopic factors are not generally as 'experimental' as their proponents claim. The experimental spectroscopic factor S_{exp} defined in **(3.12)** is the ratio of the experimental decay rate λ to λ_G, where λ_G is calculated by the substitution of some potential form into **(1.3)**. These calculations have generally been restricted to a small selection of nuclei, with somewhat arbitrary choices of potential. This work, on the other hand, relies on a fit to a large body of experimental decay data to determine the best-fit potential parameters within a consistent model. Our conclusions about acceptable values of S_{exp} are thus less arbitrary.

5. INTRODUCTION AND MOTIVATION FOR (ELASTIC) SCATTERING

The BMP model of alpha decay predicts the half lives of all alpha decays to a very high degree of accuracy considering they range over 30 orders of magnitude. Even when applied to 'exotic' decays by a simple 'extrapolation' of the cluster concept, the theory holds up well[39,40,41]. Is this success purely fortuitous? - or is there something in the model which is a necessary component of any description of alpha-decay?

One way of finding out is to see whether the model stands up to other tests. The more properties of the nucleus that one particular model can describe, without requiring changes or additions, the more likely it is that the model is a good description of the true nature of the nucleus.

Scattering experiments in which one 'bounces' objects off a nucleus and examines the pattern in which they are deflected, are another good probe into the structure of the nucleus. It is to them that we next look and ask: Does the proposed cosh potential reproduce low-energy scattering of alpha-particles off heavy nuclei and if so, can we tell anything about the preformation factor of alpha particles from these experiments ?

For heavy nuclei the cosh potential is very similar to a Woods-Saxon potential (see Figure 5.1) - thus with the cosh potential, we expect fits to the scattering data as good as any previous optical model work. A far greater achievement would be to find a set of best fit parameters of the decay calculations in agreement with those of the scattering calculations. It is to this end that the following section is directed. The matter is not a trivial one: the optimum fit parameters for each of the two types of calculation may not agree, but a single set of parameters may give a fit to both the decay and scattering data to an acceptable level of accuracy; ambiguities in parameter searches are rife; and with the inclusion of an imaginary potential in the optical potential, care has to be taken not to be swamped with free variables.

5.1 THEORY OF ELASTIC SCATTERING AND INTERPRETATION

Nuclear scattering processes are fundamental in the study of nuclear structure. These scattering processes come in a variety of forms, depending on the energies involved and whether nucleons or groups of nucleons are used as incident particles.

At low energies (~10 MeV) the incident particle is likely to be elastically scattered without

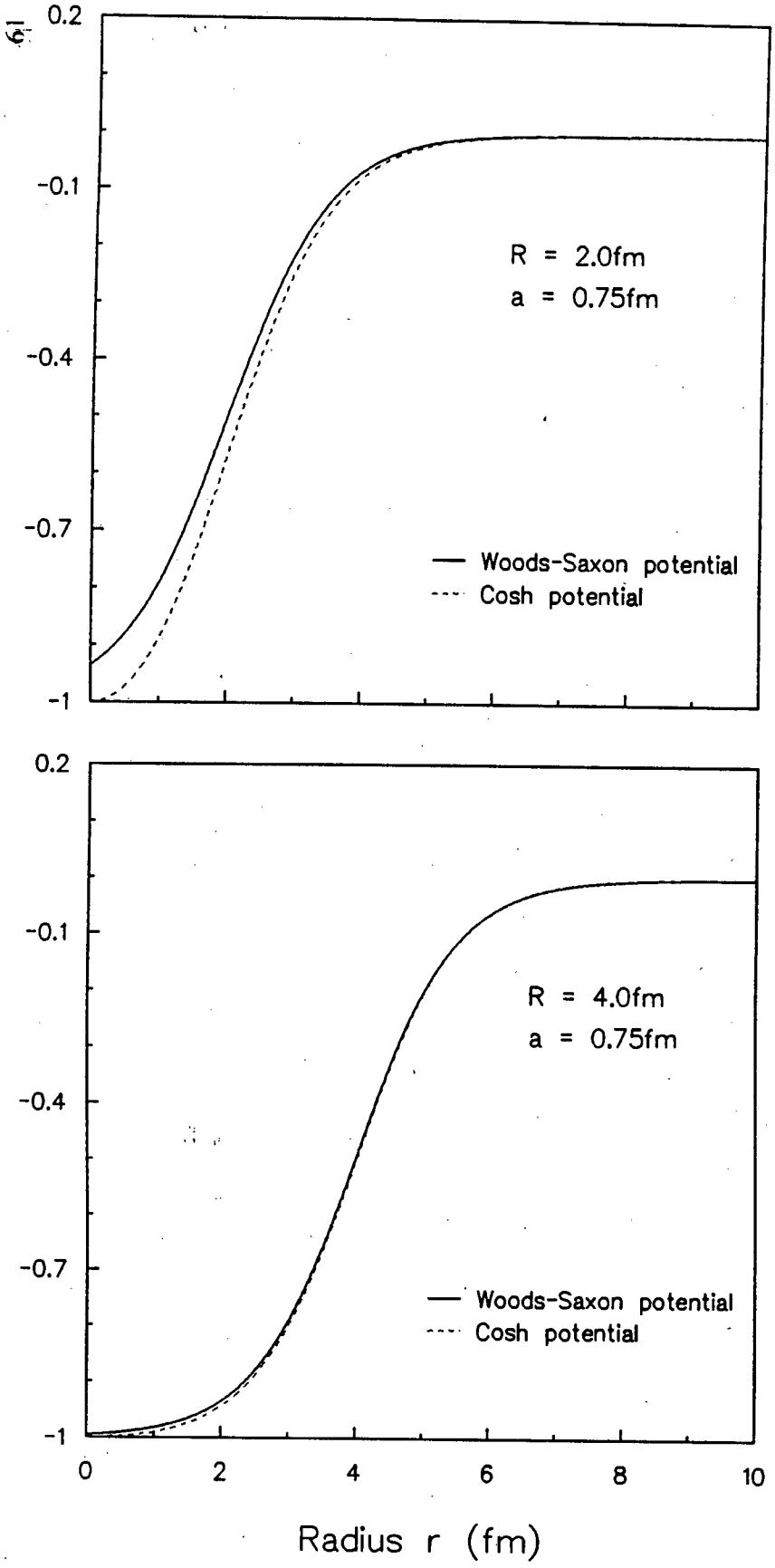

Figure 5.1 - *Comparing the Woods-Saxon and 'cosh' potentials for light and heavy nuclei. For heavy nuclei (large radius, R) the 'cosh' potential essentially degenerates to the Woods-Saxon. Both plots use a diffuseness of a=0.75fm. (a) R=2.0fm. (b) R=4.0fm.*

appreciable loss of energy, or absorbed to form a compound nucleus. As the energy rises it can gain nucleons by a pickup reaction or, if composite, lose them by stripping. Inelastic reactions leave the residual nucleus in an excited state from which nucleons and gamma rays are emitted. At higher energies still, many body channels open up, and hadrons other than protons and neutrons are produced. Elastic scattering is always present though, and invariably forms the strongest exit channel, so that its good description is crucial to the understanding of other reaction channels in DWBA.

We are concerned only with the process of elastic scattering - in other words, where the incident particle loses no energy in the interaction. This is a standard problem dealt with in many references[42,43,44]. To begin with, we restrict our discussion to a spinless, chargeless projectile of mass **a** incident upon a target of mass A_{targ} and charge, Z_{targ}. The wave function Ψ of relative motion for such a projectile obeys the Schrödinger equation:

$$-\left(\frac{\hbar^2}{2\mu}\right)\nabla^2\Psi = (E-V)\Psi \ , \qquad (5.1)$$

where V is an optical potential whose form is discussed later. E is the energy in the centre of mass system and μ the reduced mass

$$\mu = \frac{a A_{targ}}{a + A_{targ}} \quad ; \quad E = E_{cm} = E_{lab}\left(\frac{A_{targ}}{a+A_{targ}}\right) . \qquad (5.2)$$

In order to solve the Schrödinger equation we expand Ψ as a product of radial and angular parts:

$$\Psi = \sum_L \frac{u_L(r)}{r} P_L(\cos\theta), \qquad (5.3)$$

where L=0,1,2,... is the orbital angular momentum quantum number and $P_L(\cos\theta)$ is a Legendre Polynomial. After manipulation, the radial wave equation becomes

$$\left[\frac{d^2}{dr^2} + k^2\left(1-\frac{V}{E}\right) - \frac{L(L+1)}{r^2}\right]u_L = 0 \ , \qquad (5.4)$$

where

$$k = \left(\frac{2\mu E}{\hbar^2}\right)^{1/2} . \qquad (5.5)$$

From the known behaviour of u_L at r=0, **(5.4)** can be numerically integrated into the asymptotic region, where it is matched to its known behaviour. The solutions of the Schrödinger equation in the asymptotic region are required to represent an incident plane wave and a scattered spherical wave

$$\Psi \sim e^{ikz} + \frac{e^{ikr}}{r} f(\theta) \,. \tag{5.6}$$

$f(\theta)$ is the interesting quantity describing the scattering pattern. In particular, the differential scattering cross section is given by

$$\frac{d\sigma}{d\Omega} = |f(\theta)|^2 \,. \tag{5.7}$$

At large distances, the nuclear field falls off more rapidly than r^{-1} and so it may be neglected beyond a certain cut-off radius R_{co}. This is not true for the Coulomb potential which we consider later.

In the limit $r \to \infty$, **(5.4)** becomes

$$\frac{d^2u_L}{dr^2} + k^2 u_L = 0 \,, \tag{5.8}$$

which admits a general solution, written in L-dependent form

$$u_L \sim A \sin(kr - \tfrac{1}{2}L\pi + \delta_L) \,. \tag{5.9}$$

δ_L is a constant whose value is determined by the matching of internal and external solutions, and the constant term $-\tfrac{1}{2}L\pi$ is quite arbitrary, but is introduced so that $\delta_L \to 0$ as $V(r) \to 0$ for all L.

In terms of the phase shifts δ_L, the total scattering amplitude is given by

$$f(\theta) = \frac{1}{2ik} \sum_{L=0}^{\infty} (2L+1)(e^{2i\delta_L} - 1) P_L(\cos\theta) \,. \tag{5.10}$$

All the physical information is therefore carried by the δ_L from the potential to the cross-section.

Hodgson[42] illustrates this nicely when considering the radial wave function $u_0(r)$.

"In the absence of a scattering potential V(r), $\delta_l \to 0$ and the wave function is sinusoidal. If the attractive potential V(r) is now switched on, the wave function is pulled in so that it has the required shorter wavelength (corresponding to higher energy) in the region of the potential. Beyond the potential V(r) the new wave function has the same sinusoidal form as has the wave function corresponding to V(r)=0, but it is shifted in phase by an amount δ_0. Similar considerations apply to the other partial waves, and since the observed scattering is determined only by the asymptotic forms of the wave functions it becomes clear how the phase shifts δ_l carry all the physical information from the potential V(r) to the observed scattering."

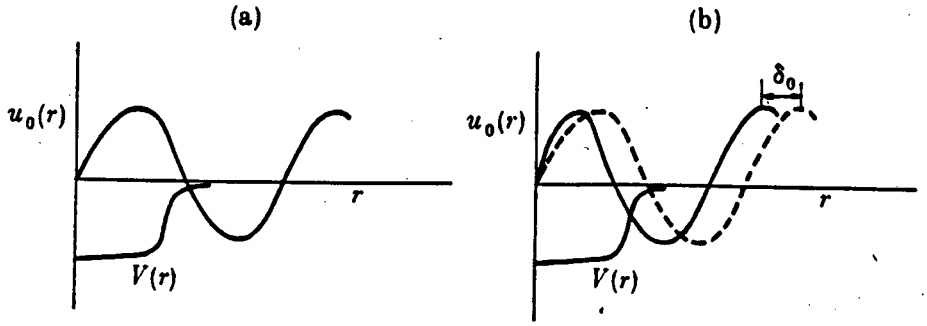

Figure 5.2 - *The scattering wave functions (a) before and (b) after switching on the potential V(r).*

If we propose a potential U that is truly a good approximation to the effective potential V, the model wave functions are good approximations to the elastic component of the exact wave function. However the only way of determining the success of a model potential is through its reproduction of the observed scattering cross-section. That is, it reproduces the asymptotic behaviour of the true wave function - outside of the region of interaction, $r > R_{co}$. Hence U and V are 'phase-equivalent' in giving the same δ_L. This does not guarantee that the model and true wave functions are equal or even similar for $r < R_{co}$. Indeed as will be seen, there may be ambiguities such that more than one model U will reproduce equally well a given set of data, but be associated with quite different model wave functions.

Until now we have been considering the case of neutral particles, ignoring Coulomb effects. To include Coulomb effects does not require a different approach. The wave equation may be solved in the interior region in the same way as before, but the analytical solution in the exterior

region is different because of the long-range nature of the Coulomb field. In the presence of the Coulomb field the scattering amplitude for alpha particles is given[44,45] by

$$f(\theta) = f_C(\theta) + \frac{1}{2ik}\sum_L (2L+1)(S_L-1)e^{2i\sigma_L}P_L(\cos\theta) \ , \qquad (5.11)$$

where the Coulomb scattering amplitude

$$f_C(\theta) = -\frac{\eta}{2k}\,\mathrm{cosec}^2(\frac{\theta}{2})\exp\left\{2i\sigma_0 - i\eta\ln[\sin^2(\frac{\theta}{2})]\right\} \ , \qquad (5.12)$$

and

$$\eta = \frac{2Z_{targ}e^2\mu}{\hbar^2 k} \ . \qquad (5.13)$$

The S_L are related to the phase shifts δ_L by

$$S_L = e^{2i\delta_L} \ . \qquad (5.14)$$

The Coulomb phase shifts σ_L may be defined by the recurrence relation

$$\sigma_{L+1}(\eta) = \sigma_L(\eta) + \tan^{-1}(\frac{\eta}{L+1}) \ , \qquad (5.15)$$

and the lowest phase shift

$$e^{2i\sigma_0} = \frac{\Gamma(1+i\eta)}{\Gamma(1-i\eta)} \ . \qquad (5.16)$$

The reaction cross section is

$$\sigma_R = \frac{\pi}{k^2}\sum_L (2L+1)(1-|S_L|^2) \ . \qquad (5.17)$$

The actual integration of the internal wave function is a standard problem for which there are a number of computer programs available. We have used a general optical model code called 'A-Three' developed at Brookhaven National Laboratory.

We now have the apparatus to take a particular given potential and create a theoretical scattering cross-section. To proceed further it is necessary to find an appropriate form for V(r).

5.2 THE FORM OF THE POTENTIAL

We might immediately suggest using the cosh potential from the decay work but a purely real potential is unable to account for the non-elastic cross sections[46]. This difficulty is overcome by adding to the potential an imaginary part whose form is to be determined. Physically this is equivalent to treating the nucleus as if it were made of a material of complex refractive index, so that it both refracts and absorbs the incident waves. In the same way that the scattering and absorption of light by a murky crystal ball can be described by a complex refractive index, the scattering and absorption of particles by a nucleus can be described by a complex potential. It is for this reason that the model is referred to as an optical model

The optical potential is commonly held to have a form

$$V(r) = V_{re}(r) + iV_{im}(r) + V_{co}(r) + V_{so}(r)\boldsymbol{l}\cdot\boldsymbol{\sigma} \qquad (5.18)$$

where the four parts V_{re}, V_{im}, V_{coul}, and V_{so} are called the real, imaginary, Coulomb, and spin-orbit parts of the potential respectively. The spin-orbital term drops out in our case as alpha particles are spin 0 particles, so we are left with

$$V(r) = V_{re}(r) + iV_{im}(r) + V_{co}(r) \ . \qquad (5.19)$$

5.2.1 Nuclear potential (real and imaginary)

For the real potential we do want to keep the cosh potential. This bears a very strong resemblance to the Woods-Saxon potential which has been the most popular form used (see Figure 5.1)

We have more leeway in choice of the imaginary (absorptive) potential but choose to keep the same form as the real potential (with possibly different parameter values) purely to keep the number of parameters to a minimum. An alternative to this widely used approach is to use a surface absorptive potential, which helps explain the existence of surface collective modes, the possibility of nucleon transfer between ions suffering peripheral collisions and the possibility of breakup of the projectile at the target surface. For such a potential, the derivative Woods-Saxon form

$$U(r) \sim \frac{e^{x_D}}{(e^{x_D}+1)^2} \quad ; \text{ where } \quad x_D = \frac{r-R}{a} \qquad (5.20)$$

is used in conjunction with the usual volume absorption term to give a 'surface-peaked' absorption. These alternate forms are equally acceptable from the point of view of fitting the data and are a form of ambiguity known as form factor ambiguity[47,48]. The ambiguity is generally dealt with in practice by choosing one form and using it consistently.

5.2.2 Coulomb potential

The potential due to the nuclear charge may be derived from the known distribution of charge in the nucleus. Detailed calculations show, however, that the scattering is very insensitive to the fine structure of the nuclear charge distribution[49,50].

In particular it is not necessary to take account of the diffuse edge of the nucleus[50] and it is sufficient for all practical purposes to take the Coulomb potential as that due to a uniformly charged sphere. This is fortunate, allowing us to use the same potential as in the decay work and saves introducing extra variables to parametrise the Coulomb potential. We use the same parametrisation as before:

$$V_C(r) = \begin{cases} \dfrac{Z_1 Z_2 e^2}{r} & \text{for } r \geq R, \\ \dfrac{Z_1 Z_2 e^2}{2R}\left[3 - \left[\dfrac{r}{R}\right]^2\right] & \text{for } r \leq R, \end{cases} \qquad (5.21)$$

where $R=r_c A^{1/3}$ is the Coulomb radius and Z_1 and Z_2 are the charges of the incident particle and target nucleus. We follow McFadden and Satchler[51] in setting $r_c = 1.3$fm.

5.3 ANALYSIS OF SCATTERING DATA

A customary measure of the agreement between the theoretical predictions and the experimental values is the chi-square:

$$\chi^2 = \frac{1}{N}\sum_{i=1}^{N}\left[\frac{\sigma_{th}(\theta_i) - \sigma_{ex}(\theta_i)}{\Delta\sigma_{ex}(\theta_i)}\right]^2 \qquad (5.22)$$

where σ_{th} and σ_{ex} are the theoretical and experimental differential cross-sections respectively at angle θ_i. N is the number of θ_i and $\Delta\sigma_{ex}(\theta_i)$ is the error associated with $\sigma_{ex}(\theta_i)$. As explained later in 5.5.1, in our scattering calculations we have used the data of Budzanowski *et al.*[52] which have previously been extensively analysed by McFadden and Satchler[51]. Budzanowski estimated the errors on the absolute values of the cross sections to vary from 2% up to 10% and hence McFadden and Satchler chose to use a constant 10% error in $\sigma_{ex}(\theta_i)$ for each nucleus. In order to compare our results with those of McFadden and Satchler, we also assume a 10% error for $\Delta\sigma_{ex}(\theta_i)$.

Automatic search routines are then used to minimize χ^2 by varying one or more of the adjustable parameters of a given model potential. One has to be very careful in using these search routines. The quantity χ^2 defines a surface in the multi-dimensional parameter space of this model which is not altogether 'smooth'. The surface may contain many local as well as absolute minima which cannot be detected without some degree of parameter scanning. In particular the ambiguities in the proposed potentials hinted at earlier lead to different 'valleys' in the parameter space.

5.4 AMBIGUITIES

When discussing the partial wave decomposition of the wave function, it was pointed out how one cannot distinguish between wave functions with different behaviour when $r<R_{co}$, but identical behaviour at $r>R_{co}$. In other words as long as the phase shifts are the same, one cannot distinguish between two trial functions. So the measured differential cross section does not necessarily determine the optical model potential uniquely.

There are several distinct types of parameter ambiguity. Some are continuous, so that all sets of parameters in a particular region of parameter space give equally good fits. Other ambiguities are discrete in the sense that only a series of particular values of the parameters gives acceptable fits while intermediate values do not. The scattering of composite particles is particularly prone to ambiguity: partly because the alpha-nucleus interaction is not as well known as the

nucleon-nucleus interaction and partly because the generally higher surface absorption makes the elastic scattering less sensitive to the nuclear interior.

5.4.1 Continuous ambiguities

Small variations in one parameter of the potential can usually be compensated for by small variations in another part so that the scattering is almost unchanged. These ambiguities are particularly sensitive toward poor data of low statistical accuracy. Statistical errors can be reduced by ensuring high enough counts at each angle but an overall normalization error, depending on the calibration of the apparatus and thickness of the target, still introduces an ambiguity into the analysis[53]. This 'normalization' error is illustrated in Figure 5.3 where some data on the elastic scattering of 12 MeV deuterons by Ni, Zr and Cd have been analysed using different normalisations. It is possible to determine the normalization factor by allowing it to be one of the parameters that is varied to optimize the fit, but this is not reliable and usually introduces substantial additional uncertainty into the values of the optical-model parameters.

Another well known ambiguity is the VR^n ambiguity[54], where n is about 2. It is found that the fit remains almost the same if r is varied (up to 10% either way from its optimum) at the same time so as to keep VR^n constant[55]. Similar ambiguities have been noted for W and for the diffuseness parameter. From their study of the elastic scattering of 11 MeV deuterons by ^{40}Ca, Bassel *et al.*[56] found that the value of the exponent in the VR^n ambiguity decreased from 1.76 for the shallowest potential, through 1.26 for the deepest potential.

A further ambiguity, the Igo ambiguity[57], arises under conditions of strong absorption in the nuclear surface, in which case only the tail of the potential is tested. At large radii the Woods-Saxon potential reduces to a simple exponential, so for given values of diffuseness, any combination of V and R which yield the same values for $V_0\exp(R/a)$ will leave the potential unaltered in this region.

5.4.2 Discrete ambiguities

If the real part of the potential is steadily deepened and at each depth all of the other parameters are adjusted to optimize the fit, it is found that χ^2 passes through a series of minima at a series of depths that vary roughly as integer multiples of some minimum value. Each of these minima is subject to some of the continuous ambiguities, so it is said that there are discrete families of potentials. Examination of the associated wave functions of successive deeper potentials show identical

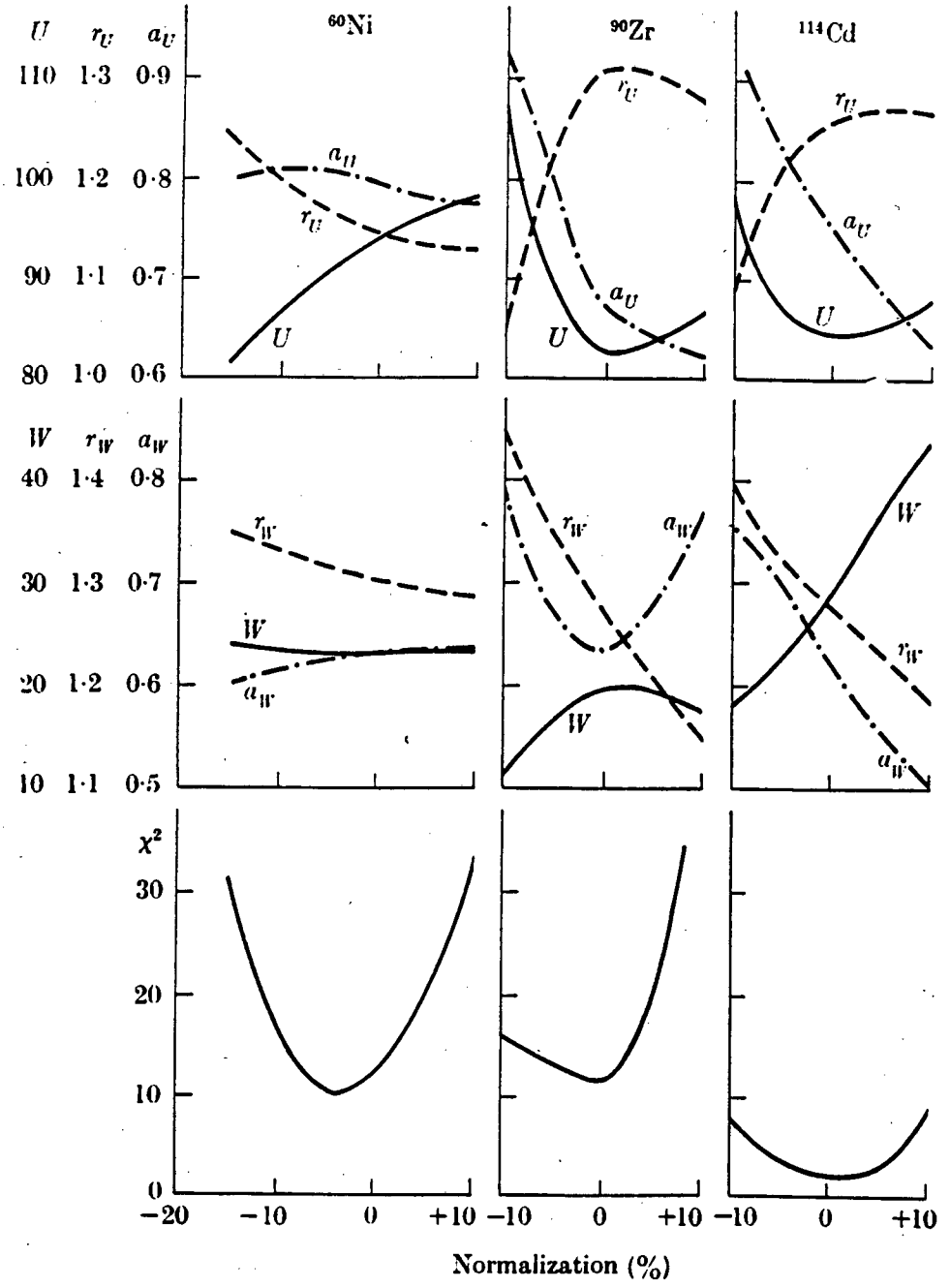

Figure 5.3 - *Optimum values of the parameters of the optical model as a function of the assumed normalization of the experimental data. These calculations were made for 12-MeV deuterons elastically scattered by ^{60}Ni, ^{90}Zr, and ^{114}Cd. {J.K. Dickens and F.G. Perey, Phys. Rev. B 138, 1080 (1965).}*

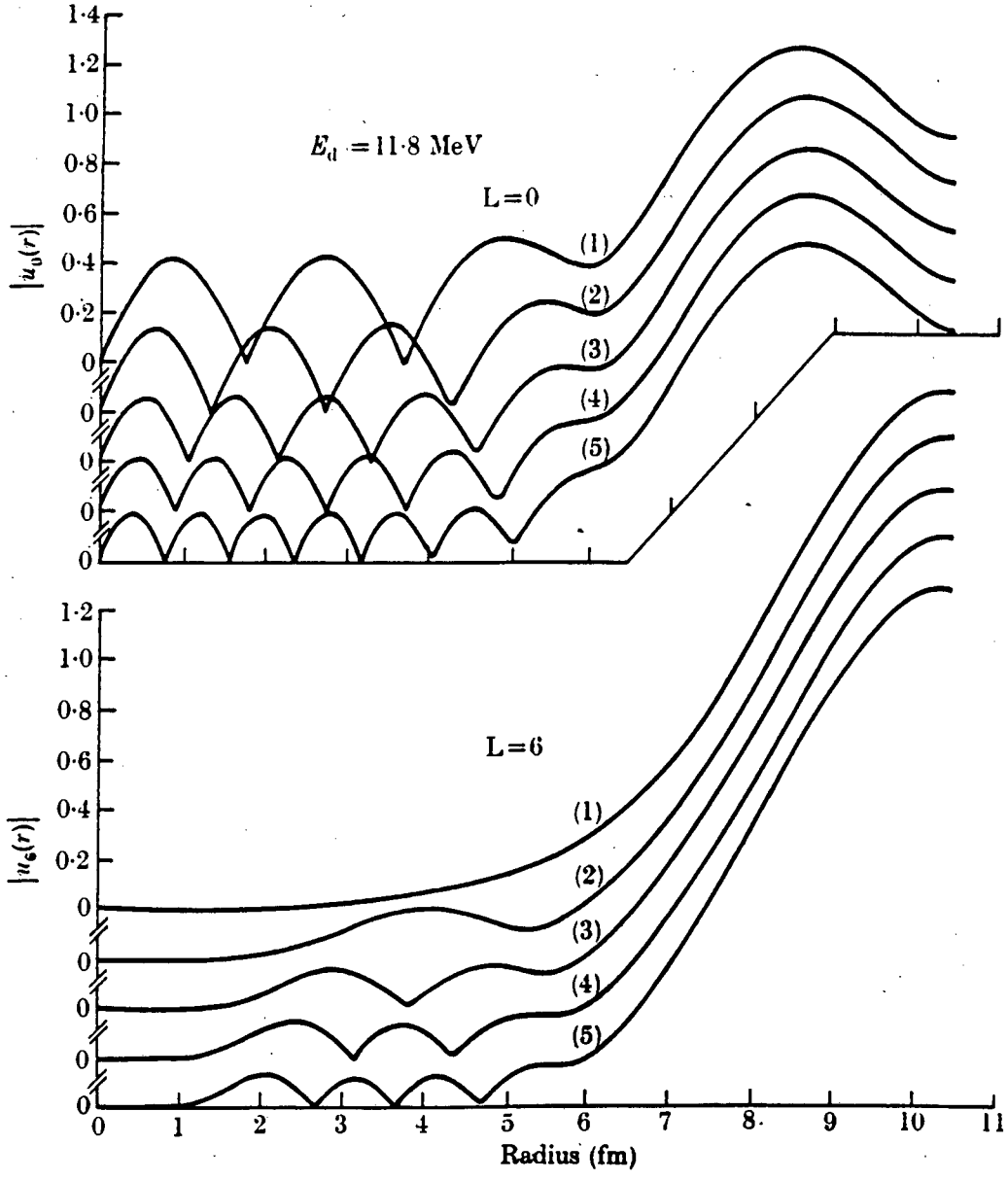

Figure 5.4 - *Moduli of the L=0 and L=6 partial waves as a function of radius for the pure surface absorption potentials that fit the elastic scattering of 11.8-MeV deuterons by copper. {C.M. Perey and F.G. Perey, Phys. Rev. 132, 755 (1963).}*

asymptotic forms but an additional half-wavelength within the potential (see Figure 5.4). This effect can be understood using the W.K.B. approximation for the partial wave amplitudes[58,59]. The reflection coefficient, or scattering matrix element can be written:

$$\eta_L \equiv S_L = \exp(2i\delta_L(r_L)) \tag{5.23}$$

where

$$\delta_L(r_L) = \int_{r_L}^{\infty}\left[k^2-\frac{2\mu}{\hbar^2}U(r)-\frac{L(L+1)}{r^2}\right]^{1/2}dr - \int_{r_L}^{\infty}\left[k^2-\frac{L(L+1)}{r^2}\right]^{1/2}dr \tag{5.24}$$

where r_L is the classical turning point for the Lth wave. So if a deeper potential is used such that δ_L is increased by π, then S_L is unchanged. Of course this needs to be done simultaneously for each partial wave that makes a significant contribution to the scattering. The more partial waves required, the more difficult this condition is to meet and the less likely this ambiguity is encountered. To remove this ambiguity thus requires higher energies. The potential is then determined at smaller radii and more phase shifts δ_L are required to reproduce the scattering.

5.5 OBTAINING SIMULTANEOUS SCATTERING AND DECAY FITS

Table XV illustrates the very considerable range in optical parameters obtained for just one particular target, ^{208}Pb. Having so thoroughly examined the theory of elastic scattering and defined an optical potential to use as the optical 'analog' of the BMP decay potential, the presence of the discrete and continuous ambiguities seems liable to destroy any hope of obtaining meaningful results from low-energy scattering experiments. Certainly a unique optical potential seems beyond the reach of these scattering experiments alone. That however is of not much concern to us. Our aim in this chapter is to see whether the BMP potential, which is so successful in predicting alpha decay half-lives from heavy nuclei can simultaneously describe the low-energy scattering of these particles from the same nuclei - in other words, does it's optical analog coincide with one of the many possible optical potentials that describe the scattering data? If so, we obtain a further indication of the validity of the model. We also gain an indication of which of the many optical potentials is most likely to be 'correct'; and as will be seen, provides an experimental limit on the preformation factor.

Table XV - *Optical model parameters for ^{208}Pb deduced from various low-energy alpha-scattering experiments. (At. Data and Nucl. Data Tables, Vol 17, No.1, January 1976)*

E_α	Real Potential			Vol. Imag. Potential			Surf. Imag. Potential		
MeV	V	R	a	W	R_i	a_i	WD	RD	AD
19.0	96.44	1.376	0.625				32.0	1.216	0.42
19.5	20.0	1.22	0.57	38.0	1.22	0.57			
20.0	174.0	1.47	0.47	16.83	1.47	0.47			
20.0	96.44	1.376	0.625				32.0	1.216	0.42
21.0	32.0	1.22	0.57	15.0	1.22	0.57			
22.0	96.44	1.376	0.625				32.0	1.216	0.42
22.5	33.0	1.22	0.57	6.	1.22	0.57			
24.5	37.0	1.22	0.57	5.	1.22	0.57			
25.5	41.0	1.22	0.57	2.	1.22	0.57			

5.5.1 Potential model and data used

The potential used has already been extensively discussed in 5.2. We use an optical potential with real, imaginary and Coulomb parts (spin-orbital potentials not playing a role in alpha scattering). The Coulomb potential is obtained from assuming a uniform charge distribution within the nucleus with no diffuse edge (equation **(5.21)**); whilst a cosh potential is used for the real and imaginary parts.

The data used has been kindly provided by G.R.Satchler and has been previously used by McFadden and Satchler[51] in an extensive optical model analysis of the scattering of 24.7 MeV alpha particles. The data originates from the experiments of Budzanowski *et al.*[52] in which scattering cross sections were measured of 24.7 MeV alpha particles off: O, Mg, Al, Si, Ca, Mn, Co, Ni, Cu, Ge, Zr, Ag, In, Sn, Hf, W, Au, Bi and U. For the purposes of investigating heavy nuclei, we have chosen to use the data for Hf, W, Au, Bi and U nuclei only.

At this stage it may be asked how effective the optical potential is in influencing the scattering of such fairly low energy (24.7 MeV) alpha particles off nuclei with such high Coulomb barriers (23MeV at 12fm for U). Calculations were made by McFadden and Satchler, for a potential with V=185MeV, W=20MeV, r_0=1.4fm and a=0.55fm for Hf and U, using only the real part, only the imaginary part, and then both. The results are shown in Figure 5.4. The real potential alone

produces strong oscillations in the angular distributions even for U. The imaginary potential alone causes a smooth falloff from the Rutherford value, but much less than that observed experimentally. Combining the two parts damps out the oscillations and causes a more rapid falloff in cross section; reproducing the experimental cross-section. Thus, even at 24.7MeV, alpha scattering is sensitive to the nuclear potential.

5.5.2 Parameter search approach

The only free parameter in the Coulomb potential is the radius r_c to which a value of 1.3fm has already been assigned. This leaves 6 independent parameters in the real and imaginary potentials:

REAL POTENTIAL			IMAGINARY POTENTIAL		
V	-	potential depth	W	-	potential depth
r_r	-	radius	r_i	-	radius
a_r	-	diffuseness	a_i	-	diffuseness

The most straightforward method of finding a self-consistent set of potential parameter values that adequately fit the decay data, and adequately fit the scattering data, would be the following: For P=1, for example, we would systematically scan the entries of Table VIII, using each set in turn to fix the real part of the optical potential. For each such set we would then search on the parameters of the imaginary part of the optical potential and determined the overall goodness-of-fit to the elastic scattering for the targets for which we have data. If an adequate fit to the decay and scattering data can be found, this technique would then produce the corresponding set of self-consistent parameter values. Unfortunately, this programme turns out to be too ambitious. Indeed, McFadden and Satchler[51] were unable to find a single set of optical model parameter values to fit the scattering data alone. At a less ambitious level, we can determine regions of parameter space within which we can adequately describe the decay and scattering data. To this end, we carry out the following calculations for each nucleus for which we have scattering data. Focussing our attention on Hf, for example:

1. We set $a_i=a_r$. Due to the insensitivity of the scattering in particular to the diffuseness of the imaginary potential we have decreased the number of independent variables by equating the imaginary diffuseness with the real diffuseness.

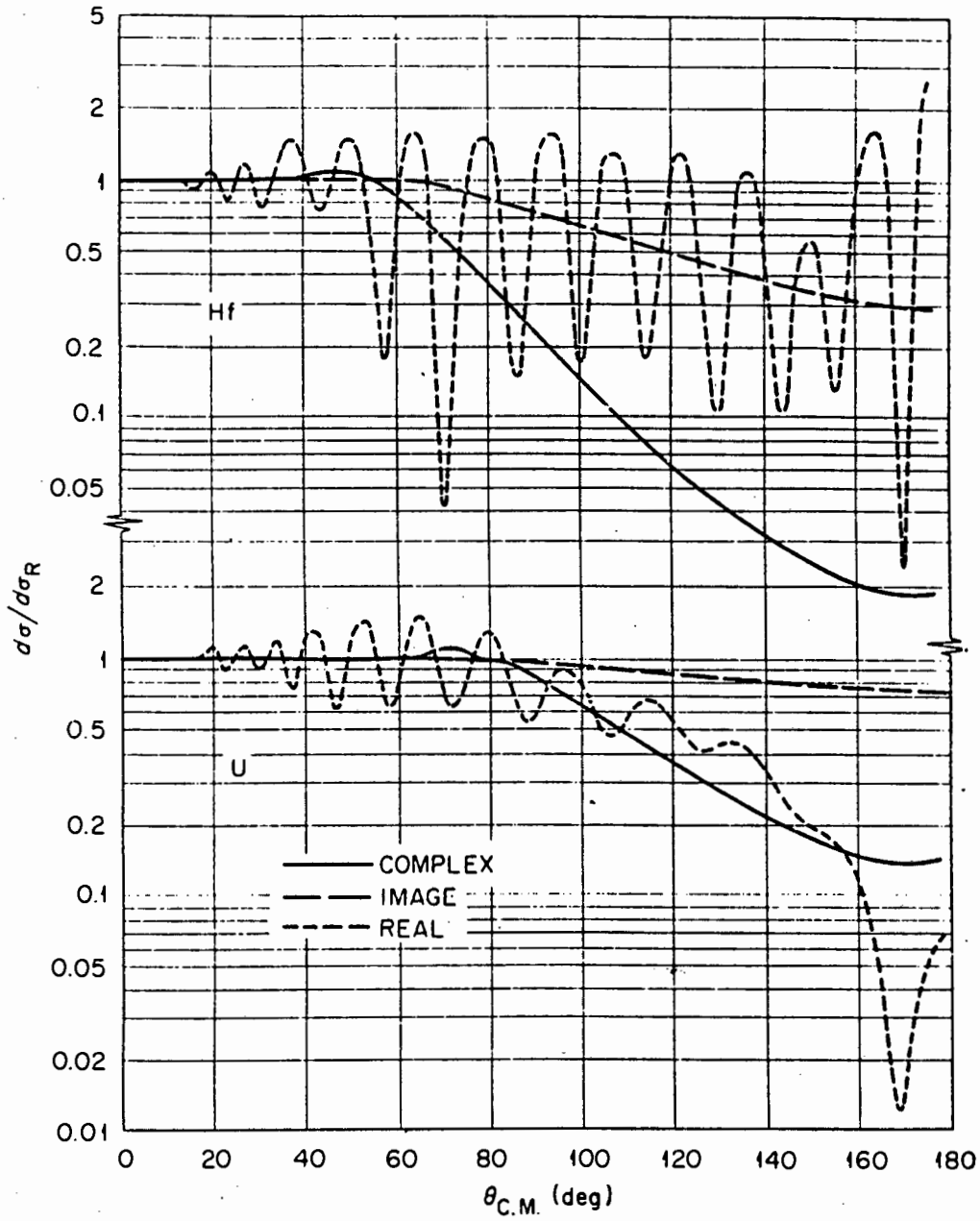

Figure 5.5 - *Effects of the real and imaginary parts of the optical potentials on the scattering of 24.7MeV α-particles from Hf and U. {L.McFadden and G.R.Satchler,* Nucl. Phys. **84**, 177 (1966)*} Neither component individually reproduces the observed scattering, as the complex potential does. Despite these heavy targets being Coulomb dominated, the scattering is still sensitive to the nuclear potential.*

2. We set W=20 MeV. Again, the imaginary depth is poorly determined and this value of W is in line with typical values found by other researchers (Table XV and ref.[51,60]).

3. For each value of diffuseness we fix the real potential depth, V, to the best-fit value of the decay calculations for that diffuseness, and search on the last remaining independent variables: r_r and r_i. At the risk of 'muddying the waters' with an excess of data, we do this for the three G-families that gave the best radius fits to the decay data. In other words, we set the diffuseness in each case to a value from 0.20fm to 1.00fm (in increments of 0.05fm), and use the potential depths found for that diffuseness, first in the case $G_<$=14, then $G_<$=16 and finally $G_<$=18 (see Table VIII).

Once the fitting has been performed, and values of r_r, r_i and χ^2 obtained, the radius as obtained from the decay calculations can be compared with the radius of the real part of the optical potential. For a simultaneous fit to the scattering data, and to the scattering from Hf, these radii should be the same. The calculations are then repeated for W, Bi, Au and U. For overall self-consistency, the parameters V and *a* obtained in the simultaneous fits for each target should then be identical.

5.5.3 Decay radii

In this section we consider exactly which radii from which decays are to be compared with the results of the optical model fitting. Complicating the comparison of the decay and scattering results, is the fact that the scattering experiments were performed on naturally occurring (stable) samples of the elements, whilst decays are obviously from unstable nuclei. The two properties (stability and instability) are in general, exclusive of each other.

Thus if we are considering the scattering of alpha particles off $^{238}_{92}$U, the decay to be considered, is that of $^{242}_{94}$Pu ($^{238}_{92}$U core + alpha cluster) and not that of $^{238}_{92}$U itself. In this case there is no problem since $^{242}_{94}$Pu decays by alpha emission. We have scattering data for Hf, W, Au, Bi and U. As shown in Table XVI, ideally we would like to have for comparison, the potential parameters for the alpha decay of $^{182}_{74}$W, $^{188}_{76}$Os, $^{201}_{81}$Tl, $^{213}_{85}$At, $^{242}_{94}$Pu respectively.

$^{201}_{81}$Tl and $^{213}_{85}$At pose a problem as we have considered only even-even alpha decays. Fortunately the dependence of r_0 on A and Z is weak. Typically, ΔA=1 results in a 0.1% change in radius and ΔZ=1, a 0.01% change in radius. We are thus able to use the radii of neighbouring nuclei with little introduction of error. We hence choose to use the radii for the decays of $^{194}_{82}$Pb (for

$^{201}_{81}Tl$) and $^{214}_{86}Rn$ (for $^{213}_{85}At$)

Although $^{182}_{74}W$ and $^{188}_{76}Os$ are even-even, they are stable nuclei and no alpha decay half life is measurable. Again, neighbouring nuclei have to be used. $^{182}_{78}Pt$ is used for $^{182}_{74}W$ and $^{188}_{78}Pt$ is used instead of $^{188}_{76}Os$.

Table XVI - *Listing of what nuclei were used in scattering experiments, hence what decay radius should be used and thirdly, the compromise nucleus used in cases where the ideal nucleus is too stable or is not even-even.*

Scattering nucleus	Ideal decay	Decay used
$^{178.5}_{72}Hf$	$^{182}_{74}W$	$^{182}_{78}Pt$
$^{183.9}_{74}W$	$^{188}_{76}Os$	$^{188}_{78}Pt$
$^{197}_{79}Au$	$^{201}_{81}Tl$	$^{194}_{82}Pb$
$^{209}_{83}Bi$	$^{213}_{85}At$	$^{214}_{86}Rn$
$^{238}_{92}U$	$^{242}_{94}Pu$	$^{242}_{94}Pu$

5.5.4 Results: Comparing scattering and decay radii (P=1.0)

Table XVII-Table XXI list the results of the optical model parameter searches described in 5.5.2. The decay radii of the nuclei discussed in 5.5.3 are included for comparison together with χ^2_{opt}, the lowest value of χ^2 found by McFadden and Satchler[51], in their more general four parameter fits (on V, W, $r_r=r_i$, $a_r=a_i$), with parameter values tailored to each target in turn. Two important patterns are obvious.

Firstly the behaviour of χ^2. For values of diffuseness $a\leq 0.45$fm, fixing V and a from the decay calculations results in a completely unacceptable fit to the elastic scattering. χ^2 goes through a minimum in the region of a=0.50fm to a=0.65fm and then very gradually increases with higher diffuseness. Uranium, for example, has a minimum chi of 0.108 at a=0.50fm. At a=0.80fm, χ^2=0.115, an increase of 6%. At this stage it is important to point out that the quality of these fits is identical to those of the four parameter fits of McFadden and Satchler. This is a great relief, as it shows that fixing the potential depth to that of the decay potential does not affect the quality of

the fits significantly and our search method is *a posteriori* justified. The possibility of a simultaneous fit between the scattering data and the decay data is also not ruled out.

The other observation is in the behaviour of the radii. The best-fit radii of the optical model start at very high values (~1.70fm) for low diffuseness and decrease rapidly with increasing diffuseness. The radii of the decay calculations similarly decrease with increasing diffuseness, but at a much slower rate. The values 'overlap' for each nucleus in the range a=0.75fm to 0.85fm. At these points the parameters of the decay potential and the real part of the optical potential are identical and we find simultaneous fits to both the decay and scattering data.

A diffuseness of a~0.80fm is considerably greater than the values of 0.50fm to 0.60fm obtained by McFadden and Satchler in their 4 parameter fits to the same data. By 'scanning' through different values of diffuseness rather than letting the optical model fitting program search on it as an independent variable, we have observed a behaviour in the fits not previously noted; that being the insensitivity of the fits to the diffuseness for $a \geq 0.45$fm. In so doing, we find that although we reproduce McFadden and Satchler's results with a minimum chi in the range a=0.50fm to a=0.60fm, values as high as a=0.80fm are not strongly excluded. These higher values of a (coupled with lower values of r_r) are predicted by folding models. For example, Buck and Merchant in BM1 and BM2 find that a double folding of the experimental densities of ^{208}Pb and ^{4}He with a δ function for the nucleon-nucleon interaction results in a potential which can be perfectly reproduced by a cosh potential with a=0.75fm and r_r=1.06fm. We note also that a double folded potential of this type successfully[60] reproduces α scattering data in ^{209}Bi at incident energies ranging from 22-104MeV.

Although the fits to the scattering data are not optimal, and there is some spread in the values of a from nucleus to nucleus (showing that we have not obtained complete consistency between a single set of decay potential parameters, and a single set of scattering potential parameters), a region of parameter space within which we can adequately describe the decay and scattering data is clearly delineated. We shall return to the question of a completely consistent potential that adequately describes both the decay and scattering data in 5.8.

5.6 ALTERNATIVE VALUES OF P

The assumption that P=1.0 for all nuclei was an attempt to restrict the number of free variables. So what happens if we decide to free this variable and repeat the calculations with different values of P ?

Table XVII - *Optical model fits to Hf scattering data. For each value of diffuseness we give the value of χ^2; the fitted parameters r_r and r_i; and the relevant decay radius for comparison. (P=1.0) Shaded sections mark approximately where decay and scattering parameters 'overlap'. Table VIII provides the additional information on the relevant decay S and V_0.*

The format is:

χ^2	r_r
	r_i
	r_{decay}

$\chi^2_{opt}=0.150$

Diffuseness	14-16		16-18		18-20	
0.30	12.	1.8	12.	1.8	13.	1.8
		1.2		1.2		1.5
		1.274		1.267		1.260
0.35	4.9	1.65	4.9	1.64	4.9	1.6
		1.27		1.18		1.1
		1.259		1.248		1.241
0.40	1.8	1.531	1.8	1.520	1.8	1.508
		1.153		1.071		1.062
		1.237		1.229		1.222
0.45	0.5139	1.441	0.5248	1.429	0.5325	1.416
		0.944		0.994		1.022
		1.223		1.211		1.197
0.50	0.1702	1.366	0.1721	1.352	0.1742	1.339
		1.086		1.093		1.104
		1.203		1.188		1.176
0.55	0.1561	1.319	0.1556	1.302	0.1549	1.286
		1.325		1.322		1.319
		1.183		1.165		1.152
0.60	0.1508	1.269	0.1505	1.251	0.1503	1.233
		1.346		1.344		1.343
		1.164		1.148		1.129
0.65	0.1503	1.215	0.1500	1.194	0.1499	1.175
		1.344		1.342		1.341
		1.146		1.123		1.107
0.70	0.1548	1.157	0.1540	1.135	0.1534	1.114
		1.331		1.331		1.330
		1.122		1.103		1.081
0.75	0.1643	1.097	0.1636	1.073	0.1632	1.050
		1.314		1.313		1.312
		1.099		1.078		1.056
0.80	0.1787	1.036	0.1780	1.009	0.1773	0.986
		1.291		1.291		1.290
		1.077		1.051		1.033
0.85	0.1984	0.973	0.1978	0.944	0.1973	0.922
		1.274		1.269		1.271
		1.056		1.031		1.010
0.90	0.2242	0.909	0.2235	0.877	0.2231	0.855
		1.251		1.245		1.244
		1.030		1.008		0.989

Table XVIII - *Optical model fits to W scattering data. For each value of diffuseness we give the value of χ^2; the fitted parameters r_r and r_i; and the relevant decay radius for comparison. (P=1.0) Shaded sections mark approximately where decay and scattering parameters 'overlap'. Table VIII provides the additional information on the relevant decay S and V_0.*

The format is:

χ^2	r_r
	r_i
	r_{decay}

$\chi^2_{opt}=0.214$

Diffuseness	14-16		16-18		18-20	
0.30	4.4	1.71	4.5	1.7	4.4	1.7
		1.18		1.1		1.3
		1.27		1.26		1.26
0.35	2.29	1.62	2.37	1.611	2.3	1.6
		0.69		1.130		0.8
		1.25		1.24		1.24
0.40	1.24	1.544	1.25	1.533	1.26	1.522
		1.164		1.178		1.199
		1.23		1.22		1.22
0.45	0.6157	1.477	0.6239	1.464	0.6288	1.081
		0.9881		1.054		1.452
		1.227		1.204		1.197
0.50	0.3134	1.416	0.3183	1.401	0.3167	1.409
		1.024		1.048		1.047
		1.198		1.181		1.176
0.55	0.2127	1.359	0.2165	1.343	0.2214	1.328
		1.080		1.116		1.148
		1.178		1.159		1.145
0.60	0.2166	1.310	0.2158	1.293	0.2155	1.275
		1.267		1.260		1.253
		1.159		1.143		1.122
0.65	0.2290	1.262	0.2277	1.241	0.2264	1.223
		1.300		1.296		1.295
		1.141		1.117		1.100
0.70	0.2454	1.210	0.2450	1.189	0.2451	1.168
		1.300		1.299		1.298
		1.117		1.097		1.075
0.75	0.2649	1.157	0.2642	1.134	0.2633	1.111
		1.287		1.286		1.284
		1.095		1.073		1.050
0.80	0.2857	1.102	0.2843	1.077	0.2834	1.053
		1.267		1.266		1.265
		1.073		1.046		1.027
0.85	0.3087	1.044	0.3053	1.013	0.3027	0.997
		1.248		1.247		1.250
		1.050		1.023		1.005
0.90	0.3343	0.988	0.3275	0.962	0.3222	0.935
		1.224		1.225		1.227
		1.023		1.001		0.981

Table XIX - *Optical model fits to Au scattering data. For each value of diffuseness we give the value of χ^2; the fitted parameters r_r and r_i; and the relevant decay radius for comparison. (P=1.0) Shaded sections mark approximately where decay and scattering parameters 'overlap'. Table VIII provides the additional information on the relevant decay S and V_0.*

The format is:

χ^2	r_r
	r_i
	r_{decay}

$\chi^2_{opt}=0.135$

Diffuseness	14-16		16-18		18-20	
0.30	6.4	1.8	6.5	1.8	6.8	1.8
		0.8		1.1		1.1
		1.267		1.257		1.249
0.35	2.5	1.677	2.5	1.668	2.6	1.659
		1.178		1.096		1.140
		1.253		1.238		1.227
0.40	0.8888	1.577	1.0480	1.579	1.1025	1.571
		1.199		1.199		1.199
		1.231		1.220		1.206
0.45	0.2517	1.496	0.2594	1.484	0.2603	1.472
		1.019		1.200		1.075
		1.217		1.202		1.186
0.50	0.1311	1.431	0.1313	1.417	0.1316	1.403
		1.294		1.287		1.283
		1.197		1.179		1.166
0.55	0.1402	1.386	0.1409	1.368	0.1393	1.355
		1.412		1.399		1.408
		1.178		1.157		1.142
0.60	0.1512	1.336	0.1504	1.319	0.1497	1.301
		1.423		1.421		1.408
		1.159		1.141		1.142
0.65	0.1664	1.283	0.1654	1.263	0.1648	1.244
		1.416		1.414		1.414
		1.141		1.115		1.097
0.70	0.1856	1.226	0.1847	1.205	0.1840	1.184
		1.401		1.400		1.399
		1.117		1.095		1.072
0.75	0.2081	1.167	0.2072	1.144	0.2065	1.122
		1.381		1.380		1.379
		1.095		1.072		1.048
0.80	0.2328	1.108	0.2319	1.083	0.2313	1.060
		1.357		1.356		1.356
		1.073		1.045		1.025
0.85	0.2600	1.049	0.2586	1.022	0.2577	0.998
		1.322		1.324		1.327
		1.055		1.027		1.004
0.90	0.2892	0.990	0.2880	0.959	0.2864	0.930
		1.292		1.294		1.295
		1.032		1.001		0.980

Table XX - *Optical model fits to Bi scattering data. For each value of diffuseness we give the value of χ^2; the fitted parameters r_r and r_i; and the relevant decay radius for comparison. (P=1.0) Shaded sections mark approximately where decay and scattering parameters 'overlap'. Table VIII provides the additional information on the relevant decay S and V_0.*

The format is:

χ^2	r_r
	r_i
	r_{decay}

$\chi^2_{opt}=0.142$

Diffuseness	14-16		16-18		18-20	
0.30	1.4857	1.686	1.4939	1.681	1.5037	1.673
		1.034		0.851		1.028
		1.314		1.301		1.289
0.35	0.8414	1.621	0.8476	1.612	0.8518	1.603
		1.118		1.161		1.184
		1.298		1.281		1.267
0.40	0.4699	1.561	0.4728	1.550	0.4757	1.540
		1.187		1.000		1.125
		1.276		1.262		1.244
0.45	0.2618	1.506	0.2647	1.494	0.2674	1.482
		1.012		1.050		1.093
		1.261		1.243		1.223
0.50	0.1636	1.453	0.1649	1.440	0.1660	1.426
		1.000		1.023		1.045
		1.240		1.219		1.202
0.55	0.1408	1.404	0.1414	1.388	0.1422	1.373
		1.134		1.158		1.180
		1.220		1.196		1.178
0.60	0.1501	1.359	0.1497	1.342	0.1495	1.325
		1.332		1.328		1.325
		1.200		1.179		1.154
0.65	0.1610	1.312	0.1604	1.292	0.1600	1.275
		1.350		1.348		1.347
		1.181		1.153		1.132
0.70	0.1731	1.263	0.1726	1.242	0.1722	1.222
		1.343		1.342		1.341
		1.157		1.132		1.132
0.75	0.1862	1.212	0.1856	1.190	0.1852	1.168
		1.326		1.325		1.324
		1.134		1.108		1.081
0.80	0.2003	1.161	0.1996	1.137	0.1991	1.114
		1.303		1.302		1.301
		1.111		1.080		1.056
0.85	0.2154	1.080	0.2150	1.049	0.2143	1.027
		1.279		1.280		1.277
		1.088		1.052		1.028
0.90	0.2315	1.030	0.2310	1.002	0.2308	0.980
		1.250		1.258		1.253
		1.065		1.033		1.004

Table XXI - *Optical model fits to U scattering data. For each value of diffuseness we give the value of χ^2; the fitted parameters r_r and r_i; and the relevant decay radius for comparison. (P=1.0) Shaded sections mark approximately where decay and scattering parameters 'overlap'. Table VIII provides the additional information on the relevant decay S and V_0.*

The format is:

χ^2	r_r
	r_i
	r_{decay}

$\chi^2_{opt}=0.106$

Diffuseness	14-16		16-18		18-20	
0.30	0.5019	1.583	0.5064	1.576	0.5096	1.569
		1.092		1.132		1.268
		1.330		1.307		1.287
0.35	0.2677	1.524	0.2696	1.515	0.2706	1.507
		1.165		1.184		1.109
		1.315		1.287		1.264
0.40	0.1564	1.471	0.1576	1.461	0.1582	1.451
		1.004		1.050		1.062
		1.292		1.268		1.243
0.45	0.1130	1.422	0.1135	1.410	0.1144	1.399
		0.7983		0.692		1.052
		1.278		1.249		1.222
0.50	0.1088	1.378	0.1087	1.364	0.1087	1.352
		1.301		1.310		1.306
		1.256		1.226		1.202
0.55	0.1092	1.334	0.1091	1.319	0.1108	1.304
		1.352		1.350		1.369
		1.236		1.203		1.178
0.60	0.1099	1.288	0.1099	1.272	0.1099	1.255
		1.346		1.345		1.344
		1.217		1.187		1.155
0.65	0.1110	1.241	0.1109	1.222	0.1109	1.205
		1.328		1.327		1.326
		1.198		1.160		1.133
0.70	0.1123	1.193	0.1122	1.174	0.1122	1.154
		1.302		1.302		1.301
		1.173		1.140		1.107
0.75	0.1138	1.146	0.1138	1.125	0.1137	1.104
		1.272		1.272		1.271
		1.150		1.119		1.089
0.80	0.1155	1.100	0.1154	1.076	0.1154	1.054
		1.239		1.238		1.238
		1.128		1.088		1.060
0.85	0.1174	1.054	0.1174	1.030	0.1173	1.004
		1.206		1.205		1.207
		1.105		1.060		1.034
0.90	0.1194	1.010	0.1193	0.987	0.1193	0.958
		1.170		1.171		1.169
		1.082		1.032		1.001

To maintain the same rate of decay for a nucleus a drop in P must be met with an increased tunnelling probability. This is ensured by increasing the nuclear radius, reducing the Coulomb barrier thickness. We can thus expect an increase in decay radius when using a lower value of P. This is borne out in the tables of Appendix E in which we have repeated the optical model fits of 5.5 with values of P=0.1, 0.01, 0.001 and 0.0001. Study of these tables shows that decreasing P increases the decay radius, leading to coincidence of the decay and scattering radii at a smaller diffuseness. These results have been summarised in Table XXII. For each value of P and each target we list the diffuseness at which a simultaneous fit of scattering and decay data occurs. Furthermore we list the quality of fit to the scattering data for each of these points. For ease of comparison in assessing the quality of individual fits, rather than quoting our χ^2, we quote instead the ratio χ^2/χ^2_{opt}, where χ^2_{opt} is again the result of the best four parameter fit obtained by McFadden and Satchler[51] for the given target. These results have been further summarised in Figure 5.6 where the dependence of the fits on the preformation factor are shown, together with the spread in potential parameters found from nucleus to nucleus.

In Figure 5.6 we see that the overall quality of fit is significantly improved for P=0.1; is roughly the same for P=0.01 (as P=1.0); and worsens dramatically for smaller values. Not only do we have simultaneous fits to the scattering and decay data, but the varying quality of fit with changing P provides limits on what values of P are allowed. From Figure 5.6 we can conclude that P falls in the range 0.01 to 0.1, although values as high as P=1.0 are not ruled out. This we recall is consistent with the conclusions we came to in 4.6 when examining the effect of varying the preformation factor in the decay calculations. Figure 5.6 also shows that the best-fit potential parameters from the decay calculations can be used to make a good first guess at an optical potential to describe alpha scattering from heavy nuclei. We discuss this further in 5.8 after first verifying that our results are not the artifact of a 'wisely' chosen parameter search method in our scattering calculations.

5.7 ALTERNATIVE SEARCH APPROACHES

There are numerous approaches to optical model parameter fits: some keep all six optical potential parameters independent; some couple the real and imaginary radii and/or diffusenesses; some include surface imaginary potentials with either fixed or independent parameters etc. The point is, due to a large degree of ambiguity and uncertainty in the work, there is no accepted search method which is significantly superior to any other. McFadden and Satchler[51] highlighted this by performing both

Table XXII - *Quality of simultaneous fit for each nucleus.* χ^2_{opt} *corresponds to the best four parameter fit obtained by McFadden and Satchler*[51].

P	Target	Diffuseness (fm)	χ^2 / χ^2_{opt}
1.0	Hf	0.75	1.09
	W	0.82	1.35
	Au	0.82	1.84
	Bi	0.85	1.50
	U	0.76	1.05
0.1	Hf	0.62	1.00
	W	0.70	1.15
	Au	0.73	1.49
	Bi	0.75	1.29
	U	0.65	1.02
0.01	Hf	0.47	2.30
	W	0.54	1.09
	Au	0.60	1.13
	Bi	0.60	1.04
	U	0.46	1.05
0.001	Hf	0.39	13.4
	W	0.41	5.57
	Au	0.45	2.02
	Bi	0.44	2.14
	U	0.34	2.58
0.0001	Hf	0.34	~30
	W	0.33	14
	Au	0.36	19
	Bi	0.30	10.7
	U	0.22	~15

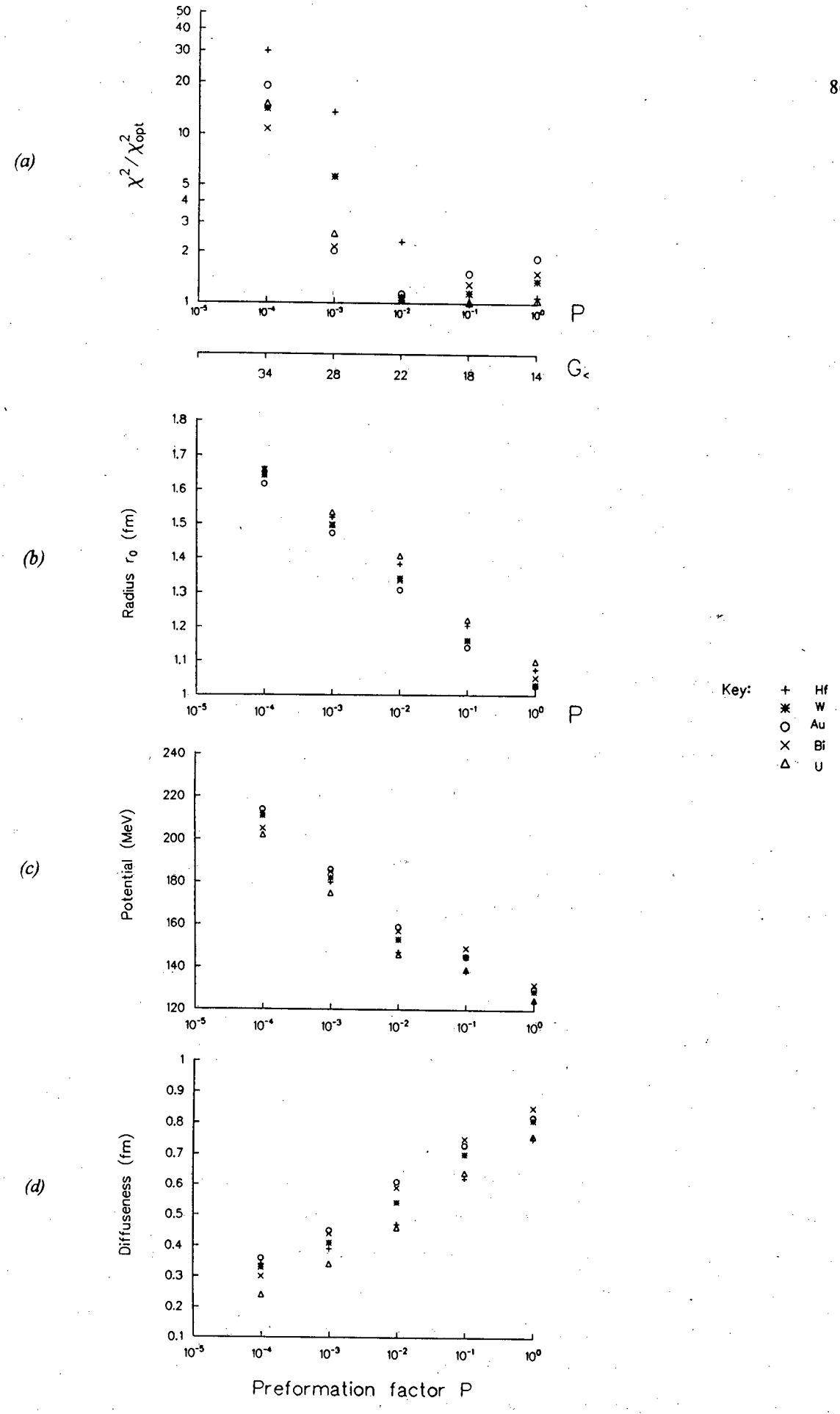

Figure 5.6 - *Summary of simultaneous decay and scattering fits (taken from Appendix E). For each nucleus we plot: (a) χ^2/χ^2_{opt} at the point of fit, as a function of the preformation factor (χ^2_{opt} is the fit obtained using Satchler's best fit parameters). The sub-axis marks the value of $G_<$ at which the fit occurs.*
(b), (c) and (d): The radius, potential and diffuseness respectively, at which the simultaneous fit occurs, again as a function of the preformation factor.

Table XXIII - *Testing alternative search approaches to performing optical model fits to the scattering data. See text for explanation of the three approaches.*

Diffuseness	Search on W and r_r ($a_r=a_i$) ($r_r=r_i$)		Search on r_r and r_i ($a_r=a_i$) (W=20MeV)		Search on W and r_r ($a_r=a_i$) (r_i=1.35fm)	
Format of results	χ^2	r_r W	χ^2	r_r r_i	χ^2	r_r W
0.35	4.5	1.576 3.43	4.9	1.6 1.1	4.3	1.58 4.42
0.40	2.083	1.499 5.107	1.8	1.508 1.062	1.908	1.499 6.891
0.45	0.7122	1.424 8.82	0.5325	1.416 1.022	0.6159	1.421 11.45
0.50	0.2380	1.348 13.28	0.1742	1.339 1.104	0.2394	1.349 13.47
0.55	0.1559	1.286 28.19	0.1549	1.286 1.319	0.1534	1.286 14.50
0.60	0.1510	1.234 56.41	0.1503	1.233 1.343	0.1502	1.233 18.69
0.65	0.1498	1.178 82.22	0.1499	1.175 1.341	0.1502	1.175 18.67
0.70	0.1520	1.118 106.8	0.1534	1.114 1.330	0.1540	1.113 17.20
0.75	0.1573	1.057 129.8	0.1632	1.050 1.312	0.1675	1.048 15.62
0.80	0.1652	0.995 150.6	0.1773	0.9858 1.290	0.1880	0.9799 13.94

3. Fix r_i and search on W and r_r. Using this approach we can manually ensure that $r_i > r_r$. Beyond this requirement, the choice of r_i is fairly arbitrary. After some investigation, we settled on r_i=1.35fm. Other values gave almost identical results but with different values of W.

The results of these alternative search methods on the Hf target are shown in Table XXIII. The results are very similar, with the only major discrepancies occurring for diffusenesses less than 0.45fm. In this region the fits are all uniformly so poor that the discrepancies are not a major concern. With these results we feel fairly safe that our results are not a consequence of a fortuitous choice of search method.

5.8 CONCLUSION

The virtues of the BMP model as a means of predicting alpha decay half lives have already been stressed. In this chapter we have seen the model go beyond just predicting this one property of heavy nuclei. Using the scattering data of Budzanowski *et al.*[52], previously analysed by McFadden and Satchler[51], we find the BMP model can simultaneously describe the decay rates of heavy nuclei and the low-energy scattering of alpha particles off these same nuclei. In its own right, this is a result of great interest, but it has a number of further consequences.

By wedding the scattering and decay calculations to find a physically acceptable parameter set that describes both sets of data optimally we find the strengths of the one approach support the weaknesses of the other in a way which helps one distinguish between ambiguities and uncertainties in both methods. The decay approach is a fairly poor test of diffuseness allowing a wide range of $G_<$ values and not a very strong indication of a within any of these families. The combined work sets much tighter bounds on $G_<$ and a ($G_<$~20 and a~0.70fm). The optical model fits on their own shed very little light on V, anything from 100 MeV to 180 MeV being feasible. The combined results restrict this range to 140-150MeV.

For each nucleus for which we have scattering data we have thus been able to find a set of potential parameters which simultaneously gives an acceptable fit to all the decay data and to the elastic scattering data for that nucleus. However, the scatter in potential parameters from nucleus to nucleus evident in Figure 5.6 shows that we have not been able to find a single set of potential parameters which gives acceptable fits to all the decay data, and to all the elastic scattering data. McFadden and Satchler[51] (who concentrated on the elastic scattering alone) were also unable to find such a set. Nevertheless, the smallness of this scatter is indicatory of a technique useful in making

a first guess at an optical potential for heavy nuclei.

Using the following parameter set, we are able to reproduce the alpha decay half-lives of all heavy nuclei, with a goodness of fit indicator S=4.5. With r_r fixed to within, on average, 3% of the decay radius predicted by the B-S condition, we can then also reproduce the elastic scattering data for Hf, W, Au, Bi and U with an average goodness of fit $\frac{1}{5}\sum \chi_i^2/\chi_{i(opt)}^2 = 1.17$. We stress again that $\chi_{i(opt)}^2$ corresponds to the best fit obtained in four parameter searches by McFadden and Satchler[51] with parameter values tailored to each target in turn.

$G_<$	= 18	$(a_i=)a_r$	= 0.70 fm
P	= 0.1	r_{decay}	= fixed by B-S condition
V	= 145 MeV	r_r	~ r_{decay}
W	= 20 Mev	r_i	= 1.3fm

The application of this first guess is not necessarily restricted to 24.7MeV alphas. It has been shown[62] that in the case of alpha particles, there is a smooth energy behaviour in the potential parameters over a broad incident energy range. Delbar *et al.*[62] find the energy variation of the real potential is $V = 198.6(1 - 0.00168E_\alpha)$ which implies a very slow change in the potential parameters with increasing energy and justifies our use of a common value of V in the decay calculations (E_α~5-10MeV), and in the scattering calculations (E_α~24.7MeV). Hopefully, it may also indicate that our first guess at an optical potential is likely to retain the same degree of applicability at higher bombarding energies.

Finally, in the process of obtaining simultaneous good fits to the scattering and decay data, we have delineated a range P=0.01 to 0.1 for the alpha preformation probability, with the value of P=1.0 not ruled out. This result is largely free of arbitrary choices in the parametrisation of the potential used. In 4.7 we pointed out the dangers inherent in previous determinations of 'experimental' preformation probabilities based on potentials of possibly limited validity. We have removed any subjective choice in such matters by requiring our potential to simultaneously reproduce a large body of scattering and decay data. The downside of this is that we have found an acceptable range of P running over two orders of magnitude. The upside

is that we are not led to an automatic dismissal of the theoretical value P=0.3 very recently obtained by Varga *et al.*[37], nor of the value P=1.0 used successfully in the BMP analyses of alpha decay data. Such large values run contrary to earlier[63] 'experimental' determinations of P which typically suggest $P \leq 0.01$.

6. SUMMARY

The discovery of exotic decays by Rose and Jones in 1984 has been the stimulus for a great deal of work on cluster models of heavy nuclei. A particularly successful model has been that of Buck, Merchant and Perez, especially in its application to alpha decay. A considerable degree of the success of this model can be attributed to the assignment of a large global quantum number, G, to the alpha cluster, which increases sharply (by $\Delta G=2$) at neutron shell closures. This work has looked for evidence of a similar change in G at proton shell closures by considering alternative values of ΔG and an alternative approach to determining the nuclear potential parameters. We find the original approach of Buck *et al.*, a radius fit with $\Delta G=2$, is still the most successful but that a potential fit with $\Delta G=4$ remains competitive, lending support to the suggestion that the proton shell closure is also felt, but possibly obscured by a complicated interaction of the G and P values for the transitional nuclei.

We then turned to scattering experiments of alpha particles off heavy nuclei and find that the potential parameters of the BMP model are close to those which provide a good fit to the scattering data; further evidence for the general validity and applicability of the BMP model.

In the process of performing these calculations we have examined the effect of using values of P other than the P=1.0 of Buck *et al.* Our results are masked by ambiguities in best-fit parameters, both in the decay and scattering work, and these ambiguities are exacerbated by a probable scatter of P about its assumed constant value. Nevertheless we are able to conclude that the fluctuations in P about its average value are surprisingly small (~50%), and that its most probable average value lies in the range $0.01 \leq P \leq 0.1$ with the value of P=1.0 not ruled out.

APPENDIX A - Data set (excluding transitional nuclei)

Z	A		Q (MeV)	$T_{1/2}^{exp}$ (s)
60	144	Nd	1.902	7.2E+22
62	146	Sm	2.545	3.25E+15
62	148	Sm	2.007	2E+23
64	148	Gd	3.293	2.35E+9
64	150	Gd	2.823	5.65E+13
64	152	Gd	2.220	3.41E+21
66	150	Dy	4.412	1.20E+3
66	152	Dy	3.751	8.6E+6
66	154	Dy	2.972	9.2E+13
68	152	Er	4.953	1.10E+1
68	154	Er	4.301	4.7E+4
70	154	Yb	5.485	4.1E-1
70	156	Yb	4.834	2.6E+2
70	158	Yb	4.200	3E+6
72	156	Hf	6.059	2.5E-2
72	158	Hf	5.429	6.3E+0
72	160	Hf	4.923	5.2E+2
72	162	Hf	4.445	4E+5
72	174	Hf	2.585	6.3E+22
74	158	W	6.645	1.4E-3
74	160	W	6.102	8.6E-2
74	162	W	5.702	3.0E+0
74	164	W	5.306	2.5E+2
74	166	W	4.877	2.7E+3
76	162	Os	6.806	1.9E-3
76	166	Os	6.163	1.0E-1
76	168	Os	5.853	4.5E+0
76	170	Os	5.568	5.9E+1
76	172	Os	5.253	9.5E+3
76	174	Os	4.893	2.0E+5
76	186	Os	2.846	6.3E+22
78	170	Pt	6.734	6.0E-3
78	172	Pt	6.494	1.05E-1
78	184	Pt	6.212	1.1E+0
78	176	Pt	5.924	1.7E+1
78	178	Pt	5.604	2.7E+2
78	180	Pt	5.284	2.0E+4
78	182	Pt	4.974	8.0E+5
78	184	Pt	4.624	1.0E+8
78	186	Pt	4.354	5.1E+9
78	188	Pt	4.029	3.4E+12
78	190	Pt	3.273	1.9E+19
80	176	Hg	6.935	3.4E-2
80	178	Hg	6.608	5.2E-1
80	180	Hg	6.285	6.1E+0
80	182	Hg	6.035	7.4E+1
80	184	Hg	5.695	2.8E+3
80	186	Hg	5.235	5.2E+5
80	188	Hg	4.735	5.3E+8
82	182	Pb	7.131	5.5E-2
82	184	Pb	6.806	5.5E-1
82	186	Pb	6.496	4.79E+0
82	188	Pb	6.146	1.1E+2
82	190	Pb	5.727	8.0E+3
82	192	Pb	5.256	3.5E+6

Z	A		Q (MeV)	$T_{1/2}^{exp}$ (s)
82	194	Pb	4.666	9.9E+9
84	212	Po	8.985	2.98E-7
84	214	Po	7.865	1.64E-9
84	216	Po	6.938	1.5E-1
84	218	Po	6.147	1.87E+2
86	214	Rn	9.243	2.7E-7
86	216	Rn	8.234	4.5E-5
86	218	Rn	7.300	3.5E-2
86	220	Rn	6.438	5.56E+1
86	222	Rn	5.623	3.31E+5
88	216	Ra	9.560	1.82E-7
88	218	Ra	8.581	2.56E-5
88	220	Ra	7.627	2.5E-2
88	222	Ra	6.712	3.8E+1
88	224	Ra	5.823	3.16E+5
88	226	Ra	4.905	5.049E+10
90	218	Th	9.882	1.09E-7
90	220	Th	8.987	9.7E-6
90	222	Th	8.163	2.8E-3
90	224	Th	7.340	1.3E+0
90	226	Th	6.489	2.5E+3
90	228	Th	5.555	8.5E+7
90	230	Th	4.806	3.1E+12
90	232	Th	4.118	5.8E+17
92	222	U	9.766	1.0E-6
92	224	U	8.660	7E-4
92	226	U	7.598	5E-1
92	230	U	6.029	2.67E+6
92	232	U	5.449	3.17E+9
92	234	U	4.894	1.07E+13
92	236	U	4.609	9.99E+14
92	238	U	4.310	1.8E+17
94	232	Pu	6.753	1.7E+4
94	234	Pu	6.347	8.0E+5
94	236	Pu	5.905	1.32E+8
94	238	Pu	5.630	3.87E+9
94	240	Pu	5.292	2.82E+11
94	242	Pu	5.020	1.5E+13
94	244	Pu	4.702	3.24E+15
96	240	Cm	6.435	3.3E+6
96	242	Cm	6.254	1.90E+7
96	244	Cm	5.940	7.48E+8
96	246	Cm	5.512	1.89E+11
96	248	Cm	5.200	1.43E+13
98	240	Cf	7.765	6.36E+1
98	242	Cf	7.555	2.6E+2
98	244	Cf	7.373	1.55E+3
98	246	Cf	6.901	1.647E+5
98	248	Cf	6.405	3.48E+7
98	250	Cf	6.169	4.88E+8
100	246	Fm	8.416	1.2E+0
100	248	Fm	8.042	4.5E+1
100	252	Fm	7.194	1.08E+5
102	252	No	8.588	4.2E+0
102	254	No	8.277	7.2E+1

APPENDIX B - Data set (transitional nuclei)

Z	A		Q (MeV)	$T_{1/2}^{exp}$ (s)
82	210	Pb	3.823	3.7E+16
84	192	Po	7.347	3.4E-2
	194	Po	7.027	4.4E-1
	196	Po	6.687	5.5E+0
	198	Po	6.347	1.5E+2
	200	Po	6.017	4.6E+3
	202	Po	5.737	1.3E+5
	204	Po	5.517	1.9E+6
	206	Po	5.358	1.4E+7
	208	Po	5.247	9.146E+7
	210	Po	5.439	1.19557E+7
86	200	Rn	7.078	1.1E+0
	202	Rn	6.798	1.2E+1
	204	Rn	6.578	1.1E+2
	206	Rn	6.418	5.5E+2
	208	Rn	6.288	2.4E+3
	210	Rn	6.191	9.0E+3
	212	Rn	6.418	1.4E+3
88	206	Ra	7.459	2.4E-1
	208	Ra	7.309	1.4E+0
	210	Ra	7.189	3.7E+0
	212	Ra	7.064	1.3E+1
	214	Ra	7.306	2.46E+0
90	212	Th	7.980	3.0E-2
	214	Th	7.860	8.6E-2
	216	Th	8.100	2.8E-2

APPENDIX C - Decay fit results including transitional nuclei.

This Appendix consists of Tables C.1 to C.6 and lists the results of decay fits to the extended data set of Chapter 4.5.

C.1 to C.3 list the results of the potential fitting approach.

C4. to C.6 list the results of the radius fitting approach.

Table C.1 - *Potential fits with $\Delta G=2$ (transitional nuclei included). The tabulated quantities are the optimum values of S (quality of fit) as a function of the radius and the global quantum number, G (the radius of each nucleus is given by $R=r_0A^{1/3}$). The subscripted quantity is the diffuseness at which the best fit occurs. The shaded regions mark absolute best fits within a family of G values.*

Radius (r_0) (fm)	Values of $G_<$ and $G_>$					
	14-16	**16-18**	**18-20**	**20-22**	**22-24**	**24-26**
1.15	$9.61_{0.70}$	$10.16_{0.64}$	$10.60_{0.59}$	$11.02_{0.54}$	$11.27_{0.51}$	$11.54_{0.48}$
1.16	$9.59_{0.67}$	$10.11_{0.61}$	$10.57_{0.57}$	$10.93_{0.52}$	$11.19_{0.49}$	$11.45_{0.46}$
1.17	$9.55_{0.65}$	$10.05_{0.59}$	$10.50_{0.54}$	$10.86_{0.50}$	$11.11_{0.47}$	$11.38_{0.44}$
1.18	$9.58_{0.63}$	$10.03_{0.57}$	$10.44_{0.52}$	$10.80_{0.48}$	$11.07_{0.45}$	$11.33_{0.42}$
1.19	$9.59_{0.60}$	$10.08_{0.55}$	$10.43_{0.50}$	$10.77_{0.46}$	$11.03_{0.43}$	$11.30_{0.40}$
1.20	$9.63_{0.58}$	$10.07_{0.52}$	$10.45_{0.48}$	$10.76_{0.44}$	$11.02_{0.41}$	$11.29_{0.38}$
1.21	$9.70_{0.55}$	$10.11_{0.50}$	$10.53_{0.45}$	$10.78_{0.42}$	$11.03_{0.39}$	$11.29_{0.36}$
1.22	$9.79_{0.53}$	$10.21_{0.47}$	$10.53_{0.43}$	$10.83_{0.40}$	$11.07_{0.37}$	$11.31_{0.34}$
1.23	$9.87_{0.50}$	$10.26_{0.45}$	$10.59_{0.41}$	$10.93_{0.38}$	$11.13_{0.35}$	$11.34_{0.32}$
1.24	$10.04_{0.47}$	$10.41_{0.43}$	$10.73_{0.39}$	$10.96_{0.35}$	$11.22_{0.33}$	$11.38_{0.30}$
1.25	$10.14_{0.45}$	$10.49_{0.40}$	$10.79_{0.36}$	$11.04_{0.33}$	$11.30_{0.30}$	$11.45_{0.28}$
1.26		$10.67_{0.37}$	$10.93_{0.34}$	$11.18_{0.31}$	$11.38_{0.28}$	
1.27		$10.80_{0.35}$	$11.09_{0.31}$	$11.34_{0.28}$	$11.49_{0.26}$	
1.28		$10.97_{0.32}$	$11.24_{0.29}$	$11.45_{0.26}$	$11.64_{0.24}$	
1.29		$11.21_{0.30}$	$11.45_{0.29}$	$11.65_{0.24}$	$11.85_{0.22}$	
1.30		$11.41_{0.27}$	$11.64_{0.24}$	$11.84_{0.21}$		

Table C.2 - *Potential fits with $\Delta G=4$ (transitional nuclei included). The tabulated quantities are the optimum values of S (quality of fit) as a function of the radius and the global quantum number, G (the radius of each nucleus is given by $R=r_0A^{1/3}$). The subscripted quantity is the diffuseness at which the best fit occurs. The shaded regions mark absolute best fits within a family of G values.*

Radius (r_0) (fm)	Values of $G_<$ and $G_>$					
	14-18	**16-20**	**18-22**	**20-24**	**22-26**	**24-28**
1.02	$7.07_{0.94}$					
1.03	$7.03_{0.92}$					
1.04	$7.01_{0.90}$					
1.05	$6.99_{0.88}$	$7.36_{0.82}$	$7.95_{0.76}$	$8.46_{0.72}$	$9.01_{0.68}$	$9.60_{0.65}$
1.06	$6.99_{0.86}$	$7.33_{0.80}$	$7.89_{0.74}$	$8.40_{0.70}$	$8.96_{0.66}$	$9.45_{0.63}$
1.07	$7.00_{0.84}$	$7.32_{0.78}$	$7.83_{0.73}$	$8.38_{0.68}$	$8.96_{0.65}$	$9.39_{0.61}$
1.08	$7.01_{0.82}$	$7.33_{0.76}$	$7.80_{0.71}$	$8.39_{0.66}$	$8.85_{0.63}$	$9.39_{0.60}$
1.09	$7.03_{0.80}$	$7.34_{0.74}$	$7.80_{0.69}$	$8.34_{0.65}$	$8.79_{0.61}$	$9.27_{0.58}$
1.10	$7.07_{0.78}$	$7.37_{0.72}$	$7.81_{0.67}$	$8.31_{0.63}$	$8.78_{0.59}$	$9.21_{0.56}$
1.11	$7.12_{0.76}$	$7.42_{0.70}$	$7.84_{0.65}$	$8.31_{0.61}$	$8.80_{0.57}$	$9.22_{0.54}$
1.12	$7.19_{0.74}$	$7.47_{0.68}$	$7.88_{0.63}$	$8.33_{0.59}$	$8.85_{0.55}$	$9.27_{0.52}$
1.13	$7.29_{0.72}$	$7.54_{0.66}$	$7.94_{0.61}$	$8.37_{0.57}$	$8.89_{0.54}$	$9.23_{0.51}$
1.14	$7.42_{0.70}$	$7.64_{0.64}$	$8.00_{0.59}$	$8.42_{0.55}$	$8.95_{0.52}$	$9.25_{0.49}$
1.15	$7.48_{0.67}$	$7.75_{0.62}$	$8.09_{0.57}$	$8.49_{0.53}$	$8.97_{0.50}$	$9.27_{0.47}$
1.16	$7.59_{0.65}$	$7.88_{0.59}$	$8.19_{0.55}$	$8.57_{0.51}$	$9.10_{0.49}$	$9.31_{0.45}$
1.17	$7.74_{0.63}$	$7.97_{0.57}$	$8.31_{0.53}$	$8.67_{0.49}$	$9.24_{0.47}$	$9.39_{0.43}$

Table C.3 - *Potential fits with ΔG=2/4 (transitional nuclei included). The tabulated quantities are the optimum values of S (quality of fit) as a function of the radius and the global quantum number, G (the radius of each nucleus is given by $R=r_0A^{1/3}$). The subscripted quantity is the diffuseness at which the best fit occurs. The shaded regions mark absolute best fits within a family of G values.*

Radius (r_0) (fm)	Values of $G_<$ and $G_>$					
	14-16-18	**16-18-20**	**18-20-22**	**20-22-24**	**22-24-26**	**24-26-28**
1.04	$10.42_{0.89}$					
1.05	$10.39_{0.87}$	$10.57_{0.81}$	$10.92_{0.76}$	$11.19_{0.71}$	$11.57_{0.67}$	$11.88_{0.64}$
1.06	$10.37_{0.88}$	$10.51_{0.79}$	$10.81_{0.74}$	$11.14_{0.69}$	$11.51_{0.66}$	$11.80_{0.62}$
1.07	$10.36_{0.83}$	$10.47_{0.77}$	$10.73_{0.72}$	$11.11_{0.68}$	$11.35_{0.64}$	$11.70_{0.61}$
1.08	$10.36_{0.81}$	$10.45_{0.75}$	$10.68_{0.70}$	$10.99_{0.66}$	$11.27_{0.62}$	$11.55_{0.59}$
1.09	$10.38_{0.79}$	$10.44_{0.73}$	$10.65_{0.68}$	$10.92_{0.64}$	$11.23_{0.60}$	$11.49_{0.57}$
1.10	$10.40_{0.77}$	$10.44_{0.71}$	$10.64_{0.64}$	$10.88_{0.62}$	$11.23_{0.59}$	$11.49_{0.55}$
1.11	$10.44_{0.75}$	$10.46_{0.69}$	$10.65_{0.62}$	$10.86_{0.60}$	$11.13_{0.57}$	$11.37_{0.54}$
1.12	$10.50_{0.73}$	$10.48_{0.67}$	$10.66_{0.60}$	$10.86_{0.58}$	$11.08_{0.55}$	$11.30_{0.52}$
1.13	$10.58_{0.70}$	$10.52_{0.65}$	$10.69_{0.58}$	$10.87_{0.56}$	$11.05_{0.53}$	$11.27_{0.50}$
1.14	$10.60_{0.68}$	$10.58_{0.63}$	$10.72_{0.56}$	$10.90_{0.54}$	$11.05_{0.51}$	$11.29_{0.48}$
1.15	$10.66_{0.66}$	$10.65_{0.61}$	$10.77_{0.54}$	$10.93_{0.52}$	$11.07_{0.49}$	$11.33_{0.46}$
1.16	$10.75_{0.64}$	$10.74_{0.58}$	$10.83_{0.52}$	$10.97_{0.50}$	$11.11_{0.47}$	$11.29_{0.45}$
1.17	$10.88_{0.62}$	$10.78_{0.56}$	$10.91_{0.50}$	$11.01_{0.48}$	$11.16_{0.45}$	$11.29_{0.43}$
1.18		$10.85_{0.54}$	$11.01_{0.48}$	$11.06_{0.46}$		$11.31_{0.41}$
1.19		$10.96_{0.52}$	$11.14_{0.46}$	$11.12_{0.44}$		$11.35_{0.39}$

Table C.4 - *Radius fits with ΔG=2 (transitional nuclei included). The tabulated quantities are the optimum values of S (quality of fit) as a function of the diffuseness and the global quantum number, G. The subscripted quantity is the potential depth (in MeV) at which the best fit occurs. The shaded regions mark absolute best fits within a family of G values and the dotted line demarcates those values of G and a which require potential depths, V_0, outside the parameter range we consider physically acceptable.*

Diffuseness (fm)	Values of $G_<$ and $G_>$					
	14-16	**16-18**	**18-20**	**20-22**	**22-24**	**24-26**
0.20	13.24_{92}	9.00_{108}	7.15_{126}	6.86_{146}	7.58_{168}	8.92_{193}
0.25	12.50_{94}	8.63_{111}	7.04_{129}	6.92_{150}	7.81_{173}	9.31_{198}
0.30	11.84_{96}	8.29_{113}	6.93_{133}	7.05_{154}	8.11_{178}	9.76_{204}
0.35	11.21_{99}	7.90_{116}	6.86_{136}	7.24_{159}	8.50_{183}	10.3_{211}
0.40	10.43_{101}	7.62_{119}	6.83_{140}	7.46_{163}	8.88_{189}	10.8_{218}
0.45	9.98_{104}	7.41_{123}	6.87_{144}	7.74_{168}	9.37_{195}	11.5_{225}
0.50	9.30_{106}	7.13_{126}	7.03_{148}	8.06_{174}	9.89_{202}	12.7_{233}
0.55	8.77_{109}	7.02_{130}	7.13_{153}	8.48_{180}	10.50_{209}	13.0_{242}
0.60	8.32_{112}	7.03_{133}	7.36_{158}	8.94_{186}	11.19_{217}	13.8_{251}
0.65	8.00_{115}	7.11_{137}	7.69_{164}	9.51_{193}	11.97_{225}	14.8_{262}
0.70	7.58_{119}	7.00_{142}	8.05_{169}	10.1_{200}	12.8_{235}	
0.75	7.35_{123}	7.11_{147}	8.49_{176}	10.8_{208}	13.8_{245}	
0.80	7.15_{127}	7.32_{153}	9.04_{183}	11.6_{217}	14.8_{256}	
0.85	7.05_{131}	7.62_{158}	9.62_{190}	12.5_{226}		
0.90	7.03_{136}	7.98_{165}	10.3_{198}	13.46_{237}		
0.95	7.10_{141}	8.43_{171}	11.1_{207}	14.47_{248}		
1.00	7.29_{146}	8.96_{179}	11.92_{217}			

Table C.5 - *Radius fits with $\Delta G=4$ (transitional nuclei included). The tabulated quantities are the optimum values of S (quality of fit) as a function of the diffuseness and the global quantum number, G. The subscripted quantity is the potential depth (in MeV) at which the best fit occurs. The shaded regions mark absolute best fits within a family of G values and the dotted line demarcates those values of G and a which require potential depths, V_0, outside the parameter range we consider physically acceptable.*

Diffuseness (fm)	Values of $G_<$ and $G_>$					
	14-18	**16-20**	**18-22**	**20-24**	**22-26**	**24-28**
0.20	90.5_{99}	67.8_{116}	50.8_{135}	38.2_{156}	29.0_{179}	22.3_{204}
0.25	87.4_{101}	65.2_{118}	48.6_{138}	36.4_{160}	27.6_{184}	21.3_{210}
0.30	84.4_{103}	62.6_{121}	46.4_{142}	34.7_{164}	26.3_{189}	20.3_{216}
0.35	81.1_{106}	59.9_{125}	44.3_{146}	33.0_{169}	25.1_{196}	19.3_{224}
0.40	78.0_{109}	57.2_{128}	42.1_{150}	31.3_{174}	23.6_{202}	18.3_{231}
0.45	74.8_{111}	54.6_{132}	40.1_{155}	29.6_{180}	22.3_{208}	17.4_{239}
0.50	71.5_{115}	52.0_{135}	37.9_{159}	28.0_{186}	21.1_{215}	16.5_{248}
0.55	68.1_{118}	49.3_{140}	35.8_{164}	26.3_{192}	19.9_{223}	15.7_{258}
0.60	64.8_{121}	46.6_{144}	33.8_{170}	24.8_{199}	18.8_{232}	14.9_{268}
0.65	61.5_{125}	44.0_{149}	31.7_{176}	23.3_{207}	17.7_{241}	14.3_{280}
0.70	58.3_{129}	41.4_{154}	29.7_{182}	21.8_{215}		
0.75	55.1_{133}	38.9_{159}	27.9_{189}	20.5_{224}		
0.80	52.0_{138}	36.5_{165}	26.2_{198}	19.3_{233}		
0.85	49.0_{143}	34.3_{172}	24.5_{206}	18.2_{244}		
0.90	46.0_{148}	32.1_{179}	23.0_{215}	17.3_{256}		
0.95	43.4_{154}	30.1_{186}	21.6_{225}	16.4_{268}		
1.00	40.8_{160}	28.3_{195}	20.4_{235}			

Table C.6 - *Radius fits with ΔG=2/4 (transitional nuclei included). The tabulated quantities are the optimum values of S (quality of fit) as a function of the diffuseness and the global quantum number, G. The subscripted quantity is the potential depth (in MeV) at which the best fit occurs. The shaded regions mark absolute best fits within a family of G values and the dotted line demarcates those values of G and a which require potential depths, V_0, outside the parameter range we consider physically acceptable.*

Diffuseness (fm)	Values of $G_<$ and $G_>$					
	14-16-18	**16-18-20**	**18-20-22**	**20-22-24**	**22-24-26**	**24-26-28**
0.20	74.2_{102}	54.4_{119}	40.1_{138}	29.8_{160}	22.4_{183}	17.4_{209}
0.25	71.4_{104}	52.1_{122}	38.2_{142}	28.3_{164}	21.3_{188}	16.5_{215}
0.30	68.6_{107}	49.8_{125}	36.4_{146}	26.9_{169}	20.2_{194}	15.8_{222}
0.35	65.8_{109}	47.6_{128}	34.5_{150}	25.5_{174}	19.2_{200}	15.0_{229}
0.40	62.8_{112}	45.2_{132}	32.7_{154}	24.1_{179}	18.2_{207}	14.3_{237}
0.45	60.0_{115}	43.1_{135}	30.9_{159}	22.7_{185}	17.2_{214}	13.6_{245}
0.50	57.1_{118}	40.6_{140}	29.2_{164}	21.4_{191}	16.3_{221}	13.0_{254}
0.55	54.3_{122}	38.3_{144}	27.4_{169}	20.1_{198}	15.4_{229}	12.5_{264}
0.60	51.3_{125}	36.1_{149}	25.7_{175}	18.9_{205}	14.6_{238}	12.1_{275}
0.65	48.5_{129}	34.0_{154}	24.1_{181}	17.7_{213}	13.8_{248}	11.7_{287}
0.70	45.7_{133}	31.8_{159}	22.6_{188}	16.7_{221}		
0.75	43.0_{138}	29.8_{165}	21.1_{196}	15.8_{230}		
0.80	40.3_{143}	27.8_{171}	19.8_{204}	14.9_{241}		
0.85	37.8_{148}	26.0_{178}	18.5_{212}	14.2_{252}		
0.90	35.5_{153}	24.3_{185}	17.5_{221}	13.6_{264}		
0.95	33.2_{160}	22.78_{193}	16.5_{232}			
1.00	31.6_{165}	21.39_{202}	15.6_{243}			

APPENDIX D - Decay fit results using alternative values of the preformation factor, P.

This Appendix consists of Tables D.1 to D.4 and lists the results of decay fits (radius fit approach, with $\Delta G=2$) using alternative values of the preformation factor, as described in Chapter 4.6.

D.1 - P = 0.1

D.2 - P = 0.01

D.3 - P = 0.001

D.4 - P = 0.0001

Table D.1 - *Radius fits with P=0.1 (ΔG=2; transitional nuclei are excluded). The tabulated quantities are the optimum values of S (quality of fit) as a function of the diffuseness and the global quantum number, G. The subscripted quantity is the potential depth (in MeV) at which the best fit occurs. The shaded regions mark absolute best fits within a family of G values and the dotted line demarcates those values of G and a which require potential depths, V_0, outside the parameter range we consider physically acceptable..*

Diffuseness (fm)	Values of $G_<$ and $G_>$					
	14-16	**16-18**	**18-20**	**20-22**	**22-24**	**24-26**
0.20	16.0_{82}	10.0_{96}	6.50_{111}	4.95_{128}	4.58_{147}	5.00_{168}
0.25	15.2_{83}	9.34_{98}	6.21_{114}	4.80_{131}	4.59_{151}	5.18_{172}
0.30	14.1_{85}	8.65_{100}	5.79_{116}	4.70_{135}	4.64_{155}	5.36_{177}
0.35	13.1_{87}	8.03_{102}	5.46_{119}	4.55_{138}	4.73_{159}	5.60_{182}
0.40	12.2_{89}	7.59_{104}	5.18_{122}	4.52_{142}	4.90_{164}	5.92_{187}
0.45	11.4_{91}	7.48_{106}	4.96_{125}	4.52_{146}	5.06_{168}	6.23_{193}
0.50	10.5_{93}	6.51_{110}	4.79_{129}	4.53_{150}	5.30_{173}	6.63_{199}
0.55	9.78_{95}	6.10_{113}	4.61_{132}	4.63_{154}	5.56_{179}	7.06_{206}
0.60	9.03_{98}	5.69_{116}	4.50_{136}	4.76_{159}	5.91_{185}	7.56_{213}
0.65	8.29_{100}	5.30_{119}	4.46_{140}	4.96_{164}	6.30_{191}	8.14_{221}
0.70	7.60_{103}	5.05_{122}	4.51_{145}	5.24_{170}	6.77_{198}	8.77_{229}
0.75	7.00_{106}	4.78_{126}	4.56_{149}	5.57_{176}	7.30_{205}	9.49_{238}
0.80	6.45_{109}	4.62_{130}	4.71_{154}	5.94_{182}	7.91_{213}	10.28_{248}
0.85	5.97_{112}	4.54_{134}	4.90_{160}	6.41_{189}	8.58_{222}	
0.90	5.59_{116}	4.49_{139}	5.19_{166}	6.96_{196}	9.33_{231}	
0.95	5.28_{119}	4.54_{144}	5.53_{172}	7.55_{205}	10.1_{242}	
1.00	5.03_{123}	4.66_{149}	5.95_{179}	8.22_{214}	11.0_{253}	

Table D.2 - *Radius fits with P=0.01 (ΔG=2; transitional nuclei are excluded). The tabulated quantities are the optimum values of S (quality of fit) as a function of the diffuseness and the global quantum number, G. The subscripted quantity is the potential depth (in MeV) at which the best fit occurs. The shaded regions mark absolute best fits within a family of G values and the dotted line demarcates those values of G and a which require potential depths, V_0, outside the parameter range we consider physically acceptable.*

Diffuseness (fm)	Values of $G_<$ and $G_>$					
	16-18	**18-20**	**20-22**	**22-24**	**24-26**	**26-28**
0.20	16.1_{84}	10.7_{98}	7.46_{112}	5.65_{129}	4.97_{147}	4.90_{166}
0.25	15.1_{86}	10.0_{100}	6.94_{115}	5.40_{132}	4.83_{150}	4.94_{170}
0.30	14.3_{88}	9.34_{102}	6.62_{118}	5.16_{135}	4.75_{154}	5.01_{175}
0.35	13.5_{90}	8.72_{104}	6.19_{120}	4.99_{138}	4.71_{158}	5.10_{179}
0.40	12.6_{91}	8.24_{106}	5.82_{123}	4.83_{142}	4.72_{162}	5.23_{184}
0.45	11.8_{93}	7.59_{109}	5.52_{126}	4.75_{145}	4.77_{167}	5.39_{190}
0.50	10.9_{96}	7.15_{112}	5.28_{130}	4.65_{149}	4.85_{171}	5.61_{195}
0.55	10.1_{98}	6.66_{114}	4.97_{133}	4.58_{154}	4.97_{176}	5.87_{201}
0.60	9.33_{100}	6.21_{117}	4.79_{137}	4.56_{158}	5.10_{182}	6.14_{208}
0.65	8.87_{102}	5.82_{121}	4.65_{141}	4.60_{163}	5.32_{188}	6.50_{215}
0.70	8.01_{105}	5.39_{124}	4.51_{145}	4.69_{168}	5.58_{194}	6.93_{223}
0.75	7.34_{108}	5.15_{127}	4.45_{149}	4.86_{174}	5.91_{201}	7.39_{231}
0.80	6.78_{111}	4.84_{131}	4.43_{154}	5.07_{180}	6.29_{208}	7.93_{240}
0.85	6.32_{114}	4.65_{135}	4.49_{159}	5.31_{186}	6.73_{216}	8.51_{249}
0.90	5.78_{118}	4.47_{140}	4.60_{165}	5.63_{193}	7.25_{224}	9.17_{260}
0.95	5.42_{122}	4.43_{145}	4.78_{171}	6.03_{200}	7.81_{234}	9.88_{271}
1.00	5.10_{126}	4.39_{150}	5.00_{177}	6.48_{208}	8.42_{244}	10.7_{283}

Table D.3 - *Radius fits with P=0.001 (ΔG=2; transitional nuclei are excluded). The tabulated quantities are the optimum values of S (quality of fit) as a function of the diffuseness and the global quantum number, G. The subscripted quantity is the potential depth (in MeV) at which the best fit occurs. The shaded regions mark absolute best fits within a family of G values and the dotted line demarcates those values of G and a which require potential depths, V_0, outside the parameter range we consider physically acceptable.*

Diffuseness (fm)	Values of $G_<$ and $G_>$					
	20-22	**22-24**	**24-26**	**26-28**	**28-30**	**30-32**
0.20	12.0_{99}	8.85_{113}	6.98_{129}	5.91_{145}	5.50_{163}	5.48_{183}
0.25	11.4_{101}	8.45_{116}	6.65_{131}	5.68_{149}	5.38_{167}	5.50_{187}
0.30	10.7_{103}	7.88_{118}	6.33_{134}	5.49_{152}	5.31_{172}	5.52_{192}
0.35	10.1_{105}	7.46_{121}	6.00_{138}	5.31_{156}	5.22_{176}	5.55_{197}
0.40	9.51_{108}	7.08_{124}	5.69_{141}	5.17_{160}	5.23_{181}	5.60_{203}
0.45	8.86_{110}	6.69_{127}	5.52_{145}	5.08_{164}	5.24_{186}	5.72_{209}
0.50	8.32_{113}	6.27_{130}	5.26_{148}	5.02_{169}	5.26_{191}	5.85_{215}
0.55	7.81_{115}	5.88_{133}	5.08_{152}	4.98_{173}	5.35_{196}	6.04_{221}
0.60	7.25_{118}	5.62_{136}	4.96_{156}	4.98_{178}	5.47_{202}	6.26_{228}
0.65	6.78_{121}	5.30_{140}	4.81_{161}	5.00_{184}	5.62_{209}	6.52_{236}
0.70	6.36_{125}	5.05_{144}	4.76_{166}	5.10_{190}	5.83_{216}	6.83_{244}
0.75	5.89_{128}	4.87_{148}	4.73_{171}	5.21_{196}	6.07_{223}	7.20_{253}
0.80	5.56_{132}	4.71_{153}	4.76_{176}	5.38_{202}	6.37_{231}	7.60_{262}
0.85	5.25_{136}	4.62_{158}	4.82_{182}	5.61_{209}	6.73_{239}	8.07_{272}
0.90	4.95_{140}	4.54_{163}	4.97_{189}	5.87_{217}	7.14_{249}	8.60_{283}
0.95	4.71_{144}	4.54_{168}	5.13_{195}	6.21_{225}	7.61_{259}	9.17_{295}
1.00	4.54_{149}	4.58_{174}	5.36_{203}	6.60_{234}	8.12_{270}	9.80_{308}

Table D.4 - *Radius fits with P=0.0001 (ΔG=2; transitional nuclei are excluded). The tabulated quantities are the optimum values of S (quality of fit) as a function of the diffuseness and the global quantum number, G. The subscripted quantity is the potential depth (in MeV) at which the best fit occurs. The shaded regions mark absolute best fits within a family of G values and the dotted line demarcates those values of G and* a *which require potential depths, V_0, outside the parameter range we consider physically acceptable.*

Diffuseness (fm)	Values of $G_<$ and $G_>$					
	24-26	**26-28**	**28-30**	**30-32**	**32-34**	**34-36**
0.20	11.4_{114}	8.94_{128}	7.64_{143}	6.82_{160}	6.46_{178}	6.38_{198}
0.25	10.6_{116}	8.58_{130}	7.28_{147}	6.56_{164}	6.30_{183}	6.33_{203}
0.30	9.94_{118}	8.11_{133}	6.94_{150}	6.35_{168}	6.16_{187}	6.26_{208}
0.35	9.51_{121}	7.71_{136}	6.71_{154}	6.17_{172}	6.06_{192}	6.20_{213}
0.40	8.91_{123}	7.35_{140}	6.41_{157}	6.02_{176}	5.98_{197}	6.21_{219}
0.45	8.40_{126}	6.93_{143}	6.16_{161}	5.86_{181}	5.92_{202}	6.22_{225}
0.50	7.92_{129}	6.63_{146}	5.95_{165}	5.76_{186}	5.90_{208}	6.27_{231}
0.55	7.48_{132}	6.29_{150}	5.76_{170}	5.66_{191}	5.90_{214}	6.35_{238}
0.60	7.10_{135}	6.00_{154}	5.60_{174}	5.61_{196}	5.93_{220}	6.47_{245}
0.65	6.65_{139}	5.76_{158}	5.47_{179}	5.58_{202}	6.00_{227}	6.61_{253}
0.70	6.31_{143}	5.55_{163}	5.39_{185}	5.60_{208}	6.10_{234}	6.80_{262}
0.75	5.98_{147}	5.37_{167}	5.30_{190}	5.65_{215}	6.25_{242}	7.03_{271}
0.80	5.65_{151}	5.22_{172}	5.28_{196}	5.73_{222}	6.43_{250}	7.31_{280}
0.85	5.39_{155}	5.09_{178}	5.32_{203}	5.88_{230}	6.66_{259}	7.61_{291}
0.90	5.16_{160}	5.04_{184}	5.38_{209}	6.04_{238}	6.95_{269}	7.99_{302}
0.95	4.98_{165}	5.00_{190}	5.47_{217}	6.27_{247}	7.27_{279}	8.41_{315}
1.00	4.87_{171}	5.02_{196}	5.63_{225}	6.54_{256}	7.66_{291}	8.86_{328}

APPENDIX E - Opical model fits using alternative values of the preformation factor, P.

This Appendix consists of Tables E.Hf1 to E.U4 and lists the results of optical potential fits to the scattering of 24.7MeV alpha particles off Hf, W, Au, Bi and U respectively, using values of the preformation factor P=0.1, 0.01, 0.001 and 0.0001 in turn (see Chapter 5.6).

Table E.Hf1 - *Optical model fits to Hf scattering data (P=0.1). For each value of diffuseness we give the value of χ^2; the fitted parameters r_r and r_i; and the relevant decay radius for comparison. Shaded sections mark approximately where decay and scattering parameters 'overlap'. Table D.1 provides the additional information on the relevant decay S and V_0.*

The format is: χ^2 r_r r_i r_{decay} $\chi^2_{opt}=0.150$

Diffuseness	18-20		20-22		22-24	
0.30	12.0	1.8	12.0	1.8	13.0	1.9
		1.2		1.3		0.8
		1.365		1.355		1.350
0.35	4.9562	1.640	4.9795	1.632	4.9988	1.624
		1.182		1.214		1.244
		1.345		1.335		1.329
0.40	1.8244	1.519	1.8401	1.509	1.8559	1.500
		1.086		1.130		1.165
		1.322		1.313		1.303
0.45	0.5212	1.427	0.5303	1.416	0.5429	1.405
		0.9537		1.003		1.065
		1.305		1.291		1.283
0.50	0.1740	1.351	0.1757	1.338	0.1763	1.326
		1.113		1.114		1.118
		1.280		1.269		1.259
0.55	0.1558	1.301	0.1549	1.286	0.1543	1.272
		1.322		1.319		1.317
		1.262		1.243		1.232
0.60	0.1503	1.249	0.1503	1.233	0.1507	1.217
		1.344		1.343		1.342
		1.238		1.222		1.206
0.65	0.1499	1.193	0.1499	1.175	0.1496	1.158
		1.342		1.341		1.340
		1.216		1.198		1.181
0.70	0.1541	1.133	0.1534	1.114	0.1528	1.095
		1.330		1.330		1.329
		1.189		1.174		1.153
0.75	0.1636	1.073	0.1632	1.050	0.1631	1.030
		1.313		1.312		1.312
		1.168		1.147		1.126
0.80	0.1780	1.009	0.1773	0.9858	0.1766	0.9635
		1.291		1.290		1.290
		1.143		1.119		1.097

Table E.Hf2 - *Optical model fits to Hf scattering data (P=0.01). For each value of diffuseness we give the value of χ^2; the fitted parameters r_r and r_i; and the relevant decay radius for comparison. Shaded sections mark approximately where decay and scattering parameters 'overlap'. Table D.2 provides the additional information on the relevant decay S and V_o.*

The format is: χ^2 r_r r_i r_{decay} $\chi^2_{opt}=0.150$

Diffuseness	20-22		22-24		24-26	
0.30	12.0	1.8	12.0	1.8	12.0	1.8
		1.0		1.0		1.1
		1.463		1.459		1.453
0.35	4.9583	1.640	4.9907	1.631	5.0007	1.624
		1.185		1.003		1.157
		1.447		1.439		1.430
0.40	1.8260	1.519	1.8401	1.509	1.8500	1.500
		1.164		1.130		1.137
		1.426		1.414		1.408
0.45	0.5213	1.426	0.5684	1.419	0.5460	1.406
		0.9544		1.248		1.080
		1.405		1.395		1.381
0.50	0.1693	1.349	0.1671	1.338	0.1727	1.327
		1.250		1.353		1.104
		1.378		1.371		1.360
0.55	0.1560	1.300	0.1549	1.286	0.1548	1.274
		1.321		1.319		1.318
		1.358		1.343		1.334
0.60	0.1502	1.248	0.1504	1.233	0.1513	1.219
		1.344		1.343		1.342
		1.333		1.321		1.306
0.65	0.1498	1.192	0.1499	1.176	0.1493	1.159
		1.342		1.341		1.340
		1.309		1.295		1.279
0.70	0.1541	1.133	0.1533	1.115	0.1530	1.098
		1.330		1.330		1.329
		1.286		1.270		1.252
0.75	0.1636	1.073	0.1633	1.052	0.1631	1.033
		1.313		1.312		1.312
		1.263		1.241		1.223
0.80	0.1780	1.009	0.1773	0.9874	0.1767	0.9669
		1.291		1.291		1.290
		1.236		1.213		1.195

Table E.Hf3 - *Optical model fits to Hf scattering data (P=0.001). For each value of diffuseness we give the value of χ^2; the fitted parameters r_r and r_i; and the relevant decay radius for comparison. Shaded sections mark approximately where decay and scattering parameters 'overlap'. Table D.3 provides the additional information on the relevant decay S and V_0.*

The format is: χ^2 r_r r_i r_{decay} $\chi^2_{opt}=0.150$

Diffuseness	24-26		26-28		28-30	
0.30	12.0	1.8 1.0 1.570	12.0	1.8 1.4 1.563	12.0	1.8 1.1 1.554
0.35	4.9942	1.628 1.149 1.543	4.9927	1.625 1.150 1.538	5.0029	1.618 1.162 1.531
0.40	1.8377	1.509 1.1170 1.522	1.8428	1.501 1.110 1.514	1.8509	1.492 1.131 1.504
0.45	0.5325	1.416 1.022 1.495	0.5533	1.407 1.106 1.490	0.5676	1.398 1.128 1.478
0.50	0.1725	1.339 1.092 1.475	0.1700	1.328 1.094 1.462	0.1728	1.318 1.130 1.452
0.55	0.1548	1.288 1.320 1.450	0.1559	1.275 1.319 1.439	0.1586	1.263 1.318 1.427
0.60	0.1508	1.235 1.343 1.426	0.1515	1.221 1.342 1.413	0.1505	1.207 1.340 1.339
0.65	0.1498	1.177 1.341 1.398	0.1488	1.162 1.340 1.383	0.1484	1.147 1.430 1.339
0.70	o.1533	1.117 1.330 1.370	0.1534	1.100 1.330 1.354	0.1537	1.084 1.329 1.330
0.75	0.1634	1.054 1.312 1.025	0.1629	1.036 1.312 1.326	0.1621	1.019 1.312 1.310
0.80	0.1773	0.9905 1.291 1.009	0.1769	0.9710 1.290 1.299	0.1768	0.9520 1.290 1.279

Table E.Hf4 - *Optical model fits to Hf scattering data (P=0.0001). For each value of diffuseness we give the value of χ^2; the fitted parameters r_r and r_i; and the relevant decay radius for comparison. Shaded sections mark approximately where decay and scattering parameters 'overlap'. Table D.4 provides the additional information on the relevant decay S and V_o.*

The format is: χ^2 r_r r_i r_{decay} $\chi^2_{opt}=0.150$

Diffuseness	28-30		30-32		32-34	
0.30			12.0	1.8		
				1.1		
				1.669		
0.35	5.0002	1.634	5.0035	1.620	5.0130	1.613
		1.247		1.255		1.268
		1.651		1.644		1.637
0.40	1.8382	1.503	1.8442	1.495	1.8447	1.487
		1.117		1.133		1.086
		1.627		1.620		1.610
0.45	0.5540	1.408	0.5597	1.399	0.5624	1.391
		1.102		1.106		1.121
		1.601		1.591		1.584
0.50	0.1688	1.330	0.1902	1.325	0.1935	1.312
		1.093		1.251		1.186
		1.576		1.563		1.554
0.55	0.1570	1.277	0.1583	1.266	0.1551	1.254
		1.320		1.316		1.314
		1.546		1.536		1.525
0.60	0.1510	1.223	0.1492	1.211	0.1498	1.199
		1.342		1.341		1.341
				1.510		1.505
0.65	0.1486	1.165	0.1494	1.151	0.1499	1.138
		1.341		1.340		1.340
				1.480		1.466
0.70	0.1538	1.103	0.1532	1.089	0.1523	1.074
		1.330		1.329		1.329
				1.452		1.437
0.75	0.1627	1.040	0.1625	1.024	0.1628	1.008
		1.312		1.312		1.312
				1.420		1.405
0.80	0.1772	0.9753	0.1762	0.9576	0.1761	0.9408
		1.290		1.290		1.290
				1.390		1.374

Table E.W1 - *Optical model fits to W scattering data (P=0.1). For each value of diffuseness we give the value of χ^2; the fitted parameters r_r and r_i; and the relevant decay radius for comparison. Shaded sections mark approximately where decay and scattering parameters 'overlap'. Table D.1 provides the additional information on the relevant decay S and V_0.*

The format is: χ^2 r_r r_i r_{decay} $\chi^2_{opt}=0.214$

Diffuseness	18-20		20-22		22-24
0.30	4.5	1.706	4.4	1.699	1.703
		1.104		1.259	0.734
		1.358		1.346	1.341
0.35	2.29	1.602	2.33	1.600	1.587
		0.6403		0.7795	0.7789
		1.337		1.328	1.320
0.40	1.252	1.532	1.263	1.522	1.513
		1.193		1.209	1.230
		1.317		1.305	1.294
0.45	0.6199	1.463	0.6265	1.452	1.441
		1.015		1.064	1.118
		1.298		1.282	1.274
0.50	0.3208	1.400	0.3250	1.388	1.375
		1.066		1.085	1.105
		1.273		1.261	1.251
0.55	0.2157	1.342	0.2214	1.328	1.314
		1.110		1.148	1.175
		1.255		1.240	1.224
0.60	0.2167	1.291	0.2155	1.275	1.258
		1.262		1.253	1.242
		1.232		1.215	1.198
0.65	0.2277	1.241	0.2264	1.223	1.206
		1.297		1.295	1.295
		1.209		1.191	1.173
0.70	0.2445	1.187	0.2451	1.168	1.149
		1.298		1.298	1.298
		1.183		1.164	1.146
0.75	0.2643	1.133	0.2633	1.111	1.091
		1.286		1.284	1.283
		1.162		1.137	1.119
0.80	0.2843	1.077	0.2834	1.053	1.031
		1.266		1.265	1.265
		1.137		1.112	1.090

Table E.W2 - *Optical model fits to W scattering data (P=0.01). For each value of diffuseness we give the value of χ^2; the fitted parameters r_r and r_i; and the relevant decay radius for comparison. Shaded sections mark approximately where decay and scattering parameters 'overlap'. Table D.2 provides the additional information on the relevant decay S and V_0.*

The format is: χ^2 r_r r_i r_{decay} $\chi^2_{opt}=0.214$

Diffuseness	20-22		22-24		24-26	
0.30	4.5	1.7	4.4	1.701	4.4	1.696
		1.1		0.9057		0.7533
		1.454		1.450		1.443
0.35	2.29	1.599	2.33	1.601	2.32	1.590
		0.6263		0.7795		0.7710
		1.439		1.430		1.420
0.40	1.254	1.532	1.263	1.522	1.268	1.513
		1.197		1.209		1.204
		1.418		1.405		1.398
0.45	0.6184	1.463	0.6288	1.452	0.6382	1.442
		1.002		1.080		1.130
		1.397		1.386		1.371
0.50	0.3218	1.399	0.3234	1.388	0.3258	1.376
		1.072		1.076		1.091
		1.370		1.363		1.350
0.55	0.2147	1.341	0.2214	1.328	0.2271	1.316
		1.101		1.148		1.166
		1.351		1.335		1.325
0.60	0.2171	1.290	0.2147	1.275	0.2109	1.260
		1.264		1.251		1.239
		1.326		1.313		1.297
0.65	0.2279	1.240	0.2266	1.223	0.2276	1.207
		1.297		1.295		1.297
		1.302		1.287		1.270
0.70	0.2445	1.187	0.2455	1.169	0.2458	1.151
		1.298		1.298		1.297
		1.279		1.262		1.244
0.75	0.2643	1.133	0.2629	1.112	0.2608	1.093
		1.286		1.284		1.283
		1.256		1.233		1.215
0.80	0.2843	1.077	0.2837	1.055	0.2849	1.034
		1.266		1.265		1.265
		1.230		1.206		1.187

Table E.W3 - *Optical model fits to W scattering data (P=0.001). For each value of diffuseness we give the value of χ^2; the fitted parameters r_r and r_i; and the relevant decay radius for comparison. Shaded sections mark approximately where decay and scattering parameters 'overlap'. Table D.3 provides the additional information on the relevant decay S and V_o.*

The format is: χ^2 r_r r_i r_{decay} $\chi^2_{opt}=0.214$

Diffuseness	24-26		26-28		28-30	
0.30	4.5	1.7	4.5	1.7	4.5	1.7
		1.1		1.1		1.2
		1.560		1.553		1.543
0.35	2.33	1.600	2.37	1.596	2.36	1.591
		0.7795		0.7843		0.8923
		1.533		1.527		1.520
0.40	1.260	1.522	1.258	1.513	1.251	1.504
		1.199		1.147		1.109
		1.512		1.503		1.493
0.45	0.6288	1.452	0.6458	1.444	0.6595	1.434
		1.080		1.159		1.192
		1.489		1.480		1.467
0.50	0.3219	1.388	0.3240	1.377	0.3321	1.367
		1.067		1.083		1.128
		1.466		1.452		1.442
0.55	0.2220	1.329	0.2232	1.317	0.2183	1.305
		1.147		1.141		1.123
		1.441		1.429		1.417
0.60	0.2133	1.276	0.2110	1.263	0.2152	1.250
		1.248		1.249		1.265
		1.418		1.403		1.390
0.65	0.2272	1.225	0.2298	1.210	0.2318	1.195
		1.297		1.299		1.297
		1.389		1.374		1.359
0.70	0.2457	1.171	0.2444	1.154	0.2409	1.138
		1.298		1.296		1.293
		1.362		1.345		1.330
0.75	0.2623	1.115	0.2614	1.097	0.2639	1.080
		1.284		1.284		1.285
		1.337		1.317		1.301
0.80	0.2845	1.058	0.2851	1.038	0.2825	1.020
		1.266		1.265		1.264
		1.311		1.291		1.271

Table E.W4 - *Optical model fits to W scattering data (P=0.0001). For each value of diffuseness we give the value of χ^2; the fitted parameters r_r and r_i; and the relevant decay radius for comparison. Shaded sections mark approximately where decay and scattering parameters 'overlap'. Table D.4 provides the additional information on the relevant decay S and V_o.*

The format is: χ^2 r_r r_i r_{decay} $\chi^2_{opt}=0.214$

Diffuseness	28-30		30-32		32-34	
0.30	4.5	1.696 1.184 1.663	4.5	1.7 1.3 1.657	4.5	1.7 1.4 1.652
0.35	2.37	1.599 0.8783 1.636	2.41	1.591 1.292 1.632	2.43	1.585 1.334 1.625
0.40	1.241	1.514 1.022 1.616	1.24	1.508 1.006 1.608	1.256	1.501 1.145 1.598
0.45	0.6486	1.445 1.169 1.590	0.6512	1.435 1.166 1.580	0.6389	1.426 1.128 1.572
0.50	0.3297	1.382 1.113 1.565	0.3381	1.369 1.145 1.552	0.3487	1.360 1.166 1.542
0.55	0.2170	1.318 1.105 1.536	0.2129	1.308 1.110 1.525	0.2242	1.298 1.177 1.514
0.60	0.2138	1.266 1.260 1.514	0.2208	1.254 1.272 1.500	0.2212	1.241 1.258 1.486
0.65	0.2308	1.213 1.298 1.486	0.2274	1.199 1.291 1.470	0.2232	1.186 1.290 1.456
0.70	0.2427	1.157 1.295 1.456	0.2426	1.143 1.296 1.442	0.2469	1.129 1.298 1.426
0.75	0.2631	1.101 1.285 1.428	0.2642	1.084 1.284 1.410	0.2599	1.069 1.282 1.395
0.80	0.2842	1.043 1.265 1.399	0.2818	1.025 1.264 1.380	0.2848	1.008 1.265 1.364

Table E.Au1 - *Optical model fits to Au scattering data (P=0.1). For each value of diffuseness we give the value of χ^2; the fitted parameters r_r and r_i; and the relevant decay radius for comparison. Shaded sections mark approximately where decay and scattering parameters 'overlap'. Table D.1 provides the additional information on the relevant decay S and V_0.*

The format is: χ^2 r_r r_i r_{decay} $\chi^2_{opt}=0.135$

Diffuseness	18-20		20-22		22-24
0.30	6.5	1.814	6.5	1.802	1.8
		1.124		0.7193	1.1
		1.353		1.340	1.334
0.35	2.55	1.666	2.57	1.659	1.651
		0.9828		1.145	1.182
		1.332		1.322	1.313
0.40	1.053	1.578	0.9027	1.554	1.545
		1.199		0.8203	1.150
		1.313		1.299	1.288
0.45	0.2564	1.483	0.2603	1.471	1.461
		1.053		1.070	1.091
		1.293		1.277	1.268
0.50	0.1311	1.415	0.1315	1.403	1.391
		1.287		1.283	1.283
		1.269		1.256	1.245
0.55	0.1420	1.367	0.1532	1.348	1.336
		1.395		1.377	1.378
		1.251		1.235	1.218
0.60	0.1503	1.317	0.1497	1.301	1.286
		1.421		1.420	1.419
		1.228		1.210	1.193
0.65	0.1654	1.262	0.1648	1.244	1.228
		1.414		1.414	1.413
		1.206		1.187	1.168
0.70	0.1847	1.203	0.1840	1.184	1.166
		1.400		1.399	1.399
		1.180		1.160	1.141
0.75	0.2072	1.144	0.2065	1.122	1.103
		1.380		1.379	1.379
		1.159		1.134	1.115
0.80	0.2319	1.083	0.2313	1.060	1.038
		1.356		1.356	1.356
		1.135		1.109	1.086

Table E.Au2 - *Optical model fits to Au scattering data (P=0.01). For each value of diffuseness we give the value of χ^2; the fitted parameters r_r and r_i; and the relevant decay radius for comparison. Shaded sections mark approximately where decay and scattering parameters 'overlap'. Table D.2 provides the additional information on the relevant decay S and V_0.*

The format is: χ^2 r_r r_i r_{decay} $\chi^2_{opt}=0.135$

Diffuseness	20-22		22-24		24-26	
0.30	6.5	1.8	6.5	1.8	6.5	1.803
		1.1		0.7		1.118
		1.448		1.442		1.435
0.35	2.60	1.675	2.60	1.659	2.5792	1.651
		1.150		1.145		1.180
		1.433		1.423		1.412
0.40	0.8975	1.564	0.9027	1.554	1.1315	1.562
		1.124		0.8203		1.029
		1.412		1.398		1.390
0.45	0.2565	1.482	0.2602	1.472	0.2638	1.462
		1.048		1.075		1.095
		1.391		1.380		1.385
0.50	0.1310	1.415	0.1316	1.403	0.1326	1.393
		1.286		1.283		1.297
		1.365		1.356		1.343
0.55	0.1428	1.366	0.1532	1.348	0.1477	1.337
		1.393		1.377		1.378
		1.345		1.329		1.318
0.60	0.1503	1.316	0.1497	1.302	0.1492	1.287
		1.421		1.420		1.419
		1.321		1.307		1.290
0.65	0.1653	1.261	0.1648	1.245	0.1645	1.229
		1.414		1.414		1.413
		1.297		1.281		1.264
0.70	0.1847	1.203	0.1840	1.185	0.1834	1.168
		1.400		1.399		1.399
		1.274		1.256		1.238
0.75	0.2072	1.144	0.2065	1.124	0.2061	1.105
		1.380		1.379		1.379
		1.252		1.228		1.209
0.80	0.2319	1.083	0.2313	1.061	0.2307	1.041
		1.356		1.356		1.356
		1.226		1.201		1.182

Table E.Au3 - *Optical model fits to Au scattering data (P=0.001). For each value of diffuseness we give the value of χ^2; the fitted parameters r_r and r_i; and the relevant decay radius for comparison. Shaded sections mark approximately where decay and scattering parameters 'overlap'. Table D.3 provides the additional information on the relevant decay S and V_0.*

The format is: χ^2 r_r r_i r_{decay} $\chi^2_{opt}=0.135$

Diffuseness	24-26		26-28		28-30	
0.30	6.5	1.8	6.5	1.8	6.6	1.8
		1.1		1.1		1.2
		1.551		1.543		1.532
0.35	2.6025	1.666	2.5744	1.652	2.5816	1.644
		1.099		1.172		1.150
		1.524		1.518		1.509
0.40	1.1025	1.571	0.9044	1.547	0.9082	1.539
		1.199		0.9893		1.047
		1.503		1.494		1.483
0.45	0.2602	1.472	0.2635	1.463	0.2667	1.454
		1.075		1.099		1.119
		1.478		1.470		1.457
0.50	0.1316	1.404	0.1320	1.393	0.1322	1.383
		1.283		1.278		1.298
		1.458		1.443		1.432
0.55	0.1527	1.349	0.1499	1.338	0.1472	1.327
		1.376		1.377		1.379
		1.434		1.421		1.408
0.60	0.1497	1.303	0.1494	1.290	0.1494	1.277
		1.420		1.419		1.419
		1.410		1.395		1.381
0.65	0.1649	1.246	0.1646	1.231	0.1641	1.217
		1.414		1.413		1.413
		1.382		1.366		1.351
0.70	0.1840	1.187	0.1825	1.171	0.1831	1.155
		1.399		1.399		1.398
		1.355		1.337		1.322
0.75	0.2066	1.126	0.2063	1.108	0.2058	1.092
		1.380		1.379		1.379
				1.310		1.294
0.80	0.2314	1.064	0.2308	1.045	0.2304	1.027
		1.356		1.356		1.355
				1.284		1.263

Table E.Au4 - *Optical model fits to Au scattering data (P=0.0001). For each value of diffuseness we give the value of χ^2, the fitted parameters r_r and r_i, and the relevant decay radius for comparison. Shaded sections mark approximately where decay and scattering parameters 'overlap'. Table D.4 provides the additional information on the relevant decay S and V_0.*

The format is: χ^2 r_r r_i r_{decay} $\chi^2_{opt}=0.135$

Diffuseness	28-30		30-32		32-34	
0.30	6.5	1.8	6.5	1.798	6.6	1.8
		1.1		1.140		1.1
		1.652		1.645		1.640
0.35	2.5687	1.653	2.3134	1.6399	2.6241	1.637
		1.150		0.5854		0.9501
		1.625		1.621		1.612
0.40	0.9034	1.548	0.9084	1.541	0.9144	1.534
		1.069		1.073		1.096
		1.605		1.597		1.586
0.45	0.2623	1.464	0.2650	1.456	0.2703	1.448
		1.078		1.090		1.140
		1.580		1.569		1.560
0.50	0.1308	1.394	0.1302	1.386	0.1287	1.375
		1.265		1.298		1.248
		1.555		1.541		1.531
0.55	0.1515	1.339	0.1385	1.335	0.1391	1.324
		1.376		1.406		1.406
		1.526		1.515		1.503
0.60	0.1497	1.292	0.1496	1.280	0.1490	1.268
		1.419		1.419		1.418
				1.489		1.476
0.65	0.1645	1.234	0.1639	1.221	0.1637	1.208
		1.413		1.413		1.412
				1.460		1.446
0.70	0.1836	1.174	0.1835	1.160	0.1831	1.146
		1.399		1.399		1.398
				1.432		1.417
0.75	0.2063	1.112	0.2057	1.096	0.2054	1.081
		1.379		1.379		1.379
				1.401		1.385
0.80	0.2309	1.050	0.2306	1.032	0.2302	1.016
		1.356		1.356		1.355
				1.371		1.355

Table E.Bi1 - *Optical model fits to Bi scattering data (P=0.1). For each value of diffuseness we give the value of χ^2; the fitted parameters r_r and r_i; and the relevant decay radius for comparison. Shaded sections mark approximately where decay and scattering parameters 'overlap'. Table D.1 provides the additional information on the relevant decay S and V_0.*

The format is: χ^2 r_r r_i r_{decay} $\chi^2_{opt}=0.142$

Diffuseness	18-20		20-22		22-24	
0.30	1.498	1.680	1.507	1.673	1.516	1.666
		1.100		1.146		1.089
		1.391		1.375		1.367
0.35	0.8479	1.611	0.8517	1.603	0.8547	1.595
		1.164		1.191		1.150
		1.370		1.357		1.344
0.40	0.4732	1.549	0.4760	1.540	0.4786	1.530
		1.107		1.130		1.157
		1.350		1.333		1.318
0.45	0.2652	1.492	0.2676	1.481	0.2697	1.471
		1.064		1.096		1.121
		1.330		1.310		1.298
0.50	0.1644	1.438	0.1658	1.426	0.1671	1.414
		0.9934		1.037		1.074
		1.304		1.288		1.274
0.55	0.1415	1.387	0.1422	1.373	0.1432	1.360
		1.162		1.180		1.201
		1.289		1.267		1.247
0.60	0.1498	1.340	0.1495	1.325	0.1493	1.310
		1.328		1.325		1.323
		1.262		1.241		1.220
0.65	0.1604	1.292	0.1600	1.275	0.1596	1.258
		1.348		1.347		1.345
		1.239		1.217		1.195
0.70	0.1725	1.240	0.1722	1.222	0.1720	1.204
		1.342		1.341		1.340
		1.212		1.189		1.167
0.75	0.1856	1.189	0.182	1.168	0.1847	1.149
		1.325		1.324		1.323
		1.191		1.163		1.141
0.80	0.1996	1.137	0.1991	1.114	0.1988	1.093
		1.302		1.301		1.300
		1.166		1.137		1.112

Table E.Bi2 - *Optical model fits to Bi scattering data (P=0.01). For each value of diffuseness we give the value of χ^2; the fitted parameters r_r and r_i; and the relevant decay radius for comparison. Shaded sections mark approximately where decay and scattering parameters 'overlap'. Table D.2 provides the additional information on the relevant decay S and V_0.*

The format is: χ^2 r_r r_i r_{decay} $\chi^2_{opt}=0.142$

Diffuseness	20-22		22-24		24-26	
0.30	1.501	1.679	1.507	1.673	1.514	1.667
		1.106		1.146		1.082
		1.481		1.473		1.462
0.35	0.8480	1.611	0.8517	1.603	0.8549	1.596
		1.166		1.191		1.141
		1.465		1.452		1.439
0.40	0.4734	1.549	0.4760	1.540	0.4781	1.531
		1.110		1.130		1.142
		1.443		1.427		1.416
0.45	0.2654	1.492	0.2674	1.482	0.2696	1.471
		1.068		1.093		1.120
		1.422		1.408		1.389
0.50	0.1643	1.438	0.1660	1.426	0.1676	1.415
		0.983		1.045		1.085
		1.395		1.384		1.368
0.55	0.1415	1.387	0.1422	1.373	0.1428	1.361
		1.164		1.180		1.189
		1.375		1.356		1.343
0.60	0.1498	1.340	0.1494	1.325	0.1489	1.311
		1.329		1.325		1.322
		1.350		1.333		1.314
0.65	0.1604	1.291	0.1600	1.275	0.1598	1.260
		1.348		1.347		1.346
		1.326		1.307		1.287
0.70	0.1725	1.240	0.1723	1.223	0.1721	1.206
		1.342		1.341		1.340
		1.302		1.282		1.260
0.75	0.1856	1.189	0.1851	1.170	0.1846	1.151
		1.325		1.324		1.323
		1.279		1.253		1.231
0.80	0.1996	1.137	0.1992	1.116	0.1991	1.096
		1.302		1.301		1.301
		1.252		1.225		1.203

Table E.Bi3 - *Optical model fits to Bi scattering data (P=0.001). For each value of diffuseness we give the value of χ^2; the fitted parameters r_r and r_i; and the relevant decay radius for comparison. Shaded sections mark approximately where decay and scattering parameters 'overlap'. Table D.3 provides the additional information on the relevant decay S and V_o.*

The format is: χ^2 r_r r_i r_{decay} $\chi^2_{opt}=0.142$

Diffuseness	24-26		26-28		28-30	
0.30	1.506	1.673	1.510	1.667	1.514	1.661
		1.142		1.175		1.110
		1.576		1.565		1.552
0.35	0.8517	1.603	0.8548	1.596	0.875	1.590
		1.191		1.222		1.246
		1.548		1.540		1.529
0.40	0.4757	1.540	0.4775	1.532	0.4792	1.524
		1.125		1.097		1.129
		1.527		1.515		1.502
0.45	0.2674	1.482	0.2691	1.473	0.2710	1.464
		1.093		1.112		1.137
		1.501		1.491		1.476
0.50	0.1663	1.427	0.1682	1.416	0.1706	1.406
		1.055		1.100		1.138
		1.481		1.463		1.450
0.55	0.1418	1.375	0.1415	1.363	0.1408	1.351
		1.168		1.152		1.130
		1.456		1.441		1.426
0.60	0.1492	1.327	0.1488	1.313	0.1487	1.301
		1.325		1.323		1.323
		1.432		1.414		1.398
0.65	0.1601	1.277	0.1602	1.262	0.1604	1.248
		1.347		1.347		1.346
		1.403		1.385		1.367
0.70	0.1723	1.225	0.1719	1.209	0.1713	1.198
		1.41		1.340		1.339
		1.376		1.356		1.338
0.75	0.1851	1.172	0.1847	1.155	0.1847	1.138
		1.324		1.323		1.323
		1.358		1.328		1.309
0.80	0.1994	1.119	0.1992	1.100	0.1996	1.081
		1.301		1.301		1.308
		1.324		1.301		1.279

Table E.Bi4 - *Optical model fits to Bi scattering data (P=0.0001). For each value of diffuseness we give the value of χ^2; the fitted parameters r_r and r_i; and the relevant decay radius for comparison. Shaded sections mark approximately where decay and scattering parameters 'overlap'. Table D.4 provides the additional information on the relevant decay S and V_0.*

The format is: χ^2 r_r r_i r_{decay} $\chi^2_{opt}=0.142$

Diffuseness	28-30		30-32		32-34	
0.30	1.507	1.668	1.509	1.663	1.511	1.658
		1.065		1.096		1.123
		1.670		1.660		1.653
0.35	0.8553	1.597	0.8571	1.591	0.8590	1.584
		1.150		1.246		1.263
		1.642		1.635		1.625
0.40	0.4774	1.533	0.4798	1.526	0.4823	1.19
		1.103		1.166		1.198
		1.622		1.611		1.598
0.45	0.2683	1.474	0.2699	1.465	0.2719	1.457
		1.092		1.115		1.146
		1.596		1.582		1.557
0.50	0.1691	1.418	0.1707	1.408	0.1713	1.399
		1.118		1.138		1.142
		1.571		1.555		1.543
0.55	0.1397	1.364	0.1387	1.354	0.1406	1.344
		1.078		1.080		1.164
		1.541		1.528		1.514
0.60	0.1492	1.316	0.1499	1.304	0.1505	1.292
		1.325		1.327		1.327
		1.521		1.502		1.486
0.65	0.1604	1.265	0.1600	1.252	0.1592	1.239
		1.347		1.345		1.343
		1.491		1.473		1.456
0.70	0.1717	1.212	0.1714	1.198	0.1716	1.184
		1.340		1.339		1.339
		1.463		1.444		1.427
0.75	0.1850	1.159	0.1851	1.143	0.1846	1.128
		1.324		1.323		1.323
		1.432		1.413		1.395
0.80	0.1991	1.104	0.1985	1.087	0.1984	1.071
		1.301		1.300		1.304
		1.402		1.383		1.364

Table E.U1 - *Optical model fits to U scattering data (P=0.1). For each value of diffuseness we give the value of χ^2; the fitted parameters r_r and r_i; and the relevant decay radius for comparison. Shaded sections mark approximately where decay and scattering parameters 'overlap'. Table D.1 provides the additional information on the relevant decay S and V_0.*

The format is: χ^2 r_r r_i r_{decay} $\chi^2_{opt}=0.106$

Diffuseness	18-20		20-22		22-24	
0.30	0.5070	1.575	0.5102	1.569	0.5116	1.562
		1.136		1.067		1.100
		1.394		1.370		1.354
0.35	0.2699	1.514	0.2705	1.08	0.2718	1.499
		1.150		1.100		1.150
		1.373		1.352		1.333
0.40	0.1575	1.460	0.1580	1.451	0.1415	1.443
		1.046		0.9558		0.7102
		1.353		1.329		1.308
0.45	0.1140	1.410	0.1145	1.399	0.1150	1.389
		1.011		1.069		1.093
		1.333		1.306		1.288
0.50	0.1087	1.363	0.1087	1.351	0.1087	1.340
		1.309		1.306		1.303
		1.308		1.285		1.265
0.55	0.1091	1.318	0.1091	1.305	0.1091	1.292
		1.350		1.349		1.347
		1.290		1.264		1.239
0.60	0.1099	1.270	0.1099	1.255	0.1099	1.241
		1.345		1.344		1.343
		1.267		1.239		1.213
0.65	0.1109	1.222	0.1109	1.205	0.1109	1.189
		1.327		1.326		1.326
		1.244		1.216		1.189
0.70	0.1122	1.172	0.1122	1.154	0.1122	1.137
		1.302		1.301		1.301
		1.218		1.188		1.162
0.75	0.1138	1.124	0.1137	1.104	0.1137	1.085
		1.272		1.271		1.271
		1.197		1.162		1.136
0.80	0.1155	1.076	0.1154	1.054	0.1154	1.034
		1.238		1.238		1.238
		1.172		1.138		1.108

Table E.U2 - *Optical model fits to U scattering data (P=0.01). For each value of diffuseness we give the value of χ^2; the fitted parameters r_r and r_i; and the relevant decay radius for comparison. Shaded sections mark approximately where decay and scattering parameters 'overlap'. Table D.2 provides the additional information on the relevant decay S and V_0.*

The format is: χ^2 r_r r_i r_{decay} $\chi^2_{opt}=0.106$

Diffuseness	20-22		22-24		24-26	
0.30	0.5075	1.574	0.5109	1.569	0.5118	1.563
		1.141		0.9648		1.100
		1.480		1.464		1.448
0.35	0.2698	1.514	0.2707	1.507	0.2716	1.493
		1.191		1.103		1.098
		1.465		1.445		1.425
0.40	0.1574	1.459	0.1580	1.451	0.1584	1.442
		1.041		0.9558		0.8893
		1.444		1.420		1.404
0.45	0.1141	1.409	0.1144	1.399	0.1149	1.389
		1.038		1.052		1.086
		1.423		1.402		1.378
0.50	0.1087	1.363	0.1087	1.352	0.1087	1.341
		1.309		1.306		1.302
		1.396		1.379		1.357
0.55	0.1091	1.318	0.1091	1.305	0.1091	1.293
		1.350		1.349		1.348
		1.377		1.351		1.333
0.60	0.1099	1.270	0.1099	1.256	0.1099	1.242
		1.345		1.344		1.344
		1.3552		1.329		1.305
0.65	0.1109	1.221	0.1109	1.206	0.1109	1.191
		1.327		1.326		1.326
		1.328		1.304		1.278
0.70	0.1122	1.172	0.1122	1.156	0.1122	1.139
		1.302		1.301		1.301
		1.305		1.279		1.253
0.75	0.1138	1.124	0.1137	1.105	0.1137	1.088
		1.272		1.271		1.271
		1.283		1.251		1.225
0.80	0.1155	1.076	0.1154	1.056	0.1154	1.037
		1.238		1.238		1.238
		1.257		1.224		1.198

Table E.U3 - *Optical model fits to U scattering data (P=0.001). For each value of diffuseness we give the value of χ^2; the fitted parameters r_r and r_i; and the relevant decay radius for comparison. Shaded sections mark approximately where decay and scattering parameters 'overlap'. Table D.3 provides the additional information on the relevant decay S and V_0.*

The format is: χ^2 r_r r_i r_{decay} $\chi^2_{opt}=0.106$

Diffuseness	24-26		26-28		28-30	
0.30	0.5097	1.569 1.168 1.566	0.5117	1.563 1.100 1.549	0.5132	1.558 1.134 1.5531
0.35	0.2706	1.507 1.034 1.539	0.2715	1.500 1.120 1.524	0.2722	1.493 1.150 1.435
0.40	0.1582	1.451 1.062 1.518	0.1589	1.443 1.087 1.501	0.1596	1.100 1.483
0.45	0.1144	1.399 1.052 1.493	0.1145	1.390 1.002 1.478	0.1147	1.381 0.9994 1.458
0.50	0.1087	1.352 1.306 1.473	0.1086	1.342 1.303 1.450	0.1086	1.332 1.300 1.433
0.55	0.1091	1.306 1.349 1.449	0.1091	1.295 1.348 1.429	0.1092	1.284 1.347 1.409
0.60	0.1099	1.257 1.344 1.426	0.1099	1.245 1.344 1.403	0.1099	1.232 1.343 1.383
0.65	0.1109	1.207 1.326 1.398	0.1109	1.193 1.326 1.374	0.1108	1.180 1.325 1.353
0.70	0.1122	1.157 1.301 1.371	0.1122	1.142 1.301 1.347	0.1122	1.127 1.300 1.325
0.75	0.1137	1.107 1.271 1.027	0.1137	1.091 1.271 1.320	0.1137	1.075 1.271 1.297
0.80	0.1154	1.059 1.238 1.013	0.1153	1.041 1.238 1.294	0.1153	1.023 1.237 1.268

Table E.U4 - *Optical model fits to U scattering data (P=0.0001). For each value of diffuseness we give the value of χ^2; the fitted parameters r_r and r_i; and the relevant decay radius for comparison. Shaded sections mark approximately where decay and scattering parameters 'overlap'. Table D.4 provides the additional information on the relevant decay S and V_0.*

The format is: χ^2 r_r r_i r_{decay} $\chi^2_{opt}=0.106$

Diffuseness	28-30		30-32		32-34	
0.30	0.5110	1.564 1.091 1.651	0.5119	1.559 1.115 1.637	0.5061	1.553 0.9161 1.625
0.35	0.2502	1.501 0.6361 1.625	0.2439	1.496 0.884 1.613	0.2501	1.489 0.5882 1.599
0.40	0.1591	1.444 1.108 1.605	0.1596	1.437 1.109 1.590	0.1599	1.430 1.093 1.573
0.45	0.1158	1.392 1.250 1.580	0.1136	1.383 0.8190 1.562	0.1137	1.376 0.8426 1.548
0.50	0.1087	1.344 1.300 1.556	0.1087	1.334 1.302 1.536	0.1088	1.325 1.301 1.520
0.55	0.1092	1.296 1.348 1.527	0.1092	1.286 1.347 1.510	0.1092	1.276 1.346 1.492
0.60	0.1099	1.247 1.348 1.499	0.1098	1.235 1.343 1.485	0.1098	1.224 1.343 1.466
0.65	0.1109	1.196 1.326 1.474	0.1109	1.183 1.325 1.457	0.1109	1.171 1.325 1.436
0.70	0.1122	1.145 1.301 1.453	0.1122	1.131 1.301 1.429	0.1122	1.118 1.300 1.408
0.75	0.1137	1.095 1.271 1.417	0.1137	1.080 1.271 1.399	0.1137	1.065 1.271 1.378
0.80	0.1154	1.045 1.238 1.393	0.1153	1.029 1.238 1.370	0.1153	1.013 1.237 1.348

REFERENCES

1. E. U. Condon and R. W. Gurney, *Phys.Rev.* **33**, 127 (1929).

2. G. Gamow, *Z.Phys.* **51**, 204 (1928).

3. H. J. Rose and G. A. Jones, *Nature* **307**, 245 (1984).

4. M. Curie, *C. r. Acad. Sci.*, Paris **130**, 76 (1900); also W. H. Bragg, *Phil. Mag.* **8**, 719 (1904); **10**, 600 (1905); **11**, 617 (1906).

5. E. Rutherford, *Phys. Z.* **4**, 235 (1903); also *Phil. Mag.* **5**, 177 (1903).

6. E. Rutherford and H. Geiger, *Proc. Roy. Soc.* **A81**, 141, 162 (1908); also E. Rutherford and T. Royds, *Phil. Mag.* **17**, 281 (1909).

7. E. Rutherford, *Phil. Mag.* **13**, 110 (1907).

8. H. Geiger and J. M. Nuttall, *Phil. Mag.* **22**, 613 (1911); **23**, 439 (1912).

9. E. Rutherford, *Phil. Mag.* **21**, 669 (1911).

10. N. Bohr, *Phil. Mag.* **26**, 1 (1913); **26**, 476 (1913).

11. F. A. Lindemann, *Phil. Mag.* **30**, 560 (1915).

12. D. Brink and J. J. Castro, *Nucl. Phys. A* **216**, 109 (1973).

13. W. W. Daehnick and L. J. Denes, *Phys. Rev.* B **136**, 1325 (1964).

14. K. Bethge, K. Meier-Ewart, K. Pfeiffer and R. Bock, *Phys. Lett. B* **24**, 663 (1967).

15. B. Buck, C. Dover, J.P. Vary, *Phys. Rev. C* **11**, 1803 (1975).

16. B. Buck and A. A. Pilt, *Nucl. Phys. A* **280**, 133 (1977).

17. B. Buck, H. Friedrich and A. A. Pilt, *Nucl. Phys A* **290**, 205 (1977).

18. K. F. Pal and R. G. Lovas, *Phys. Lett. B* **96**, 19 (1980).

19. A. Arima, H. Horiuchi, K. Kubodera, and N. Takigawa, in *Advances in Nuclear Physics*, edited by M. Baranger and E. Vogt (Plenum, New York, 1972), Vol. 5, p.345. For an even more extensive treatment, see K. Wildermuth and W. McClure, in *Springer Tracts in Modern Physics*, edited by G. Höhlen (Springer, New York, 1966), Vol 41.

20. S. A. Gurvitz and G. Kalbermann, *Phys. Rev. Lett.* **59**, 262 (1987).

21. P. B. Price, *Ann. Rev. Nucl. Part. Sci.* **39**, 19 (1989).

22. A. Sandalescu and W. Greiner, *Rep. Prog. Phys.* **55**, 1423 (1992).

23. H. J. Mang, *Ann. Rev. Nucl. Sci.* **14**, 1 (1964).

24. J.O.Rasmussen 1965 *Alpha-, Beta- and Gamma-Ray Spectroscopy* ed. K.Siegbahn (Amsterdam: North-Holland) p701.

25. T. Fliessbach and H. J. Mang, *Nucl. Phys. A* **236**, 75 (1976).

26. Y. Hatsukawa, H. Nakahara and D. C. Hoffman, *Phys. Rev. C* **42**, 674 (1990).

27. V. V. Burov, Yu N. Eldyshev, V. V. Lukyanov and Yu S Pol, *JINR Dubna Preprint E4-8029*, 1974.

28. R. Hofstadter, *Ann. Rev. Nucl. Sci.* **7**, 231 (1957).

29. J. Cook, *Comput. Phys. Commun.* **25**, 125 (1982).

30. I. Perlmann and J. O. Rasmussen, *Handb. Phys.* **XLII**, 109 (1957).

31. R. S. Thomas, *Prog. Theor. Phys.* **12**, 253 (1954).

32. Z. Fliessbach, *Z. Phys. A* **272**, 39 (1975); **277**, 151 (1976).

33. R. Beck, F. Dickmann and R. G. Lovas, *Ann. Phys.* **173**, 1 (1987).

34. T. Fliessbach and H. J. Mang, *Nucl. Phys. A* **263**, 75 (1976).

35. R. Blendowske, T. Fliessbach and H. Walliser, *Nucl. Phys. A* **464**, 75 (1987).

36. T. Fliessbach and S. Okabe, *Z. Phys. A* **320**, 289 (1985).

37. K. Varga, R. G. Lovas and R. J. Liotta, *Phys. Rev. Lett.* **69**, 37 (1992).

38. B. Buck, A. C. Merchant, S. M. Perez, *Phys. Rev. C* **45**, 2247 (1992).

39. B.Buck and A.C.Merchant, *Phys. Rev. C* **39**, 2097 (1989).

40. B.Buck, A.C.Merchant and S.M.Perez, *J.Phys. G: Nucl. Part. Phys.* **17**, L91 (1991).

41. B.Buck, A.C.Merchant, S.M.Perez and P.Tripe, *Phys. Rev. C* **47**, 1307 (1993).

42. P. E. Hodgson, *Nuclear Reactions and Nuclear Structure*, Clarendon Press, Oxford, 1971, Ch.3.

43. B. H. Bransden and C. J. Joachain, *Physics of Atoms and Molecules*, Longman Scientific & Technical, 1983, Ch.11.

44. A. Messiah, *Quantum Mechanics* **Vol.I**, North-Holland Publishing Company, Amsterdam, 1961, Ch.10.

45. E. Merzbacher, *Quantum Mechanics* 2nd.ed., John Wiley & Sons, 1970, Ch.11.

46. H. A. Bethe, *Phys. Rev.* **47**, 747 (1935).

47. P. E. Hodgson, *Proc. Phys. Soc.* **801**, 1161 (1962).

48. C. M. Perey and F. G. Perey, *Phys. Rev.* **132**, 755 (1963).

49. R. W. Woods and D. S. Saxon, *Phys. Rev.* **95**, 977 (1954)

50. A. E. Glassgold and P. J. Kellogg, *Phys. Rev.* **107**, 1372 (1957).

51. L. McFadden and G. R. Satchler, *Nucl. Phys.* **84**, 177 (1966).

52. A. Budzanowski, K. Grotowski, S. Micek, H. Niewodniczanski, J. Sliz, A. Strzalkowski and H. Wojciechowski, *Phys. Lett.* **11**, 74 (1964).

53. J. K. Dickens and F. G. Perey, *Phys. Rev. B* **138**, 1080 (1965).

54. P. E. Hodgson, *The Optical Model of Elastic Scattering*, Oxford University Press 1963, p.70.

55. P. E. Hodgson, *Nuclear Reactions and Nuclear Structure*, Oxford University Press 1971, p.155-6.

56. R. H. Bassel, R. M. Drisko, G. R. Satchler, L. L. Lee, J. P. Schiffer and B. Zeidman, *Phys. Rev.* B **136**, 960 (1964).

57. G. Igo, *Phys. Rev.* **115**, 1665 (1959).

58. N. Austern, *Ann. Phys.* **15**, 299 (1961).

59. R. M. Drisko, G. R. Satchler and R. H. Bassel, *Phys. Lett.* **5**, 347 (1963).

60. P. Singh, A. Chatterjee, S.K. Gupta and S.S. Kerekatte, *Phys. Rev. C* **43**, 1867 (1991).

61. P. E. Hodgson, *Phys. Rev. Lett.* **6**, 358 (1961).

62. T. Delbar *et al.*, *Phys. Rev. C* **18**, 1237 (1978).

63. R. Blendowske and H. Walliser, *Phys. Rev. Lett.* **61**, 1930 (1988).